Tuning the Auxin Transcriptional Response

Edith Pierre-Jerome

A dissertation

submitted in partial fulfillment of the

requirements for the degree of

Doctor of Philosophy

University of Washington

2015

Reading Committee:

Jennifer Nemhauser, Chair

Eric Klavins

Takato Imaizumi

Program Authorized to Offer Degree:

Biology

University of Washington

Abstract

Tuning the Auxin Transcriptional Response

Edith Pierre-Jerome

Chair of the Supervisory Committee:
Professor Jennifer Nemhauser
Biology

Auxin is involved in almost every aspect of plant growth and development. How auxin orchestrates such diverse and context-specific responses has been a longstanding question. The work presented here evaluates the potential for specificity encoded within the short nuclear auxin pathway itself. By introducing each of the core components that make up the pathway into yeast, I was able to test how component choice and circuit configuration could be used to tune an auxin response. In building the pathway from perception to transcription in a heterologous context, I also defined the minimal requirements for a transcriptional auxin response. I went on to explore the potential for diverse responses in auxin circuits of varying complexity by individually substituting family members of the core components that make up the pathway. Finally, guided by the partial structures of the two key transcriptional regulators, I broke the pathway back down to systematically characterize the underlying protein-protein and protein-DNA interactions and generated a new minimal model of auxin signaling.

TABLE OF CONTENTS

List of Figures v

Chapter 1. Tuning the Auxin Transcriptional Response 1

Chapter 2. A Synthetic Approach Reveals Tunability of Auxin Signaling 8

Chapter 3. Recapitulation of the Nuclear Auxin Response Pathway in Yeast 52

Chapter 4. Molecular Basis of Auxin Nuclear Signaling 80

Chapter 5. Perspective:Evolution as Tinkering 126

LIST OF FIGURES

Figure 1.1. Tuning the auxin response module. 2

Figure 2.1. IAA degradation is highly variable. 9
Figure 2.2. Degradation dynamics can be described using few parameters. 10
Figure 2.3. Residues outside of domain II contribute to auxin-induced degradation. 12

Figure 3.1. Auxin-induced transcription in yeast..... 53
Figure 3.2. IAAs drive auxin response dynamics. 53
Figure 3.3. Model selection and sensitivity analysis of the auxin response pathway..... 54
Figure 3.4. IAA coexpression reveals dominance relationships between IAAs..... 55

Figure 4.1. ARFs exhibit promoter specific activity..... 84
Figure 4.2. ARFs activate as dimers. 87
Figure 4.3. IAAs can function as monomers. 92
Figure 4.4. Model of auxin nuclear signaling. 96

ACKNOWLEDGEMENTS

If there is anything I learned in graduate school, it is that you cannot do everything yourself. I have gotten a lot of help and support along the way from the Biology Department, my fantastic committee, the Nemhauser, Klavins and Imaizumi labs, and my friends and family.

There are two people in particular, to whom I will forever be in debt:
my loving husband Nima for his steadfast loyalty, and my incredible mentor Jennifer for recognizing before I did that I was meant to be a scientist.

DEDICATION

This is for you dad

Journal of Experimental Botany, Vol. 64, No. 9, pp. 2557–2563, 2013
doi:10.1093/jxb/ert100 Advance Access publication 29 April, 2013

Journal of Experimental Botany
www.jxb.oxfordjournals.org

REVIEW PAPER

Tuning the auxin transcriptional response

Edith Pierre-Jerome*, Britney L. Moss* and Jennifer L. Nemhauser†

Department of Biology, University of Washington, Seattle, WA 98195, USA

*These authors contributed equally to this work.
† To whom correspondence should be addressed. E-mail: jn7@uw.edu

Received 16 January 2013; Revised 12 March 2013; Accepted 13 March 2013

Abstract

How does auxin provoke such a diverse array of responses? This long-standing question is further complicated by a remarkably short nuclear auxin signalling pathway. To crack the auxin code, several potential sources of specificity need to be evaluated. These include: specificity of interactions among the core auxin response components, specificity resulting from higher order complex dynamics, and specificity in interactions with global factors controlling protein turnover and transcriptional repression. Here, we review recent progress towards characterizing and quantifying these interactions and highlight key gaps that remain.

Key words: ARF, Aux/IAA, E3 ubiquitin ligase, phytohormones, TIR1, transcriptional repression.

Introduction

The central role of auxin in shaping plant form is made possible by context-specific responses. Cell type, developmental stage, and environment all contribute to striking differences in auxin responses, yet the many transcriptional effects of auxin rely on the same small repertoire of signalling components: receptors [TRANSPORT INHIBITOR RESPONSE1/AUXIN SIGNALING F-BOXES (TIR1/AFBs)], repressors [Auxin/INDOLE-3-ACETIC ACID (Aux/IAAs)], and transcription factors [AUXIN RESPONSE FACTORS (ARFs)]. The transmission of an auxin signal relies on interactions between these three components that comprise the core auxin signalling module. Formation of an ARF–Aux/IAA heterodimer results in repression of ARF target genes. This repression is relieved by the degradation of Aux/IAA following its auxin-induced association with a TIR1/AFB receptor. Given the large sizes of the protein families to which these components belong, it is tempting to speculate that particular combinations of signalling component family members confer auxin response specificity (Lokerse and Weijers, 2009; De Smet *et al*., 2010; Stewart and Nemhauser, 2010; Rademacher *et al*., 2012). For such a model to work, an auxin response module would need to be tuned to different auxin input properties and be able to deliver different transcriptional outputs. One likely source for varied input/output properties is differential interactions amongst the core auxin signalling components. Current models of auxin signalling are caught between the competing priorities of simplicity and capturing the most influential parameters. A key to improving these models, and to understanding the auxin code, will be the ability to rigorously quantify and rank the importance of each interaction within the auxin network. Here, we review what is currently known about differences between family members of the components that make up the auxin response complex, as well as areas of potential differences in their interactions outside of the core module (Fig. 1).

Abbreviations: APC/C, anaphase-promoting complex; ARFs, AUXIN RESPONSE FACTORS; Aux/IAAs, Auxin/INDOLE-3-ACETIC ACID; AXR1, AUXIN RESISTANT 1; CAND1, CULLIN-ASSOCIATED AND NEDDYLATION DISASSOCIATED 1; CSN, CONSTITUTIVE PHOTOMORPHOGENIC9 (COP9) SIGNALOSOME; CUL1, cullin-1; EAR, ethylene response factor-associated amphiphilic repression; ECR1, E1 C-terminal related 1; HDAC, histone deacetylase; IκB, nuclear factor-κB inhibitor; LUG, LEUNIG; NF-κB, nuclear factor-κB; NO, nitric oxide; RCE1, RUB1 CONJUGATING ENZYME 1; RUB, related to ubiquitin 1/neural precursor cell expressed developmentally down-regulated protein 8; SCF, Skp1-Cullin-F-box; TIR1/AFBs, TRANSPORT INHIBITOR RESPONSE1/AUXIN SIGNALING F-BOXES; TPR, TOPLESS-related protein; β-TrCP, β-transducin repeat-containing protein.

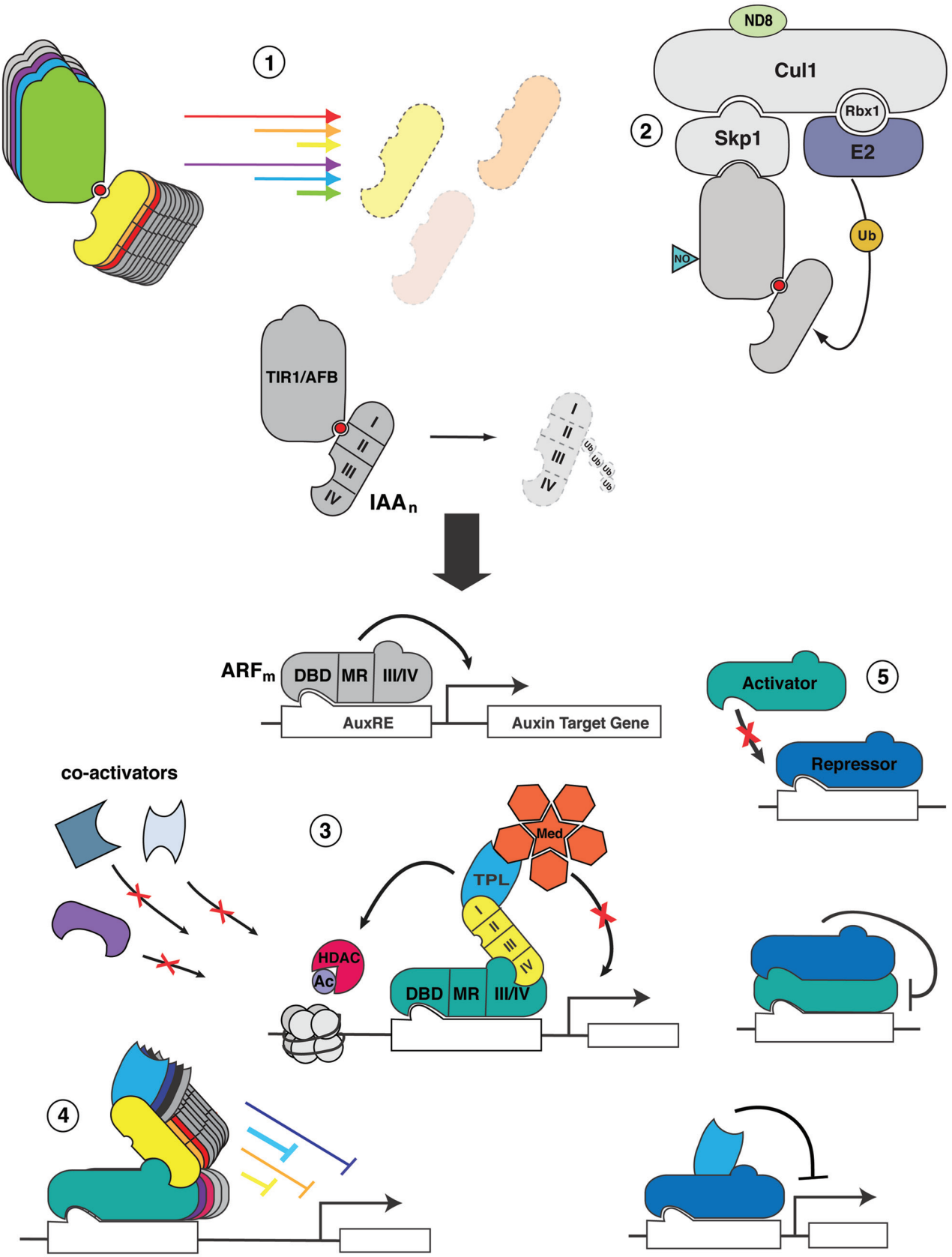

Fig. 1. Tuning the auxin response module. The activity of the auxin response module is governed by interactions between a core set of proteins: auxin receptors (TIR1/AFBs), repressors (Aux/IAAs), and transcription factors (ARFs). The basic mechanism of auxin signalling is depicted centrally in grey: the Aux/IAAs interact with the TIR1/AFBs in an auxin-dependent manner, leading to the ubiquitination and subsequent degradation of the Aux/IAA, which promotes the activity of the ARF transcription factors on auxin target genes. Modulation

The TIR1/AFB receptor family

In *Arabidopsis thaliana*, there are three ancient lineages within the AFB family of auxin receptors. Each lineage is represented by pairs of genes: TIR1 and AFB1; AFB2 and AFB3; and AFB4 and AFB5 (a fourth lineage found in angiosperms was lost in *Brassicaceae* and *Poaceae*) (Parry *et al*., 2009). Genetic studies have revealed that the two dominant auxin receptors in plants are TIR1 and AFB2, although they are not functionally equivalent (Dharmasiri *et al*., 2005b; Parry *et al*., 2009). Biochemical studies have demonstrated auxin-induced, dose-dependent interactions of AFB2 and TIR1 with several Aux/IAAs (Gray *et al*., 2001; Dharmasiri *et al*., 2005a; Kepinski and Leyser, 2005; Parry *et al*., 2009; Calderón Villalobos *et al*., 2012). Both proteins have highly similar auxin-binding and Aux/IAA interaction domains (Tan *et al*., 2007). Despite this high degree of similarity, AFB2 degrades Aux/IAAs faster than TIR1 in a yeast degradation assay (Havens *et al*., 2012).

The role of the other AFB family members in the auxin response is less clear. Single *afb1* or *afb3* loss-of-function mutants have only subtle phenotypes, although they can enhance phenotypes of *tir1* and *afb2* mutants (Dharmasiri *et al*., 2005*b*; Parry *et al*., 2009). This is consistent with the weaker interactions observed between AFB1 or AFB3 and Aux/IAAs in yeast two-hybrid or *in vitro* pull-down assays (Parry *et al*., 2009; Calderón Villalobos *et al*., 2012). *afb4* and *afb5* mutants were identified in screens for resistance to the synthetic auxin herbicide picloram (Walsh *et al*., 2006), and later shown to function as auxin receptors *in vitro* (Greenham *et al*., 2011). AFB5 binds picloram with much higher affinity than TIR1, probably as a result of amino acid substitutions within the auxin-binding pocket (Calderón Villalobos *et al*., 2012). Initial AFB4 loss-of-function studies revealed growth defects consistent with auxin hypersensitivity, leading the authors to hypothesize that AFB4 might act as a negative regulator of auxin signalling (Greenham *et al*., 2011). However, more recent studies indicate that AFB4 acts similarly to other AFB family members (Hu *et al*., 2012). Future experiments are needed to determine whether any differences in biochemical properties among AFBs contribute to specificity in auxin binding or response dynamics.

Post-translational modification of TIR1, as well as other components of the larger SCF (Skp1-Cullin-F-box) E3 ubiquitin ligase complex, is a potential additional layer of regulation. Recently, TIR1 has been shown to undergo *S*-nitrosylation, a nitric oxide (NO)-mediated protein modification (Terrile *et al*., 2012). *S*-Nitrosylation enhanced TIR1 association with Aux/IAAs, and a mutant TIR1 protein lacking a putative *S*-nitrosylation site was unable to restore auxin sensitivity when expressed in a *tir1* mutant. Additionally, SCF complex assembly and activity can be regulated through ubiquitin-related protein RUB/NEDD8 post-translational modification of the CUL1 scaffold protein (reviewed in Duda *et al*., 2011; Hua and Vierstra, 2011). In plants, mutants in several proteins involved in RUB/NEDD8 conjugation (e.g. AXR1, ECR1, and RCE1) show strong auxin resistance phenotypes (Cheng *et al*., 2004; Mockaitis and Estelle, 2008). NEDD8 modification of CUL1 is further regulated by the complex interplay of de-neddylation by the CSN [CONSTITUTIVE PHOTOMORPHOGENIC9 (COP9) SIGNALOSOME] and the inhibitory protein CAND1 (CULLIN-ASSOCIATED AND NEDDYLATION DISASSOCIATED 1); however, *csn* and *cand1* mutant plants display more subtle and complex auxin phenotypes (Gusmaroli *et al*., 2007; Stuttmann *et al*., 2009; Dohmann *et al*., 2010). While CSN and CAND1 are required for proper SCF–TIR1 function, the molecular basis of this regulation remains to be firmly established. Recent *in vitro* experiments have suggested that the F-box identity and substrate binding can also impact neddylation of the SCF (Emberley *et al*., 2012; Enchev *et al*., 2012). Together, these data suggest that the SCF complex can be regulated by post-translational modification at several levels that can influence the efficacy of F-box function and, in turn, the transmission of an auxin signal.

The Aux/IAA co-repressor family

The diversity of Aux/IAA-related phenotypes and the size of the family suggest that Aux/IAAs are excellent candidates for providing specificity in auxin responses (Lokerse and Weijers, 2009). Most Aux/IAAs have four domains thought to act modularly to confer: auxin-induced degradation through interaction with TIR1/AFBs (DII), dimerization with the ARFs and other IAAs (DIII and DIV), and transcriptional repression through the recruitment of co-repressors (DI). The interactions at each of these domains

of these interactions has the potential to fine-tune the output of the auxin response. (1) The timing and degree of auxin-induced Aux/IAA degradation can be influenced by the particular combination of TIR1/AFBs and Aux/IAAs present in a cell. (2) The auxin co-receptor is part of a larger E3 ubiquitin ligase complex whose activity can be regulated by several post-translational modifications and by interaction with E2 ubiquitin-conjugating enzymes. (3) When auxin levels are low, activator ARFs dimerize with Aux/IAAs, which in turn recruit the TOPLESS (TPL) co-repressors to inhibit transcriptional activity of the target gene. Though the mechanism of TPL repression is largely unknown, TPL probably recruits HDACs to remodel chromatin at auxin target genes and/or blocks recruitment of co-activators and the Mediator complex. (4) Differential and specific interactions between the various members of the ARF, Aux/IAA, and TPL families may also contribute to the dynamics of auxin transcriptional responses. (5) Much less is known about how repressor ARFs function, though it is speculated that they may block binding of activator ARFs, dimerize with and inhibit activator ARFs, and/or directly recruit co-repressors to target genes. ND8, NEDD8; Cul1, cullin 1; Rbx1, RING-box protein 1; Ub, ubiquitin; NO, nitric oxide; DBD, DNA-binding domain; MR, middle region; HDAC, histone deacetylase; Ac, acetyl group; Med, Mediator complex.

may act as tuning knobs to specify the output properties for a given auxin signal.

Degradation (DII)

Degradation rates differ among Aux/IAAs. Aux/IAA–reporter fusions with diverse DII sequences show a range of degradation rates when expressed in *Arabidopsis* or yeast (Dreher *et al*., 2006; Havens *et al*., 2012). These and other approaches showed that 13 amino acids within DII are both necessary and sufficient for auxin-induced degradation (Ramos *et al*., 2001; Dharmasiri *et al*., 2005a; Kepinski and Leyser, 2005). Structural studies revealed that the DII from IAA7 directly contacts both auxin and TIR1 (Tan *et al*., 2007). Interestingly, efficient auxin binding *in vitro* requires both TIR1 and a member of the Aux/IAA family, suggesting that the complex behaves as an auxin co-receptor (Calderón Villalobos *et al*., 2012). Pairs of AFBs and Aux/IAAs exhibit wide variation in auxin binding affinities, suggesting that different pairs may be tuned to different ranges of auxin concentrations. In addition, different auxin binding affinities were observed when the TIR1/IAA7 co-receptor was exposed to several auxin variants (Calderón Villalobos *et al*., 2012), suggesting that co-receptor pairs may also vary in their sensitivity to the type of auxin present.

How auxin affinity relates to Aux/IAA turnover rates is still unclear, although recently reported Aux/IAA degradation rates in yeast (Havens *et al*., 2012) were not strongly correlated with measured dissociation constants of purified complex components (Calderón Villalobos *et al*., 2012). Several studies indicate that sequences outside of DII play a role in regulating both complex association and Aux/IAA degradation rates (Dreher *et al*., 2006; Calderón Villalobos *et al*., 2012; Havens *et al*., 2012). Sequences outside of the TIR1–auxin–Aux/IAA interaction surfaces may also contribute to differences in the Aux/IAA degradation rate, possibly by facilitating transfer of ubiquitin from the E2 ubiquitin-conjugating enzyme. Several substrates of the E3 anaphase-promoting complex (APC/C) share conserved sequences termed 'initiation motifs' that act in this way to accelerate substrate degradation (Williamson *et al*., 2011).

In identifying informative parameters for models of auxin signalling, it may be useful to look at how the degradation rate impacts other signalling systems. For example, the mammalian nuclear factor (NF)-κB pathway is among the best-studied degradation-triggered signalling pathways. Similar to the auxin signalling pathway, ubiquitination of several NF-κB inhibitor (IκB) repressor proteins by the β-TrCP (β-transducin repeat-containing protein) SCF E3 ligase immediately follows pathway activation (Kanarek and Ben-neriah, 2012). This facilitates de-repression of NF-κB transcription factors allowing them to activate expression of a host of genes, including the IκBs. Under prolonged or repeated exposure to the activating stimulus, this negative feedback can generate strong oscillations in NF-κB transcriptional activity that play a significant role in determining the timing and intensity of the transcriptional response (Tian *et al*., 2005; Kearns *et al*., 2006; Ashall *et al*., 2009; Sung *et al*., 2009). Much like the Aux/IAAs, the IκBs are each degraded with different kinetics (from 5 min for IκBα to 60–90 min for IκBβ and IκBε). In particular, the presence of slow degrading IκBs that are turned over out of phase with the faster IκBα can act to dampen transcriptional oscillations. It is conceivable that Aux/IAAs behave similarly to tune the intensity and duration of downstream auxin transcriptional responses.

Dimerization (DIII/IV)

Aux/IAAs modulate ARF transcriptional activity through binding at the conserved DIII and DIV domains at the C-terminus of both families (Guilfoyle *et al*., 1998; Tiwari *et al*., 2003). Expression of ARFs without DIII/DIV can lead to constitutive reporter activation in protoplast transfection assays (Tiwari *et al*., 2003; Wang *et al*., 2005), and a similarly truncated version of ARF5 acts as a gain-of-function allele in plants (Krogan *et al*., 2012). Different ARF–Aux/IAA interactions may allow for distinct auxin responses, but the degree of interaction specificity and its molecular basis have yet to be uncovered. Interaction studies suggest that Aux/IAAs can interact with one another almost non-discriminately and most Aux/IAAs can interact with a number of ARFs (Kim *et al*., 1997; Vernoux *et al*., 2011). Functional modules of ARF–Aux/IAA pairs may be generated by their shared location in time, space, and developmental context (Weijers *et al*., 2005; Walsh *et al*., 2006; Muto *et al*., 2007; Rademacher *et al*., 2012). However, the expression pattern alone cannot fully explain different functions within the Aux/IAA family, as stabilized Aux/IAAs provoke different phenotypes even when expressed from the same promoter (Weijers *et al*., 2005; Muto *et al*., 2007).

In addition, multiple ARFs and Aux/IAAs can be naturally expressed in the same cell yet generate different mutant phenotypes (Rademacher *et al*., 2011; Vernoux *et al*., 2011). For example, genetic studies suggest that IAA12–ARF5 and IAA14–ARF7/19 make up distinct functional modules despite all being expressed in lateral root founder cells (De Smet *et al*., 2010). How modules are distinguished within a cell, to what extent known Aux/IAA–ARF pairs interact with or influence one another, and how the induction of Aux/IAAs by auxin may alter Aux/IAA–ARF interactions are all open questions. Auxin-induced expression of specific Aux/IAAs may act to alter the cell's response to the next auxin cue. Such a scenario could explain the observations of a temporal offset of the IAA12 and IAA14 modules in the root (De Smet *et al*., 2010).

Dimerization within the Aux/IAA family may also contribute to the repertoire of auxin response modules, though few assays or computational models have addressed this possibility. The high degree of interaction between the Aux/IAAs observed in yeast two-hybrid assays prompted Vernoux and colleagues to include degradation of Aux/IAA dimers in their mathematical model of auxin signalling in the shoot apical meristem (Vernoux *et al*., 2011). If naturally auxin-resistant Aux/IAAs form heterodimers with auxin-degradable Aux/IAAs, they might act to fine-tune auxin transcriptional responses. Indeed, yeast interaction studies demonstrate that

these combinations are possible (Vernoux *et al*., 2011) and they could have large impacts on transcriptional dynamics in a given cell. For example, an Aux/IAA without a degron sequence could shield its partner from the SCF machinery and thereby delay activation of an ARF.

Repression (DI)

Aux/IAAs inhibit activity of ARFs by recruiting the co-repressor TOPLESS (TPL) and related proteins (TPRs) through an ethylene response factor-associated amphiphilic repression (EAR) motif in domain I (Szemenyei *et al*., 2008). This interaction can also be found in the moss *Physcomitrella patens* (Causier *et al*., 2012b), suggesting that this mechanism may be largely conserved among land plants. TPL has been shown to interact with transcriptional regulators in a number of pathways and may be recruited by diverse repression domains (Causier *et al*., 2012a). Almost all Aux/IAAs have an EAR motif, but there is some diversity in its composition (Lokerse and Weijers, 2009). Site-directed mutagenesis of EAR motifs has shown that the same mutation in different Aux/IAAs results in a range of auxin-related phenotypes (Li *et al*., 2011). This result suggests that variation in the specificity or strength of TPL/TPR recruitment may be another source of functional diversity within the Aux/IAA repressor family.

TPL belongs to the Groucho/TUP1 co-repressor family, broadly conserved across eukaryotes. How TPL confers repression is not well understood, although genetic studies connect TPL function to histone deacteylases (HDACs) (Long, 2006; Liu and Karmarkar, 2008). Another plant member of the Groucho/TUP1 family, LEUNIG (LUG), interacts both with HDACs and with components of the Mediator complex (Gonzalez *et al*., 2007). The yeast TUP1 co-repressor utilizes several repression mechanisms: HDAC recruitment, displacing Mediator interactions with activators, and nucleosome repositioning (Liu and Karmarkar, 2008). A recent study has proposed that TUP1 functions primarily by blocking recruitment of co-activators (and the Mediator complex), thereby allowing rapid transitions between on and off states in stress responses (Wong and Struhl, 2011). The identification of a similar repression mechanism for TPL would explain the rapid relief of repression upon the degradation of the Aux/IAAs. The efficiency of both short- and long-term repression mechanisms may differ across the Aux/IAA family, providing potential additional control points in auxin signalling.

The ARF transcription factor family

The auxin sensitivity of ARF transcription factors is mediated by their interaction with the Aux/IAA co-repressors (Guilfoyle *et al*., 1998; Tiwari *et al*., 2003; Wong and Struhl, 2011). Yet of the 23 ARFs in *Arabidopsis*, only five are classified as transcriptional activators. This classification is based in large part on their effect upon an auxin-inducible reporter in protoplast transfection assays (Guilfoyle *et al*., 1998; Ulmasov *et al*., 1999a; Tiwari *et al*., 2003). The other ARFs tested in these assays conferred repression, and the remaining ARFs were classified as repressors based on the shared absence of glutamine enrichment in their middle regions (Tiwari *et al*., 2003). This distinction appears to be quite ancient, as activator and repressor ARFs belong to distinct clades, with at least one clade of each class dating back to the origin of land plants (Finet *et al*., 2013). There is little evidence that repressor ARFs interact with Aux/IAAs, and it is not understood how such an interaction might mediate auxin sensitivity. Thus, repressor ARF–Aux/IAA interactions are commonly left out of models of auxin response. This fundamental difference between activators and repressors implies functional diversification of their respective DIII/DIV domains (reviewed in Guilfoyle and Hagen, 2012).

The ARF repression mechanism is not well understood, although there is evidence to support at least two distinct mechanisms. First, repressor ARFs may act through a direct repression mechanism where they inhibit activator ARF activity by dimerization or by independently conferring repression to auxin-responsive promoters. The latter scenario is supported by evidence that ARF2 can repress a yeast reporter when fused to a heterologous DNA-binding domain (Vert *et al*., 2008). In addition, several repressor ARFs have been pulled out of screens for interactions with TPL/TPR co-repressors (Causier *et al*., 2012a) and contain EAR domains in their middle regions. Repression via TPL recruitment may be evolutionarily conserved as putative repressor ARFs identified in moss can interact with moss TPL proteins (Causier *et al*., 2012b). Several ARFs contain predicted interaction domains for LUG (Lokerse and Weijers, 2009), providing additional mechanisms for blocking transcriptional activation. The dimerization scenario is based on early studies that demonstrated that some ARFs could bind DNA as either dimers or monomers, and that dimerization could enhance DNA binding (Ulmasov *et al*., 1999b). One argument against dimerization is that very few ARF–ARF interactions were detected in a recent large-scale interactome study, although for most ARFs only DIII/DIV were used (Vernoux *et al*., 2011). Little is known yet about the formation of ARF dimers *in vivo* and any partner preferences that shape which complexes may form.

An alternative means of repression is indirect. In this scenario, repressor ARFs inhibit activator ARF activity by competing for access to the same promoter elements. While many ARFs bind the same synthetic promoters (Ulmasov *et al*., 1999a; Tiwari *et al*., 2003; Lokerse and Weijers, 2009), it is unclear whether activator and repressor ARFs bind to the same *cis*-elements under natural conditions. A recent mathematical model for auxin signalling incorporates a competition between repressor and activator ARFs, largely based on their extensive co-expression (Vernoux *et al*., 2011). This model predicts that the balance of repressor and activator ARF levels maintains a constant transcriptional response even in the presence of fluctuating auxin signals.

Conclusion

The small molecule auxin accomplishes a vast array of biological tasks using a deceptively simple three-protein signal

perception and transduction module (TIR1/AFB, Aux/IAA, ARF). While much progress has been made in understanding the molecular mechanisms underlying this diversity, many questions remain. New technologies and higher precision characterization of known components can hopefully help untangle the auxin response network, and lead to a clear picture of how the auxin signal is so exquisitely fine-tuned in time and space.

Acknowledgements

Our work on auxin is supported by the Paul G. Allen Family Foundation and the National Science Foundation [IOS-0919021]. EPJ is supported by a National Science Foundation Graduate Research Fellowship and the Seattle Chapter of the Achievement Rewards for College Scientists Foundation. We thank Jessica Guseman and Kyle Havens for useful discussions and careful reading of our manuscript. We thank Eric Klavins for mentorship and lively debates about regulation of dynamic systems.

References

Ashall L, Horton CA, Nelson DE, *et al.* 2009. Pulsatile stimulation determines timing and specificity of NF-κB-dependent transcription. *Science* **324,** 242–246.

Calderón Villalobos LIA, Lee S, De Oliveira C, *et al.*. 2012. A combinatorial TIR1/AFB–Aux/IAA co-receptor system for differential sensing of auxin. *Nature Chemical Biology* **8,** 477–485.

Causier B, Ashworth M, Guo W, Davies B. 2012*a*. The TOPLESS interactome: a framework for gene repression in Arabidopsis. *Plant Physiology* **158,** 423–438.

Causier B, Lloyd J, Stevens L, Davies B. 2012*b*. TOPLESS co-repressor interactions and their evolutionary conservation in plants. *Plant Signaling Behavior* **7,** 325–328.

Cheng YF, Dai XH, Zhao Y. 2004. AtCAND1, a HEAT-repeat protein that participates in auxin signaling in arabidopsis. *Plant Physiology* **135,** 1020–1026.

De Smet I, Lau S, Voss U, *et al.*. 2010. Bimodular auxin response controls organogenesis in Arabidopsis. *Proceedings of the National Academy of Sciences, USA* **107,** 2705–2710.

Dharmasiri N, Dharmasiri S, Estelle M. 2005*a*. The F-box protein TIR1 is an auxin receptor. *Nature* **435,** 441–445.

Dharmasiri N, Dharmasiri S, Weijers D, Lechner E, Yamada M, Hobbie L, Ehrismann JS, Jürgens G, Estelle M. 2005*b*. Plant development is regulated by a family of auxin receptor F box proteins. *Developmental Cell* **9,** 109–119.

Dohmann EM, Nill C, Schwechheimer C. 2010. DELLA proteins restrain germination and elongation growth in Arabidopsis thaliana COP9 signalosome mutants. *European Journal of Cell Biology* **89,** 163–168.

Dreher KA, Brown J, Saw RE, Callis J. 2006. The Arabidopsis Aux/IAA protein family has diversified in degradation and auxin responsiveness. *The Plant Cell* **18,** 699–714.

Duda DM, Scott DC, Calabrese MF, Zimmerman ES, Zheng N, Schulman BA. 2011. Structural regulation of cullin–RING ubiquitin ligase complexes. *Current Opinion in Structural Biology* **21,** 257–264.

Emberley ED, Mosadeghi R, Deshaies RJ. 2012. Deconjugation of Nedd8 from Cul1 is directly regulated by Skp1-F-box and substrate, and the COP9 signalosome inhibits deneddylated SCF by a noncatalytic mechanism. *Journal of Biological Chemistry* **287,** 29679–29689.

Enchev RI, Scott DC, da Fonseca PC, Schreiber A, Monda JK, Schulman BA, Peter M, Morris EP. 2012. Structural basis for a reciprocal regulation between SCF and CSN. *Cell Reports* **2,** 616–627.

Finet C, Berne-Dedieu A, Scutt CP, Marletaz F. 2013. Evolution of the ARF gene family in land plants: old domains, new tricks. *Molecular Biology and Evolution* **30,** 45–56.

Gonzalez D, Bowen AJ, Carroll TS, Conlan RS. 2007. The transcription corepressor LEUNIG interacts with the histone deacetylase HDA19 and Mediator components MED14 (SWP) and CDK8 (HEN3) to repress transcription. *Molecular and Cellular Biology* **27,** 5306–5315.

Gray WM, Kepinski S, Rouse D, Leyser O, Estelle M. 2001. Auxin regulates SCF(TIR1)-dependent degradation of AUX/IAA proteins. *Nature* **414,** 271–276.

Greenham K, Santner A, Castillejo C, Mooney S, Sairanen I, Ljung K, Estelle M. 2011. The AFB4 auxin receptor is a negative regulator of auxin signaling in seedlings. *Current Biology* **21,** 520–525.

Guilfoyle TJ, Hagen G. 2012. Getting a grasp on domain III/IV responsible for Auxin Response Factor–IAA protein interactions. *Plant Science* **190,** 82–88.

Guilfoyle T, Hagen G, Ulmasov T, Murfett J. 1998. How does auxin turn on genes? *Plant Physiology* **118,** 341–347.

Gusmaroli G, Figueroa P, Serino G, Deng XW. 2007. Role of the MPN subunits in COP9 signalosome assembly and activity, and their regulatory interaction with Arabidopsis Cullin3-based E3 ligases. *The Plant Cell* **19,** 564–581.

Havens KA, Guseman JM, Jang SS, Pierre-Jerome E, Bolten N, Klavins E, Nemhauser JL. 2012. A synthetic approach reveals extensive tunability of auxin signaling. *Plant Physiology* **160,** 135–142.

Hu Z, Keceli MA, Piisila M, Li J, Survila M, Heino P, Brader G, Palva ET. 2012. F-box protein AFB4 plays a crucial role in plant growth, development and innate immunity. *Cell Research* **22,** 777–781.

Hua Z, Vierstra RD. 2011. The cullin-RING ubiquitin–protein ligases. *Annual Review of Plant Biology* **62,** 299–334.

Kanarek N, Ben-neriah Y. 2012. Regulation of NF-κB by ubiquitination and degradation of the IκBs. *Immunological Reviews* **246,** 77–94.

Kearns JD, Basak S, Werner SL, Huang CS, Hoffmann A. 2006. IκBε provides negative feedback to control NF-κB oscillations, signaling dynamics, and inflammatory gene expression. *Journal of Cell Biology* **173,** 659–664.

Kepinski S, Leyser O. 2005. The Arabidopsis F-box protein TIR1 is an auxin receptor. *Nature* **435,** 446–451.

Kim J, Harter K, Theologis A. 1997. Protein–protein interactions among the Aux/IAA proteins. *Proceedings of the National Academy of Sciences, USA* **94,** 11786–11791.

Krogan NT, Ckurshumova W, Marcos D, Caragea AE, Berleth T. 2012. Deletion of MP/ARF5 domains III and IV reveals a requirement for Aux/IAA regulation in Arabidopsis leaf vascular patterning. *New Phytologist* **194,** 391–401.

Li H, Tiwari SB, Hagen G, Guilfoyle TJ. 2011. Identical amino acid substitutions in the repression domain of auxin/indole-3-acetic acid proteins have contrasting effects on auxin signaling. *Plant Physiology* **155,** 1252–1263.

Liu Z, Karmarkar V. 2008. Groucho/Tup1 family co-repressors in plant development. *Trends in Plant Science* **13,** 137–144.

Lokerse AS, Weijers D. 2009. Auxin enters the matrix—assembly of response machineries for specific outputs. *Current Opinion in Plant Biology* **12,** 520–526.

Long JA. 2006. TOPLESS regulates apical embryonic fate in Arabidopsis. *Science* **312,** 1520–1523.

Mockaitis K, Estelle M. 2008. Auxin receptors and plant development: a new signaling paradigm. *Annual Review of Cell and Developmental Biology* **24,** 55–80.

Muto H, Watahiki MK, Nakamoto D, Kinjo M, Yamamoto KT. 2007. Specificity and similarity of functions of the Aux/IAA genes in auxin signaling of arabidopsis revealed by promoter-exchange experiments among MSG2 IAA19, AXR2/IAA7, and SLR/IAA141. *Plant Physiology* **144,** 187–196.

Parry G, Calderon-Villalobos LI, Prigge M, Peret B, Dharmasiri S, Itoh H, Lechner E, Gray WM, Bennett M, Estelle M. 2009. Complex regulation of the TIR1/AFB family of auxin receptors. *Proceedings of the National Academy of Sciences, USA* **106,** 22540–22545.

Rademacher EH, Lokerse AS, Schlereth A, *et al.*. 2012. Different auxin response machineries control distinct cell fates in the early plant embryo. *Developmental Cell* **22,** 211–222.

Rademacher EH, Moller B, Lokerse AS, Llavata-Peris CI, van den Berg W, Weijers D. 2011. A cellular expression map of the Arabidopsis AUXIN RESPONSE FACTOR gene family. *The Plant Journal* **68,** 597–606.

Ramos JA, Zenser N, Leyser O, Callis J. 2001. Rapid degradation of auxin/indoleacetic acid proteins requires conserved amino acids of domain II and is proteasome dependent. *The Plant Cell* **13,** 2349–2360.

Stewart JL, Nemhauser JL. 2010. Do trees grow on money? Auxin as the currency of the cellular economy. *Cold Spring Harbor Perspectives in Biology* **2,** a001420.

Stuttmann J, Lechner E, Guérois R, Parker JE, Nussaume L, Genschik P, Noël LD. 2009. COP9 signalosome- and 26S proteasome-dependent regulation of SCFTIR1 accumulation in Arabidopsis. *Journal of Biological Chemistry* **284,** 7920–7930.

Sung MH, Salvatore L, De Lorenzi R, Indrawan A, Pasparakis M, Hager GL, Bianchi ME, Agresti A. 2009. Sustained oscillations of NF-κB produce distinct genome scanning and gene expression profiles. *PLoS One* **4,** e7163.

Szemenyei H, Hannon M, Long JA. 2008. TOPLESS mediates auxin-dependent transcriptional repression during Arabidopsis embryogenesis. *Science* **319,** 1384–1386.

Tan X, Calderon-Villalobos LIA, Sharon M, Zheng C, Robinson CV, Estelle M, Zheng N. 2007. Mechanism of auxin perception by the TIR1 ubiquitin ligase. *Nature* **446,** 640–645.

Terrile MC, París R, Calderón-Villalobos LIA, Iglesias MJ, Lamattina L, Estelle M, Casalongué CA. 2012. Nitric oxide influences auxin signaling through S-nitrosylation of the Arabidopsis TRANSPORT INHIBITOR RESPONSE 1 auxin receptor. *The Plant Journal* **70,** 492–500.

Tian B, Nowak DE, Brasier AR. 2005. A TNF-induced gene expression program under oscillatory NF-κB control. *BMC Genomics* **6,** 137.

Tiwari SB, Hagen G, Guilfoyle T. 2003. The roles of auxin response factor domains in auxin-responsive transcription. *The Plant Cell* **15,** 533–543.

Ulmasov T, Hagen G, Guilfoyle TJ. 1999*a*. Activation and repression of transcription by auxin-response factors. *Proceedings of the National Academy of Sciences, USA* **96,** 5844–5849.

Ulmasov T, Hagen G, Guilfoyle TJ. 1999*b*. Dimerization and DNA binding of auxin response factors. *The Plant Journal* **19,** 309–319.

Vernoux T, Brunoud G, Farcot E, *et al.*. 2011. The auxin signalling network translates dynamic input into robust patterning at the shoot apex. *Molecular Systems Biology* **7,** 508.

Vert G, Walcher CL, Chory J, Nemhauser JL. 2008. Integration of auxin and brassinosteroid pathways by Auxin Response Factor 2. *Proceedings of the National Academy of Sciences, USA* **105,** 9829–9834.

Walsh TA, Neal R, Merlo AO, Honma M, Hicks GR, Wolff K, Matsumura W, Davies JP. 2006. Mutations in an auxin receptor homolog AFB5 and in SGT1b confer resistance to synthetic picolinate auxins and not to 2,4-dichlorophenoxyacetic acid or indole-3-acetic acid in Arabidopsis. *Plant Physiology* **142,** 542–552.

Wang S, Tiwari SB, Hagen G, Guilfoyle TJ. 2005. AUXIN RESPONSE FACTOR7 restores the expression of auxin-responsive genes in mutant Arabidopsis leaf mesophyll protoplasts. *The Plant Cell* **17,** 1979–1993.

Weijers D, Benkova E, Jager KE, Schlereth A, Hamann T, Kientz M, Wilmoth JC, Reed JW, Jurgens G. 2005. Developmental specificity of auxin response by pairs of ARF and Aux/IAA transcriptional regulators. *EMBO Journal* **24,** 1874–1885.

Williamson A, Banerjee S, Zhu X, Philipp I, Iavarone AT, Rape M. 2011. Regulation of ubiquitin chain initiation to control the timing of substrate degradation. *Molecular Cell* **42,** 744–757.

Wong KH, Struhl K. 2011. The Cyc8–Tup1 complex inhibits transcription primarily by masking the activation domain of the recruiting protein. *Genes and Development* **25,** 2525–2539.

A Synthetic Approach Reveals Extensive Tunability of Auxin Signaling[1][C][W][OA]

Kyle A. Havens[2], Jessica M. Guseman[2], Seunghee S. Jang[2], Edith Pierre-Jerome[2], Nick Bolten, Eric Klavins, and Jennifer L. Nemhauser*

Department of Electrical Engineering (K.A.H., S.S.J., N.B., E.K.), and Department of Biology (J.M.G., E.P.J., J.L.N.), University of Washington, Seattle, Washington 98195

Explaining how the small molecule auxin triggers diverse yet specific responses is a long-standing challenge in plant biology. An essential step in auxin response is the degradation of Auxin/Indole-3-Acetic Acid (Aux/IAA, referred to hereafter as IAA) repressor proteins through interaction with auxin receptors. To systematically characterize diversity in degradation behaviors among IAA | receptor pairs, we engineered auxin-induced degradation of plant IAA proteins in yeast (*Saccharomyces cerevisiae*). We found that IAA degradation dynamics vary widely, depending on which receptor is present, and are not encoded solely by the degron-containing domain II. To facilitate this and future studies, we identified a mathematical model able to quantitatively describe IAA degradation behavior in a single parameter. Together, our results demonstrate the remarkable tunability conferred by specific configurations of the auxin response pathway.

Auxin directs almost every aspect of plant biology, yet how specificity is generated from auxin signaling components remains largely unresolved. A range of auxin-associated phenotypes, including profound disruptions in development and severely compromised responses to environmental signals, are caused by single amino acid substitutions that stabilize transcriptional corepressor proteins called the Auxin/Indole-3-Acetic Acids (Aux/IAAs, referred to hereafter as IAAs; Chapman and Estelle, 2009). The diversity of these phenotypes and the size of the IAA family suggest that IAAs may provide specificity in auxin responses (Lokerse and Weijers, 2009). Functional studies support this idea, as stabilized IAAs provoke different phenotypes even when expressed from the same promoter (Weijers et al., 2005; Muto et al., 2007).

Auxin activates gene expression by enhancing IAA turnover through interaction with auxin receptors, a family of F-box proteins called TRANSPORT INHIBITOR RESISTANT1 (TIR1)/AUXIN SIGNALING F-BOX PROTEINS (AFBs; Dharmasiri et al., 2005a; Kepinski and Leyser, 2005), referred to here collectively as AFBs. Variation in the affinities of IAA | AFB pairs has recently been observed (Calderón Villalobos et al., 2012). How such differences relate to degradation kinetics is still unclear. Labor-intensive seedling studies on a small number of IAA proteins, in combination with analysis of stabilized IAA mutants, uncovered the importance of a conserved region, termed domain II, in determining protein stability. The degron-containing IAA domain II is both necessary and sufficient for interaction with TIR1 and the resulting auxin-induced degradation (Ramos et al., 2001; Dharmasiri et al., 2005a; Kepinski and Leyser, 2005; Tan et al., 2007). In addition, IAA-reporter fusions with diverse domain II sequences show a range of degradation rates when overexpressed in Arabidopsis (*Arabidopsis thaliana*) seedlings (Dreher et al., 2006). However, the ubiquity of the auxin pathway in plants and the difficulty in reconstituting the complete degradation machinery in vitro have hindered further characterization of the molecular determinants of IAA degradation rates.

As a complement to existing systems and to systematically characterize the potential tunability of different IAA | AFB pairs, we engineered the auxin-induced degradation of IAA proteins in the yeast *Saccharomyces cerevisiae*. Our synthetic system has several advantages: precise control of auxin input levels, the ability to study IAA | AFB pairs in isolation, and the absence of the many other plant pathways known to impact auxin signaling (Stewart and Nemhauser, 2010). Our system allowed a comprehensive survey of

[1] This work was supported by the Paul G. Allen Family Foundation and the National Science Foundation (grant nos. CISE–0832773 to E.K. and IOS–0919021 to J.L.N.). J.M.G. was supported by the National Institutes of Health (training grant no. T32HD007183). E.P.J. was supported by a National Science Foundation Graduate Research Fellowship and the Seattle Chapter of the Achievement Rewards for College Scientists Foundation.

[2] These authors contributed equally to the article.

* Corresponding author; e-mail jn7@uw.edu.

The author responsible for distribution of materials integral to the findings presented in this article in accordance with the policy described in the Instructions for Authors (www.plantphysiol.org) is: Jennifer L. Nemhauser (jn7@uw.edu).

[C] Some figures in this article are displayed in color online but in black and white in the print edition.

[W] The online version of this article contains Web-only data.

[OA] Open Access articles can be viewed online without a subscription.

www.plantphysiol.org/cgi/doi/10.1104/pp.112.202184

IAA protein turnover while recapitulating behaviors observed in plants. We discovered that the particular AFB receptor used greatly impacted the rate of degradation and that sequences outside of the degron-containing domain II accelerated or decelerated IAA degradation in an IAA-specific manner. Moreover, we identified a mathematical model that provides a single parameter to quantitatively describe degradation behavior. The synthetic toolkit described here will facilitate rapid testing of hypotheses about the ubiquitylation of IAA proteins and suggests a means to characterize other hormone-induced protein degradation pathways.

RESULTS

A Synthetic Yeast System Recapitulates Auxin-Induced IAA Degradation Dynamics

Our engineered auxin response system consisted of pairwise matings of yeast expressing either yellow fluorescent protein (YFP)-IAA fusion proteins or AFBs (Fig. 1A). In the presence of a functional AFB, YFP fluorescence (a proxy for IAA protein levels) could be both up- and down-regulated by modulating the levels of indole-3-acetic acid, hereafter referred to as auxin (Fig. 1B; Supplemental Fig. S1). The timing and extent of degradation were comparable to experimental systems relying on a much higher concentration of a synthetic auxin (Nishimura et al., 2009). Flow cytometry provided high-resolution IAA degradation profiles for each IAA|AFB pair with improved time-resolution measurements at the single cell level (Fig. 1C). In contrast to the "basal degradation" rates observed in plants (Dreher et al., 2006), YFP-IAA proteins were essentially stable in yeast in the absence of auxin or a functional AFB (Supplemental Figs. S2 and S3). This may reflect the difficulty of completely clearing auxin from plant cells or the presence of additional components in plants that are absent from our synthetic system. Following the major auxin-induced degradation

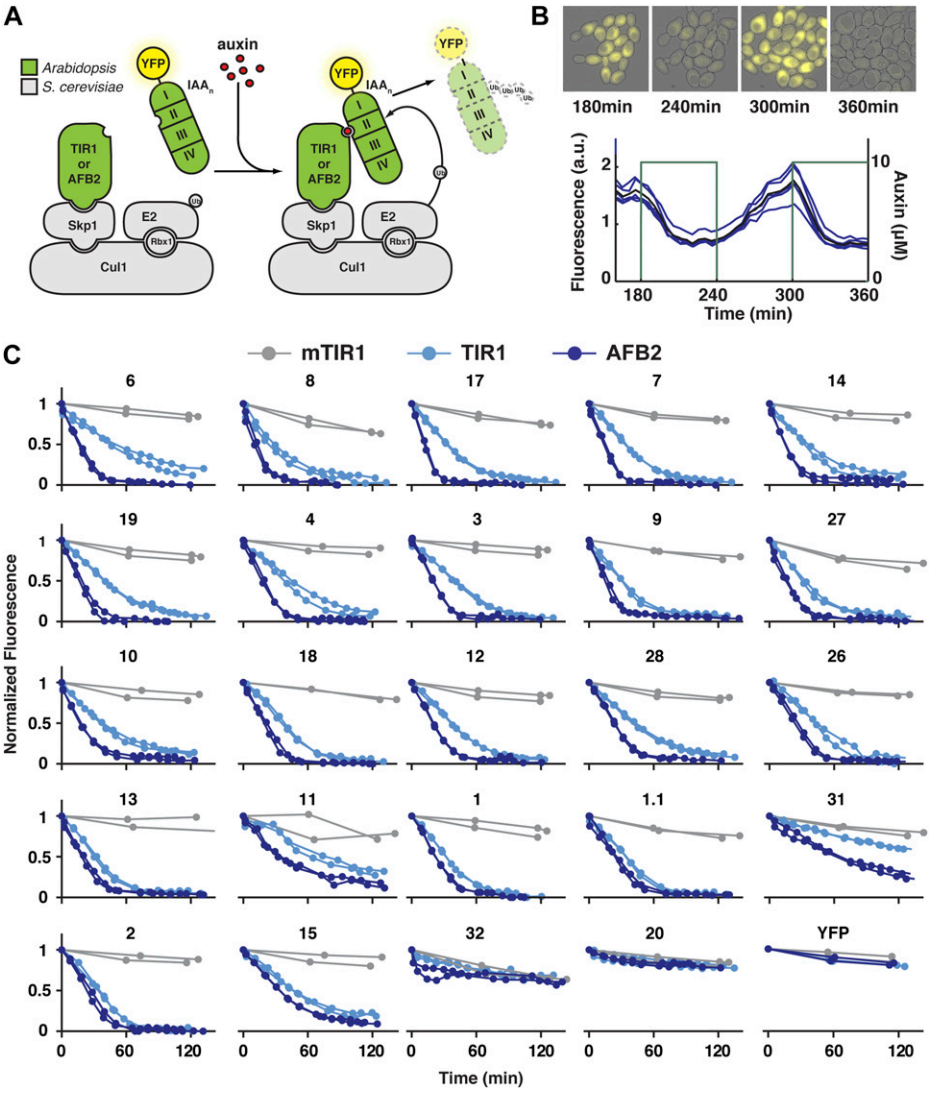

Figure 1. IAA degradation is highly variable. A, Plant auxin receptors (TIR1 or AFB2) and YFP-tagged IAA repressors were integrated into the yeast ubiquitin pathway, shown in gray. B, Yeast cells were imaged while exposed to a square wave of auxin. Auxin leads to a rapid decrease in YFP (fluorescence of individual microcolonies in blue, average value in black), which can be recovered with auxin removal. C, A range of IAA|receptor degradation rates were obtained using time-lapse flow cytometry. Degradation curves were normalized to starting fluorescence. IAAs are listed in order of the relative difference in degradation in the presence of TIR1 versus AFB2. Strains expressing the F-box-deficient mTIR1 show no auxin-dependent degradation. [See online article for color version of this figure.]

events, a more gradual decline in YFP can be observed. As this behavior was also observed in strains expressing mTIR1, we believe that this decrease in fluorescence is caused by physiological changes associated with increasing culture density and not auxin-induced degradation of YFP-IAAs.

The fine time resolution of our measurements resulted in complex degradation profiles that included an initial delay in degradation prior to an exponential decay of YFP levels (Fig. 1, B and C; Supplemental Fig. S9). Standard half-life calculations, therefore, were insufficient to describe the dynamics of degradation in our system. In order to quantitatively characterize the degradation behavior of every IAA | AFB pair, we identified a second-order nonlinear model that captures the dynamic auxin response in both time-course and dose-response experimental data (Fig. 2A; Supplemental File S1; Supplemental Figs. S9–S11; Supplemental Tables S3 and S7). This model accounts for the complex degradation behavior we observed and the nonlinear relationship between auxin concentration and steady-state YFP intensity (Supplemental Fig. S1). Among the candidate models tested, this model had the least complexity while still fitting the data with low residual error (Supplemental File S1). Auxin response is represented by YFP-IAA fluorescence intensity output y and a hypothesized internal state x, dependent on the auxin input concentration u. The hypothesized internal state x is not directly measured in our experiments and does not necessarily equate with specific active species, although one interpretation is that x is a complex formed between auxin and an AFB. Similarly, parameters k_1, k_2, k_3, k_4, and k_5 are not intended to have direct association with physical values in the system. One possibility is that these rates correlate with synthesis (k_1 for the internal state and k_3 for the IAA), degradation of the internal state (k_2), basal degradation/dilution of the IAA (k_4), and AFB-induced degradation (k_5). With this interpretation and applying the principles of global curve fitting, we reduced the total number of parameters needed to fit the entire data set (Supplemental File S1).

Modeling distilled the differences observed in degradation between the IAA | AFB pairs into a single parameter, k_5. Importantly, the k_5 value for each IAA | AFB pair is consistent with the qualitative behaviors present in the experimental data (Figs. 1C and 2C). For example, the faster degrading IAAs had the largest k_5 values, while more stable IAAs had the lowest k_5 values. Of all the parameters, k_5 best captures IAA | AFB degradation behavior and is hereafter called the degradation rate.

IAA Proteins Exhibit a Range of Degradation Rates

In our system, auxin-induced degradation differs across IAA | AFB pairs (Figs. 1C and 2C). This is consistent with previous work in Arabidopsis seedlings, where half-lives of overexpressed IAA-LUC fusions were calculated by blocking new protein production with cycloheximide and treating exogenously with the synthetic auxin 2,4-dichlorophenoxyacetic acid (Dreher et al., 2006; Supplemental Table S1). In these assays, a strong match to the consensus domain II sequence was correlated with a short protein half-life in the presence of 2,4-dichlorophenoxyacetic acid. For example, IAA17 and IAA28 have strong matches to the consensus domain II and half-lives of 5 and 15 min, respectively. In contrast, IAA31, with a diverged domain II, has a half-life of approximately 4 h. IAA20 lacks a recognizable domain II sequence and is highly stable. We observed similar patterns of degradation in yeast (Figs. 1C and 2C). In yeast expressing either TIR1 or AFB2, IAAs with consensus-matching domain II sequences degraded rapidly, IAA31 was slow to degrade, and IAA20

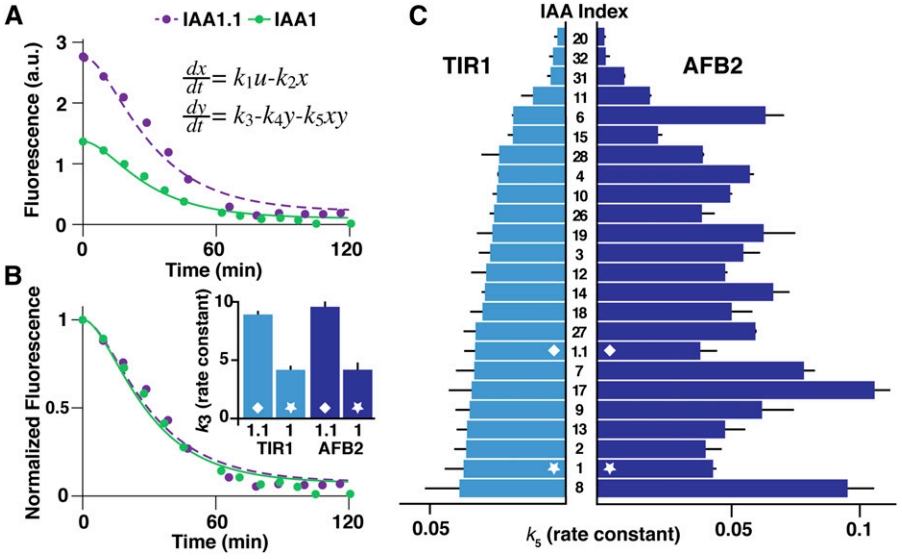

Figure 2. Degradation dynamics can be described using few parameters. A, Our model is described by two ordinary differential equations. Degradation curves for AFB2 strains expressing IAA1 or yeast codon-optimized IAA1.1 are shown. B, k_5 is largely independent of expression levels. IAA1 and IAA1.1 degradation curves overlap after normalization, although there is an approximately 2-fold difference in k_3 values. C, IAA|AFB2 pairs have increased degradation rates (k_5), a different rank order when compared with IAA/TIR1 pairs, and an increased dynamic range between the slowest and fastest pairs. Parameters were estimated for two independent replicates. All error bars represent 1 SD. Additional parameters are listed in Supplemental Tables S4 and S5. a.u., Arbitrary units. [See online article for color version of this figure.]

showed no degradation. Of the IAAs with consensus domain II sequences, most IAA | TIR1 pairs had rates similar to the fast-degrading IAA17 | TIR1 (Fig. 2C). We observed a few IAAs outside of this general trend, including the slow-degrading IAA11.

Despite being expressed from the same promoter and singly integrated in the same genomic location, IAAs displayed different basal fluorescence levels in yeast (Supplemental Fig. S3). Our model predicts that rates of IAA expression and degradation are independent of each other (Supplemental File S1). To test this prediction, we synthesized a variant allele of IAA1 (IAA1.1) with yeast-optimized codons. Basal expression of IAA1.1 was twice that of IAA1 (Fig. 2A), with a similar fold change in the estimated k_3 values (Fig. 2B). In contrast, normalized degradation curves and k_5 values overlapped (Fig. 2, B and C). This result validates our model and demonstrates that IAA degradation rates are indeed robust to fluctuations in IAA expression levels. Challenges in plant assays, including random location of insertions and multiple cell types contributing to variation in transgene expression, make this type of quantitative analysis quite difficult and highlight the benefits of using yeast as an additional resource for dynamic analysis of auxin responses.

IAA Degradation Rates Are Receptor Specific

For the majority of IAAs tested, AFB2 promoted faster degradation than TIR1 (Figs. 1C and 2C). This resulted in IAA | AFB2 pairs having degradation rates up to three times higher than IAA | TIR1 pairs. IAA | AFB2 pairs also had a wider range of degradation rates between all IAAs. Excluding the IAAs with divergent domain IIs, the fastest IAA | TIR1 pair (IAA8) had a degradation rate 3.3-fold higher than the slowest, IAA11. In contrast, the fastest IAA | AFB2 pair (IAA17) had a degradation rate 5.5-fold higher than IAA11. Strikingly, the rank order of degradation rates was not maintained between strains expressing different receptors. IAA6 showed one of the slowest rates of degradation with TIR1, yet it had one of the fastest degradation rates for IAA | AFB2 pairs. A subset of IAAs showed little difference in degradation between auxin receptors, leading to some of the widest discrepancies in relative rank order. For example, there was little or no change in IAA1 degradation when the receptor was switched from TIR1 to AFB2. This resulted in IAA1 being one of the fastest degrading IAAs in combination with TIR1 yet among the slowest when expressed with AFB2. While it is possible that AFB2 functions more efficiently than TIR1 in yeast, the identification of a subset of IAAs that show no change in degradation between the two receptors suggests that these two proteins are intrinsically different in their IAA interactions.

While TIR1 and AFB2 conferred rapid auxin-induced degradation of IAAs, AFB1 and AFB3 had little effect on IAA degradation rates (Supplemental Fig. S4). Genetic analysis suggests that TIR1 and AFB2 are the major auxin receptors in Arabidopsis, but it is still unclear the degree to which each TIR1/AFB protein contributes to specific auxin responses (Dharmasiri et al., 2005b; Parry et al., 2009). Mutations in *TIR1* or *AFB2* lead to stronger overall auxin-related phenotypes than mutations in *AFB1* or *AFB3*, although the loss of *AFB1* or *AFB3* can enhance mutations in other AFB family members (Dharmasiri et al., 2005b; Parry et al., 2009). We reasoned that AFBs might differ in their ability to interact with IAAs. This hypothesis is consistent with our findings as well as with in vitro pull-down assays showing that AFB1 and AFB3 have lower levels of interaction with IAAs than TIR1 and AFB2 (Parry et al., 2009). In addition, IAA-reporter fusions are strongly stabilized in *afb2* mutants, while loss of *AFB1* or *AFB3* alone has little effect on turnover rates (Dharmasiri et al., 2005b). An additional factor may be that our heterologous degradation assay is less sensitive than other assays to weak or transient IAA-AFB interactions. Indeed, in vitro pull-down assays and yeast two-hybrid screens have shown low levels of interaction between some IAA | AFB pairs even in the absence of auxin (Dharmasiri et al., 2005a, 2005b; Kepinski and Leyser, 2005; Parry et al., 2009; Calderón Villalobos et al., 2012), while we did not see any change in IAA stability without auxin addition (Supplemental Figs. S2 and S3). Moreover, auxin can increase interactions between AFB1-DNA-binding domain fusion proteins and IAA-activation domain fusion proteins when both constructs are highly expressed in yeast (Calderón Villalobos et al., 2012), suggesting that these weaker interactions may contribute to auxin responses in plants. Additional work in plants will be needed to discriminate among these different possibilities.

Receptor expression levels did not influence IAA degradation in our yeast assays. Degradation rates were not correlated with receptor abundance (Supplemental Fig. S5), nor could they be increased by adding a second copy of the same receptor to the genome (Supplemental Fig. S6). In addition, when TIR1 and AFB2 were coexpressed, the degradation rate of IAA6 closely matched that of AFB2 alone (Supplemental Fig. S6). Genetic studies indicate that TIR1 is the primary auxin receptor, and AFB2 is not able to substitute for TIR1 even when expressed from the TIR1 promoter (Parry et al., 2009). This suggests that degradation rate differences are not the sole distinguishing characteristic of receptors and that further functional studies of the dynamics of IAA degradation in receptor mutant backgrounds could be fruitful.

Residues Outside of Domain II Differentially Affect Degradation Rates

Residues outside of domain II have been found to contribute to IAA | AFB auxin-binding affinity in vitro (Calderón Villalobos et al., 2012) and high basal IAA

degradation rates in seedlings (Dreher et al., 2006). We engineered truncations in IAAs with disparate degradation rates (Fig. 3A; Supplemental Fig. S7) to directly test the role of nondomain II residues in auxin-induced degradation. The N-terminal half of the protein (T1) or a smaller region restricted to domain II (T2) was fused to an SV40 nuclear localization signal (NLS; Supplemental Table S2). Degradation rates of truncated proteins were compared with full-length constructs fused to the same NLS (Fig. 3, B and C). We found that sequences outside of domain II could accelerate or decelerate degradation rates in an IAA-specific manner. Relative rank order of full-length IAA degradation rates was not conserved in the truncations. IAA28.T2 was the fastest degrading of the T2 truncations, yet IAA28 showed much slower degradation rates than IAA1 or IAA6. Moreover, parallel truncations in different IAAs did not have the same effect on degradation rates. IAA6.T1 was slower than full-length IAA6, but IAA28.T1 was faster than full-length IAA28.

The recently reported DII-VENUS auxin sensor is similar to IAA28.T2 but shifted 15 amino acids toward the IAA28 N terminus (Vernoux et al., 2011; Brunoud et al., 2012). To test whether this small difference in sequence had any effect on degradation rates, we engineered the identical IAA28 truncation into our system (IAA28.T2V; Fig. 3A; Supplemental Table S2). IAA28.T2V degraded far slower than all other constructs tested (Fig. 3B). This effect is opposite to what we observed with IAA28.T1 and IAA28.T2, both of which had increased rates of degradation compared with the full-length protein. The markedly slower degradation rate we observed for IAA28.T2V could explain why it was the brightest reporter tested (Brunoud et al., 2012). In fact, our analysis predicted that IAA8 and IAA9, the other IAA truncations tested in that study, would degrade faster than IAA28 (Fig. 2; Supplemental Table S1). This is consistent with the much dimmer fluorescence observed for the DII reporters made with these IAA proteins (Brunoud et al., 2012). To directly test whether our yeast assays could predict relative degradation rates in plants, we generated transgenic seedlings expressing a modified DII-VENUS reporter where we replaced the IAA28.T2V sequence with the IAA28.T2 sequence. Consistent with the higher rate of turnover of the IAA28.T2 fusion protein in yeast, we observed significantly lower levels of fluorescence of the IAA28.T2 reporter in transgenic plants (Supplemental Fig. S8).

DISCUSSION

The size and diversity of the IAA and AFB protein families suggest that auxin specificity can be conferred by specific configurations of IAA and AFB family members (Lokerse and Weijers, 2009). In this study, we present a new method for investigating the range of diversity encoded by these large families. By porting plant proteins into yeast, we could directly test the variability in degradation rates between specific IAA | AFB pairs. We were able to reproduce auxin-induced degradation and generate high-resolution real-time data. Our yeast platform was able to recapitulate behaviors previously observed in studies of IAA turnover and allowed for an extensive survey of IAA degradation behavior.

Assessing degradation with each receptor individually, we showed that IAA degradation is highly influenced by which receptor is present and that these receptor effects are IAA specific (Figs. 1C and 2C). Our data provide evidence of receptor choice on regulating the turnover of IAAs and show that each

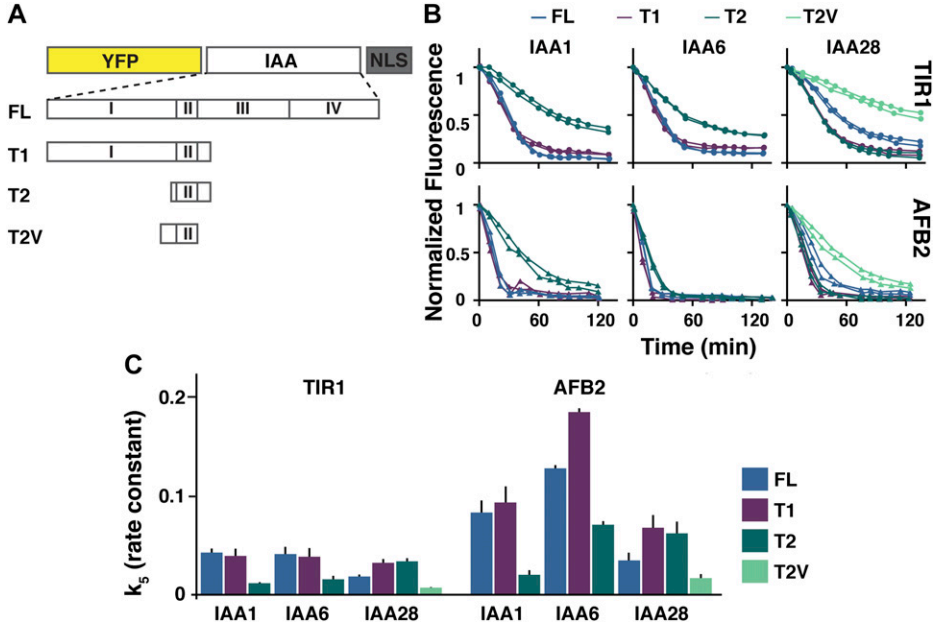

Figure 3. Residues outside of domain II contribute to auxin-induced degradation rates. A, Schematic of IAA truncations. B and C, Degradation dynamics of full-length proteins are not maintained in truncations. B, Degradation rates of truncations expressed with TIR1 or AFB2, normalized to the starting fluorescence for each strain. C, Parameters k_3 and k_5 were determined using parameters k_1, k_2, and k_4 from previous model fitting. Additional parameters are listed in Supplemental Table S6.

member of the IAA | AFB pair plays a role in determining auxin sensitivity. The high sequence similarity between TIR1 and AFB2, in combination with their shared substrates, should provide a platform to dissect how F-box proteins influence the rate of ubiquitylation, a factor known to vary among other F-box proteins (Pierce et al., 2009). The lack of detectable IAA degradation in yeast expressing AFB1 or AFB3, despite their ability to bind auxin, may have important implications for calibrating auxin responses. This implies that different combinations of receptors may produce varied response thresholds, which may each trigger a specific auxin-regulated process (Reinhardt et al., 2003; Del Bianco and Kepinski, 2011).

Surprisingly, IAA degradation rates were not strongly correlated with the few recently reported in vitro dissociation constants (Calderón Villalobos et al., 2012; Supplemental Table S1). This lack of correlation could simply be the result of the artificial nature of both systems: dissociation constants are a measure of complex formation and are determined independent of a complete ubiquitin complex, and our heterologous system has a mixture of yeast and plant components (Fig. 1A). However, a testable alternative hypothesis is that the interaction strength between TIR1 and an IAA is not a direct reflection of how quickly the IAA is degraded. Conserved sequences outside of the interaction domain have recently been shown to impact the rate of degradation of a number of substrates of the anaphase-promoting complex (Williamson et al., 2011). While similar sequences have not been identified in IAA proteins, the fact that truncations have such varied degradation rates clearly shows that additional residues play a crucial role in modulating interaction with the ubiquitin machinery (Fig. 3; Dreher et al., 2006). Identification of IAA degradation rate determinants could be accelerated by combining information from studies in yeast, in vitro, and in plants.

By utilizing a small, data-driven model, we were able to quantitatively characterize the complex degradation behavior of each IAA | AFB pair in response to auxin (Fig. 2). Mathematical modeling allowed us to distinguish IAA and AFB contributions to degradation and thereby demonstrate how auxin perception can be tuned. We chose a small, empirical model because large mechanistic models (Bridge et al., 2012) require more parameters than could be identified from the low-dimensional output available in our experiments. Small models can nevertheless be quite useful. For example, a new negative feedback loop was discovered in yeast osmoadaptation using a small-model approach (Mettetal et al., 2008). Similarly, our simple model showed that unknown molecular interactions beyond complex affinity are required to describe IAA degradation dynamics. Moreover, small models such as ours can provide a simple description of the input-output properties of a module and facilitate the rational design of new systems in synthetic biology.

In this study, we have demonstrated the utility of porting a pathway to an orthogonal organism to characterize its function. As a single-celled eukaryote with conserved cellular machinery, yeast provides a seminatural context that facilitates the study of complex signaling pathways. The rapid generation time, control of insertion site and number, and high-throughput methods for quantitative analysis, combined with the absence of other known confounding factors like auxin transport, auxin metabolism, and the coexpression of AFB and IAA family members, make studies in yeast a strong complement to plant studies. Given the obvious artificiality of our system, it is quite promising that the rank order of auxin-induced degradation rates parallels the limited number of half-lives observed in plants (Supplemental Table S1). The fact that the IAA28.T2 construct behaved as predicted when expressed in seedlings (Fig. 3; Supplemental Fig. S8) also points to overall conservation in degradation determinants between plant cells and engineered yeast. A full analysis of the similarities and differences between the systems will require more plant studies and likely better tools for measuring dynamic behaviors in plants. Our heterologous system provides a new method to investigate auxin signaling as well as suggests a means to study the many other plant pathways that rely on ubiquitin-mediated protein degradation.

MATERIALS AND METHODS

Yeast Methods

Yeast transformations were performed using a standard lithium acetate protocol (Gietz and Woods, 2002) into *MAT*a W303-1A or *MAT*α W814-29B, a gift from the Gottschling laboratory. Yeast Peptone Dextrose (YPD) and Synthetic Complete (SC) medium supplemented with 80 mg mL^{-1} adenine were made according to standard protocols. All strains used in this study are listed in Supplemental Table S9.

Strain Construction

IAAs, TIR1, and AFB were amplified from Arabidopsis (*Arabidopsis thaliana*) complementary DNA (Columbia ecotype) using the primers listed in Supplemental Table S8. A partial attB1 site and Kozak sequence (AAA) were added to the 5′ end of each forward primer (5′-AAAAAGCAGGCTTCAAA-3′), and a partial attB2 site was added to the 5′ end of each reverse primer (5′-AGAAAGCTGGGTG-3′). The remaining attB1 and attB2 sequences were added with a second PCR using generic forward and reverse adapter primers (5′-GGGGACAAGTTTGTACAAAAAAGCAGGCT-3′ and 5′-GGGGACCACTTTGTACAAGAAAGCTGGGT-3′). Products were subcloned into a Gateway pDONR221 plasmid using a standard Gateway BP reaction (BP Clonase II; Life Technologies). Each complementary DNA was fully sequenced and then cloned into destination vectors with a standard Gateway LR reaction (LR Clonase II; Life Technologies). IAAs were cloned into pGP4GY-ccdB (Trp selection), and auxin receptors were cloned into pGP5G-ccdB (Leu selection; K.A. Havens, N. Bolten, J.L. Nemhauser, and E. Klavins, unpublished data). Approximately 300 ng of each plasmid was digested with *Pme*I and transformed: pGP4GY-IAA into W303-1A, pGP5G-AFB into W814-29B. Integrations were confirmed by PCR. Strains to be mated were coinoculated at low density into YPD medium, grown overnight at 30°C, and struck out to single colonies on SC-His-Trp to select for diploids.

IAA truncations were fused to an N-terminal YFP and C-terminal SV40 NLS repeat using Gly-Ala linkers (GAGAGAGAGAGP and GAGA, respectively; Nishimura et al., 2009). The IAA17.T1 construct was synthesized with partial EYFP and the complete NLS sequence (www.genewiz.com) and then cloned into the pGP4GY-ccdB vector backbone via Gibson assembly (Gibson et al., 2009). The cloning scheme is outlined in Supplemental Figure S7.

Primers are listed in Supplemental Table S8. Gateway acceptor sites were removed by this process. Further truncation constructs were amplified from full-length IAA sequences and cloned in place of IAA17 using Gibson assembly (Gibson et al., 2009).

The DII-VENUS plasmid was a gift from Teva Vernoux. The IAA28.T2-VENUS plasmid was constructed by replacing the DII region of DII-VENUS with the IAA28.T2 degron region using Gibson assembly (Gibson et al., 2009).

Flow Cytometry

YFP intensity measurements were taken with a BD Accuri C6 flow cytometer with a CSampler plate adapter using excitation wavelengths of 488 and 640 nm and an emission detection filter at 533 nm (FL1 channel). A total of 10,000 events above a 400,000 FSC-H threshold (to exclude debris) were measured for each sample at a flow rate of 66 μL min^{-1} and core size of 22 μm using the Accuri C6 CFlow Sampler software. Cytometry data were exported as FCS 3.0 files and processed using the flowCore R software package and custom R scripts to obtain the mean FL1-A value at each time point. The script applies two polygon gates on the data to isolate single yeast cells. One gate separates the total yeast population from debris on the SSC-A and FSC-A channels. The second gate isolates single cells from cell aggregates (doublet discrimination) via their higher FSC-H (peak height) to FSC-A (peak area) ratio. Scripts are available upon request.

Degradation Assays

Cells were prepared by transferring a freshly grown colony from YPD plates into SC. The cell density (in events μL^{-1}) was estimated using cytometry data gated for yeast by a custom R script. Each culture was then diluted to 0.5 events μL^{-1} in 15 mL of SC. This dilution was split into duplicate 4-mL aliquots with the exception of controls. For IAA17 without a YFP tag and YFP without an IAA, only a single 4-mL aliquot was prepared. YFP-IAA17 was split into three aliquots to serve as an internal replicate control within each experiment. Aliquots were incubated for 16 h at 30°C with shaking. At 16 h, duplicate aliquots of each strain were mixed and split again into two tubes. Cultures were in log phase at the beginning of each experiment (density measured in the cytometer at approximately 500 events μL^{-1}) and remained in log phase for the duration of each experiment (Supplemental Fig. S2).

Measurements were taken at two time points prior to the addition of any treatment. For each strain, one replicate was mock treated (95% [v/v] ethanol) and one replicate was treated with 10 μM indole-3-acetic acid (the minimal concentration of auxin needed to promote complete IAA degradation during log-phase growth of the yeast; Supplemental Figs. S1 and S2). As soon as possible after the addition of auxin, fluorescence for the 0-min time point was recorded. Subsequent measurements were acquired at 10-min intervals for the first 2 h after auxin addition and every 30 min thereafter until the fluorescence level in most strains had plateaued (approximately 3.5 h). Controls were measured every hour for the duration of the experiment.

Modeling and Quantitative Analysis

Modeling methods and quantitative analysis are described in Supplemental File S1.

Microscopy

Yeast cells grown overnight in SC at 30°C were diluted 1:100 in SC, incubated for 4 to 5 h, and then diluted 1:20 before loading onto a Y04D plate (CellASIC). Using the CellASIC-ONIX microfluidic system and associated software, cells were pulsed with a square wave of 10 μM auxin in SC medium over a period of 2 h. An inverted Nikon Eclipse Ti microscope with a 60×, numerical aperture 1.4 oil objective was used to image the yeast cells at 5-min intervals using a YFP-HYQ 535 bandpass filter (Nikon; excitation at 515 nm, detection from 520 to 550 nm) and a CoolSNAP HQ2 14 bit camera. Image processing was done with custom MATLAB scripts, available upon request. Briefly, a segmentation algorithm was applied to bright-field images to produce a binary mask for each microcolony. This binary mask was then applied to the YFP image to calculate the average YFP intensity value within the colony. Background fluorescence level was estimated using the average fluorescence of a 100- × 100-pixel square away from the yeast colony and subtracted from total fluorescence values.

Generation and Analysis of Transgenic Plants

Columbia ecotype plants were transformed using the floral dip method (Clough and Bent, 1998). T1 plants were selected on 0.5× LS agar plates containing 30 μg mL^{-1} hygromycin B. Plates were stratified for 2 d, exposed to light for 6 h, and then grown in the dark for 3 d following a modification of the method of Harrison et al. (2006). Resistant seedlings were transferred to plates containing no antibiotics and allowed to recover for an additional 3 d. DII-VENUS seeds provided generously by Teva Vernoux were grown in identical conditions to allow a direct comparison of the IAA28.T2 and IAA28.T2V constructs in plants.

Plants were imaged using a Leica DMI 3000B microscope fitted with a Leica long-working 20× HCX PL FLUORTAR objective and illuminated with a Lumencor SOLA light source. Images were captured using Leica LAS AF version 2.6.0 software and a Leica DFC 345FX camera. Seven independent IAA28.T2 transformants were examined and compared with 10 DII-VENUS seedlings. Fiji software was used to quantify fluorescence in a region of interest centered on each image.

Supplemental Data

The following materials are available in the online version of this article.

Supplemental Figure S1. Addition of 10 μM auxin is sufficient for maximal degradation of IAAs.

Supplemental Figure S2. Fluorescence levels decrease drastically as yeast cells enter the stationary phase.

Supplemental Figure S3. AFBs do not have differential effects on basal degradation of IAAs.

Supplemental Figure S4. AFB1 and AFB3 do not promote degradation of IAA2.

Supplemental Figure S5. TIR1 is expressed at a similar level to AFB2.

Supplemental Figure S6. AFB2 expression is not rate limiting.

Supplemental Figure S7. Cloning scheme for domain II truncation constructs.

Supplemental Figure S8. Fluorescence accumulation differs between IAA28 truncations in plants.

Supplemental Figure S9. Sample time-course IAA degradation data and model fits of IAA14|TIR1.

Supplemental Figure S10. Sample dose-response data and model predicted dose response of IAA17|AFB2.

Supplemental Figure S11. Parameter variations study of the preferred model.

Supplemental Table S1. Comparison of degradation rates, half-lives, and affinities from yeast, in vitro, and plant studies.

Supplemental Table S2. Table of amino acids included in each IAA truncation.

Supplemental Table S3. The residuals and the number of distinct parameters for all candidate models.

Supplemental Table S4. Estimated parameters for IAA|TIR1 pairs using the preferred model interpretation.

Supplemental Table S5. Estimated parameters for IAA|AFB2 pairs using the preferred model interpretation.

Supplemental Table S6. Estimated parameters for degron comparison study using the preferred model interpretation.

Supplemental Table S7. Average, minimum, and maximum values of the estimated parameters.

Supplemental Table S8. Oligonucleotides used in this study

Supplemental Table S9. Yeast strains used in this study.

Supplemental File S1. Quantitative Analysis.

ACKNOWLEDGMENTS

We thank Mark Estelle, Ning Zheng, and members of the Nemhauser and Klavins groups for helpful discussions and Alec Nielson, Selma Alkafeef, and Brandi House for technical assistance.

Received June 18, 2012; accepted July 25, 2012; published July 27, 2012.

LITERATURE CITED

Bridge LJ, Mirams GR, Kieffer ML, King JR, Kepinski S (2012) Distinguishing possible mechanisms for auxin-mediated developmental control in Arabidopsis: models with two Aux/IAA and ARF proteins, and two target gene-sets. Math Biosci **235:** 32–44

Brunoud G, Wells DM, Oliva M, Larrieu A, Mirabet V, Burrow AH, Beeckman T, Kepinski S, Traas J, Bennett MJ, et al (2012) A novel sensor to map auxin response and distribution at high spatio-temporal resolution. Nature **482:** 103–106

Calderón Villalobos LI, Lee S, De Oliveira C, Ivetac A, Brandt W, Armitage L, Sheard LB, Tan X, Parry G, Mao H, et al (2012) A combinatorial TIR1/AFB-Aux/IAA co-receptor system for differential sensing of auxin. Nat Chem Biol **8:** 477–485

Chapman EJ, Estelle M (2009) Mechanism of auxin-regulated gene expression in plants. Annu Rev Genet **43:** 265–285

Clough SJ, Bent AF (1998) Floral dip: a simplified method for Agrobacterium-mediated transformation of Arabidopsis thaliana. Plant J **16:** 735–743

Del Bianco M, Kepinski S (2011) Context, specificity, and self-organization in auxin response. Cold Spring Harb Perspect Biol **3:** a001578

Dharmasiri N, Dharmasiri S, Estelle M (2005a) The F-box protein TIR1 is an auxin receptor. Nature **435:** 441–445

Dharmasiri N, Dharmasiri S, Weijers D, Lechner E, Yamada M, Hobbie L, Ehrismann JS, Jürgens G, Estelle M (2005b) Plant development is regulated by a family of auxin receptor F box proteins. Dev Cell **9:** 109–119

Dreher KA, Brown J, Saw RE, Callis J (2006) The *Arabidopsis* Aux/IAA protein family has diversified in degradation and auxin responsiveness. Plant Cell **18:** 699–714

Gibson DG, Young L, Chuang R-Y, Venter JC, Hutchison CA III, Smith HO (2009) Enzymatic assembly of DNA molecules up to several hundred kilobases. Nat Methods **6:** 343–345

Gietz RD, Woods RA (2002) Transformation of yeast by lithium acetate/single-stranded carrier DNA/polyethylene glycol method. Methods Enzymol **350:** 87–96

Harrison SJ, Mott EK, Parsley K, Aspinall S, Gray JC,, Cottage A (2006) A rapid and robust method of identifying transformed Arabidopsis thaliana seedlings following floral dip transformation. Plant Methods **2:** 19

Kepinski S, Leyser O (2005) The Arabidopsis F-box protein TIR1 is an auxin receptor. Nature **435:** 446–451

Lokerse AS, Weijers D (2009) Auxin enters the matrix: assembly of response machineries for specific outputs. Curr Opin Plant Biol **12:** 520–526

Mettetal JT, Muzzey D, Gómez-Uribe C, van Oudenaarden A (2008) The frequency dependence of osmo-adaptation in Saccharomyces cerevisiae. Science **319:** 482–484

Muto H, Watahiki MK, Nakamoto D, Kinjo M, Yamamoto KT (2007) Specificity and similarity of functions of the *Aux/IAA* genes in auxin signaling of Arabidopsis revealed by promoter-exchange experiments among *MSG2/IAA19*, *AXR2/IAA7*, and *SLR/IAA14*. Plant Physiol **144:** 187–196

Nishimura K, Fukagawa T, Takisawa H, Kakimoto T, Kanemaki M (2009) An auxin-based degron system for the rapid depletion of proteins in nonplant cells. Nat Methods **6:** 917–922

Parry G, Calderon-Villalobos LI, Prigge M, Peret B, Dharmasiri S, Itoh H, Lechner E, Gray WM, Bennett M, Estelle M (2009) Complex regulation of the TIR1/AFB family of auxin receptors. Proc Natl Acad Sci USA **106:** 22540–22545

Pierce NW, Kleiger G, Shan SO, Deshaies RJ (2009) Detection of sequential polyubiquitylation on a millisecond timescale. Nature **462:** 615–619

Ramos JA, Zenser N, Leyser O, Callis J (2001) Rapid degradation of auxin/indoleacetic acid proteins requires conserved amino acids of domain II and is proteasome dependent. Plant Cell **13:** 2349–2360

Reinhardt D, Pesce E-R, Stieger P, Mandel T, Baltensperger K, Bennett M, Traas J, Friml J, Kuhlemeier C (2003) Regulation of phyllotaxis by polar auxin transport. Nature **426:** 255–260

Stewart JL, Nemhauser JL (2010) Do trees grow on money? Auxin as the currency of the cellular economy. Cold Spring Harb Perspect Biol **2:** a001420

Tan X, Calderon-Villalobos LI, Sharon M, Zheng C, Robinson CV, Estelle M, Zheng N (2007) Mechanism of auxin perception by the TIR1 ubiquitin ligase. Nature **446:** 640–645

Vernoux T, Brunoud G, Farcot E, Morin V, Van den Daele H, Legrand J, Oliva M, Das P, Larrieu A, Wells D, et al (2011) The auxin signalling network translates dynamic input into robust patterning at the shoot apex. Mol Syst Biol **7:** 508

Weijers D, Benkova E, Jäger KE, Schlereth A, Hamann T, Kientz M, Wilmoth JC, Reed JW, Jürgens G (2005) Developmental specificity of auxin response by pairs of ARF and Aux/IAA transcriptional regulators. EMBO J **24:** 1874–1885

Williamson A, Banerjee S, Zhu X, Philipp I, Iavarone AT, Rape M (2011) Regulation of ubiquitin chain initiation to control the timing of substrate degradation. Mol Cell **42:** 744–757

Supplementary Information for
A synthetic approach reveals extensive tunability of auxin signaling

Kyle A. Havens[1*], Jessica M. Guseman[2*], Seunghee S. Jang[1*], Edith Pierre-Jerome[2*], Nick Bolten[1], Eric Klavins[1#], and Jennifer L. Nemhauser[2#]

[1]Department of Electrical Engineering
[2]Department of Biology
University of Washington, Seattle, WA, 98195
[*]co-first authors
[#]correspondence should be addressed to klavins@uw.edu or jn7@uw.edu

Contents

1 Quantitative Analysis **2**
1.1 Objectives and Approach . . . 2
1.2 Model Development and Discrimination . . . 2
1.2.1 M_0 . . . 3
1.2.2 M_1 . . . 3
1.2.3 M_2 . . . 4
1.2.4 M_3 . . . 4
1.2.5 Summary . . . 5
1.3 Parameter Reduction . . . 5
1.4 Summary . . . 8

Supplementary Figures

1 Addition of 10μM auxin is sufficient for maximal degradation of IAAs. . . . 10
2 Fluorescence levels decrease drastically as yeast cells enter stationary phase. . . . 11
3 AFBs do not have differential effects on basal degradation of IAAs. . . . 12
4 AFB1 and AFB3 do not promote degradation of IAA2. . . . 13
5 TIR1 is expressed at a similar level to AFB2. . . . 14
6 AFB2 expression is not rate limiting. . . . 15
7 Schematic of cloning strategy for domain II truncations. . . . 16
8 Yeast degradation experiments predict relative degradation rates in plants. . . . 17
9 Sample time-course IAA degradation data and model fits of IAA14|TIR1. . . . 18
10 Sample dose-response data and model predicted dose-response of IAA17|AFB2. . . . 19
11 Parameter variations study of the preferred model. . . . 20

Supplementary Tables

1 Comparison of degradation rates, half-lives, and affinities from yeast, *in vitro* and plant studies. . . . 21

2 Table of amino acids included in each IAA truncation. 24
3 The residuals and the number of distinct parameters for all candidate models. 25
4 Estimated parameters for IAA|TIR1 pairs using the preferred model interpretation. 26
5 Estimated parameters for IAA|AFB2 pairs using the preferred model interpretation. 27
6 Estimated parameters for degron comparison study using the preferred model interpretation. 28
7 Average, minimum and maximum values of the estimated parameters 29
8 Oligonucleotides used in this study 30
9 Yeast strains used in this study 33

1 Quantitative Analysis

1.1 Objectives and Approach

The primary objective of our quantitative analysis is to identify a small model, with as few parameters as possible, that describes the differential degradation of IAA|AFB pairs observed in experiments. Having few parameters avoids over-fitting, facilitates comparison among available pairs, and provides a guide for the selection of parts during the rational design of new networks. A computationally intractable number of candidate models can be generated by, for example, various assumptions about the mechanism of degradation and the many molecular species involved. Computational limits, therefore, require that we limit the number of candidate models by employing current knowledge of the auxin signal pathway, basic assumptions about protein synthesis, and simple input-output concepts.

We assess candidate models by fitting their parameters to the entire data set, analyzing their qualitative fit, and then computing their residual fit. We fit our models to experimental data using the nonlinear optimization function `FindFit` in *Mathematica* (Wolfram) where the cost function is defined as

$$J(\theta^{(s)}, M_s) \;=\; \sum_{i,j} \sum_{t_m \in \mathrm{T}} \left\| y_{ij}(t_m) - \hat{y}_{ij}(t_m, \theta_{ij}^{(s)}, M_s) \right\|_2 , \tag{1}$$

where i denotes the index of an IAA, j denotes the index of a AFB, s denotes the index of a model, $y_{ij}(t_m)$ denotes the measured output at $t = t_m$, T denotes the set of measurement times, $\theta_{ij}^{(s)}$ denotes the parameter vector for a model M_s and $\mathrm{IAA}_i|\mathrm{AFB}_j$, $\hat{y}_{ij}(t_m, \theta_{ij}, M_s)$ denotes the predicted output using the model M_s and its parameter vector θ_{ij} at $t = t_m$, $\theta^{(s)}$ denotes the union of all parameter vectors of IAA|AFB pairs under the model M_s and $\|\cdot\|_2$ denotes the 2-norm[1] of the given vector. Following the estimation, the residual of a model is defined as

$$G(M_s) = \sum_{i,j} \sum_{t_m \in \mathrm{T}} \frac{1}{dim\ y_{ij}} \left\| \frac{y_{ij}(t_m) - \hat{y}_{ij}\left(t_m, M_s, \theta_{ij}^{(s)*}\right)}{y_{ij}(t_m)} \right\|_2 \tag{2}$$

where $\theta^{(s)*}$ denotes the optimal estimated parameter vector obtained from minimizing the cost function (1), and *dim* denotes the dimension of the vector (e.g. number of data points in the time course).

1.2 Model Development and Discrimination

Our approach is to develop candidate models with good qualitative fits, low residuals, and a small number of parameters by incrementally increasing complexity via refinements that are based on known mechanisms. In the model discrimination step, both quantitative and qualitative metrics of each model are evaluated. It is true that quantitatively low residual is desired in general, however, the analytical metric takes precedence. If a model is shown to be analytically incapable of fitting critical features of experimental observation, the model is deemed structurally flawed, and is eliminated, even if the quantitative metric is relatively low. Following are the two general qualitative features observed in the experimental data.

[1] $\|x\|_p = \left(\sum_{i=1}^{n} |x_i|^p\right)^{1/p}$

1. Each degradation time-course includes an inflection point, such that the curve switches from concave to convex (Figure 1C).

2. Each dose-response curve (steady-state fluorescence measurement vs auxin concentration) is nonlinear (Supplementary Figure 1).

These two features were used as qualitative criteria to which all models were subjected to. The number of parameters for the model is computed over all experimental data sets, such that the total number of parameters equals the number of parameters in the model multiplied by the number of experiments (i.e. the number of distinct IAA|AFB pairs). After a model has been selected, we reduced the total number of parameters by assuming that some of the parameters can be consolidated for a specific group of experiments.

1.2.1 M_0

We first consider the synthetic yeast system as a grey-box with a single input (auxin) and a single output (YFP intensity). Therefore, we propose the following model, M_0, which is a combination of simple synthesis/degradation dynamics and exponential decay:

$$\frac{d\,y(t)}{dt} = k_1 - k_2\,y(t) - k_3\,u(t)\,y(t), \tag{3}$$

where t denotes time, y denotes the output, and u denotes the input. This model encodes the hypothesis that the YFP-IAA fusion protein is subject to zeroth-order synthesis and first-order degradation, and that the output degrades at a rate proportional to the input. The first two terms, k_1 and $k_2\,y(t)$, represent the input-independent synthesis and degradation of the output, respectively. The last term represents the degradation of output with the overall rate proportional to itself and the input. Thus, k_1 is the synthesis rate, k_2 is the basal degradation rate, and k_3 is the input mediated degradation rate.

This model has residual $G(M_0) = 49.31$, and requires 144 distinct parameters (3 per IAA|AFB pair) to fit the entire data set. The model has a closed form analytical solution,

$$y(t) \;=\; \frac{k_1}{k_2 + k_3 u}\left(1 + \frac{e^{-t(k_2+k_3u)}k_3 u}{k_2}\right), \tag{4}$$

which demonstrates the nonlinear relationship between u and the y^*, which is consistent with the qualitative observation of the experimental data (Supplementary Figure 9, purple curve). However, the model cannot capture the inflection of the curve (Supplementary Figure 9, purple curve). For a function to have change in its convexity, the second derivative has to equal zero at some $t > 0$ (and that t is the inflection point). However, M_0 has second-order derivative,

$$\frac{d^2y}{dt^2} \;=\; \frac{k_1 k_3 u\,(k_2 + k_3 u)}{k_2} e^{-t(k_2+k_3u)} \tag{5}$$

which shows that for all parameters $k_1, k_2, k_3 > 0$ and $u \geq 0$, $d^2y/dt^2 > 0$. This represents M_0 is fundamentally unable to capture one of the crucial features of the system.

1.2.2 M_1

The inflection point and the related initial delay in the degradation curves suggest that the IAA degradation mechanism comprises additional intermediate processes (e.g. formation of an intermediate species). To model this feature, we add an internal state x. At this point, we do not assume that x is any specific species or combination of species – just that it is formed and degraded. In particular, we assume that the

rate at which x is synthesized is proportional to the input, and that x affects the non-basal degradation of y. This second-order linear model, M_1, is defined by

$$\begin{aligned}\frac{d\,x(t)}{dt} &= k_1\,u(t) - k_2\,x(t)\\ \frac{d\,y(t)}{dt} &= k_3 - k_4\,y(t) - k_5\,x(t).\end{aligned} \tag{6}$$

The model has residual $G(M_1) = 81.68$, and requires 240 distinct parameters (5 per IAA|AFB pair) to fit the entire data set. The model captures the inflection point in time-course degradation curve (Supplementary Figure 9, blue curve). However, the dose-response predicted by M_1 is qualitatively different from our observations. Analytically, the steady-state solution of M_1 has a closed form,

$$\begin{aligned}x^* &= \frac{k_1\,u}{k_2}\\ y^* &= \frac{k_3}{k_4} - \frac{k_5\,k_1}{k_2\,k_4}u,\end{aligned} \tag{7}$$

which demonstrates that y^* has a linear relationship to u. Furthermore, because of this linear relationship, the model predicts that the steady-state fluorescence decreases indiscriminately with increasing amount of input, to the point where negative fluorescence is predicted (Supplementary Figure 10, blue curve). The fact that M_2 makes predictions that starkly contradict physical constraints demonstrates that M_1 is qualitatively unfit for the given experimental data.

1.2.3 M_2

Since the dose-response is nonlinear, we modify M_1 by introducing a nonlinear term, making the degradation term dependent on $y(t)$. This second-order nonlinear model, M_2, is,

$$\begin{aligned}\frac{dx(t)}{dt} &= k_1\,u(t) - k_2\,x(t)\\ \frac{dy(t)}{dt} &= k_3 - k_4\,y(t) - k_5\,x(t)\,y(t),\end{aligned} \tag{8}$$

which has a residual of $G(M_2) = 24.54$ and requires 240 distinct parameters (5 per IAA|AFB pair) to fit the entire data set. The steady-state of output predicted by M_2 are,

$$\begin{aligned}x^* &= \frac{k_1\,u}{k_2}\\ y^* &= \frac{k_2 k_3}{k_2 k_4 + k_1 k_5 u},\end{aligned} \tag{9}$$

which demonstrates a nonlinear relationship between y^* and u, which satisfies one of the qualitative features. There is no closed-form solution for the model because it is nonlinear, however, numerical solution demonstrates that the model captures the inflection point in the predicted time-course curves (Supplementary Figures 9 and 10, green curve).

1.2.4 M_3

As mentioned before, the internal state x represents an unknown intermediate species (or combination of species) that interacts with auxin input and the YFP-IAA output. It is feasible that more than a single intermediate species is required to encompass the underlying dynamics. To investigate whether this might be the case, we added a second internal state, z, as an intermediate state between x and y. This third-order

nonlinear model, M_3, is

$$\begin{aligned}\frac{dx(t)}{dt} &= k_1\,u(t) - k_2\,x(t),\\ \frac{dz(t)}{dt} &= k_3\,x(t) - k_4\,z(t),\\ \frac{dy(t)}{dt} &= k_5 - k_6\,y(t) - k_7\,z(t)\,y(t),\end{aligned} \tag{10}$$

which has a residual of $G(M_3) = 33.30$ and requires 336 distinct parameters (7 parameters per IAA|AFB pair) to fit the entire data set. As in the case with M_2, M_3 captures the two qualitative features of the system (Supplementary Figures 9 and 10, red curve). It is notable that the computed residual is larger than $G(M_2)$, however, this is most likely the result of standard estimation error (e.g. non-optimal initial condition or insufficient search space). Alternatively, M_3 may represent a point at which the saturation of model benefit gained by increasing model complexity is saturated.

1.2.5 Summary

We generated and evaluated four candidate models, M_0, M_1, M_2, and M_3, with respect to how well each model captures the experimental observation, both quantitatively and qualitatively. M_0 did not capture the inflection observed in time-course degradation curves; M_1 did capture the inflection, but did not capture the nonlinear dose-response behavior; M_2 captures both the time-course and dose-response data qualitatively; and M_3 matches these behaviors with comparable quantitative metric to M_2. However, given the limitations of the experimental dataset (time-course to auxin step-input and auxin dose response), M_3, nor any more complex models, may not provide verifiable insights to the system. Said differently, more complex models may result in lower quantitative fit metric, however, to balance the estimation uncertainty associated with higher complexity models, we require richer perturbation of the system that reveals the appropriately higher complexity of the internal mechanism. Therefore, M_2 is arguably the simplest explanation for the observed phenomenon.

1.3 Parameter Reduction

Aside from M_0, the model candidates considered in the previous section include one or more internal states, x (and z), that are not readily associated with biological complexes. One way to approach this is to consider the internal state simply as a mathematical necessity for fitting the experimental observation. Another approach is to consider hypotheses as to what biological complex – that we know to exist in the auxin-mediated IAA degradation pathway – can be associated with x, and examine whether these hypotheses lend a useful quality to our model. One of the hypothetical interpretations of x is that it is a complex formed between auxin and AFB. A simple description of the mechanism in which IAA degrades in the presence of auxin and AFB is shown in Figure 1A, where auxin serves as a molecular glue, binding with an AFB and allowing the protein to bind with IAA, further triggering the ubiquitylation of IAA. Therefore, we postulate that x is a proxy of such a species.

Building on the hypothesis of model interpretation that x is a proxy of the auxin-bound AFB complex, we associate each of the model parameters to the identity of the two different proteins, IAA and AFB. Firstly, parameters k_1 and k_2 are rates associated with synthesis and degradation of auxin-bound receptor protein, where the synthesis is directly proportional to the input. In which case, we further hypothesized that these two parameters are dependent on the identity of AFB but are independent of the identity of the co-expressed IAA. Secondly, analogous interpretations are given to k_3 and k_4; these are rates of synthesis and basal (input-independent) degradation of IAA-YFP, and they are only dependent on the identity of the IAA and not on the identity of the AFB. Finally, k_5 is unique among the model parameters such that it is dependent on the identities of both proteins. Mathematically, k_5 is the rate constant for how fast the output degrades, and such a degradation process is proportional to the amount of x and y in

the system. One can then assign a biochemically feasible interpretation to the term, "when active AFB and IAA interact, the IAA degrades at a rate proportional to k_5". As shown in Figure 1C, the unifying feature of all IAA|AFB pairs is that they degrade when auxin is added to the system in varying degrees. Such variation in degradation among the IAA|AFB pairs can serve as a unique identifier for each pair, and we investigated whether a subset of parameters can serve as the quantitative identifier. Note that these association of parameters to reaction rates are based on a possible interpretation of the model, and should not be taken as a direct representation of a "true system". The parameters may be crude amalgamations of multiple biochemical processes but the resulting model is an elegant abstraction rid of unwieldy details.

In the previous section, when we fit candidate models to experimental data, all five of the M_2 parameters,

$$\theta_{ij}^{(2)} = \{k_1^{(i,j)}, k_2^{(i,j)}, k_3^{(i,j)}, k_4^{(i,j)}, k_5^{(i,j)}\}, \tag{11}$$

were allowed to vary, resulting in five different parameter values for each IAA|AFB pair[2]. This method, which allowed us to easily compare candidate models, makes it difficult to compare the parameters of one IAA|AFB pair to another. For example, suppose we want to directly compare the degradation rates of IAA17|TIR1 and IAA17|AFB2, which have mean fitted k_5 values of 0.034 and 0.21, respectively. The large discrepancy in the two values suggests a large difference in the respective degradation dynamics, but because each pair has other parameters that vary as well, the differences in k_5 are not the only explanation for the variation.

Therefore, we asked if some parameters may be common to a subset of the IAA|AFB pairs, and if consolidating these common parameters would reduce estimation uncertainty. This approach is often called global curve fitting. A systematic generation of all possible global fitting hypotheses for parameter reduction (identifying all possible combinations of common parameters across the 48 IAA|AFB pair, and five parameter model) would have been computationally expensive. Fortunately, the model interpretation provides a feasible guide as to which hypotheses are more likely than others, such as dividing the 48 pairs into smaller subsets. With this estimation approach, we can reduce the variability caused by other parameters and fairly compare parameter values. As mentioned before, k_5 is unique to the identity of each IAA|AFB pair, therefore, the parameter is the primary quantity of interest in comparing the differential degradation among the pairs.

First of all, we address an extreme case of parameter reduction, where we only let k_5 vary for all IAA|AFB pairs, and fix the rest of the parameters to be the same across all pairs. We denote this hypothesis H_1, which provides an additional constraint on the optimization problem, defined by

$$\begin{aligned} \min J(\theta^{(s)}, M_s) \quad &= \quad \sum_{i,j} \sum_{t_m \in \mathrm{T}} \left\| y_{ij}(t_m) - \hat{y}_{ij}(t_m, \theta_{ij}^{(s)}, M_s) \right\|_2, \\ \text{subject to} \qquad & k_l^{(i,j)} = k_l^{(i',j')} \qquad \forall i, i' \in \mathcal{I},\ \forall j, j' \in \mathcal{J},\ \text{and } l = 1,2,3,4, \end{aligned} \tag{12}$$

where, $\mathcal{I}$ and $\mathcal{J}$ denote the sets of IAA and AFB indices, respectively, and l denotes the parameter index. The resulting parameter vector, θ_{H_1}, has 52 distinct parameters (4 + 48 per pair) and results in $G(M_2, \theta_{H_1}) = 48.9$. Thus, H_1 reduces the cardinality of the parameter vector to the point where an IAA|AFB pair has only one parameter that differs from another pair. However, because H_1 makes both k_3 and k_4 be the same for all IAA|AFB pairs, it implies that the initial output value at $t = 0$ for all IAA|AFB pairs are equal ($y_{ij}(0) = k_3^{(i,j)}/k_4^{(i,j)}$). This is inconsistent with the experimental data where initial levels of expression vary (Figure S4). Therefore, H_1 is invalidated based on its conflict between the interpretation of the model and the experimental data.

[2] $k_l^{(i,j)}$ denotes the k_l value for IAA$_i$|AFB$_j$, where $l = 1, 2, 3, 4, 5$.

Next, we propose an alternative hypothesis to H_1 in which k_1, k_2, k_3 and k_4 are constrained, but across a smaller subset of IAA|AFB pairs. For example, it was shown that the AFBs do not have differential effect on basal dynamics of IAA (Supplementary Figure S4). Therefore, two IAA|AFB pairs with the same IAA have a similar initial output - suggesting equal k_3 and k_4 values for these two pairs. For this hypothesis, H_{11}, we have the following optimization constraints.

$$\text{subject to} \qquad k_l^{(i,j)} = k_l^{(i,j')} \qquad \forall j, j' \in \mathcal{J}, \text{ and } l = 1, 2, 3, 4. \tag{13}$$

The resulting parameter vector, denoted $\theta_{H_{11}}$, has 144 distinct parameters, and results in $G(M_2, \theta_{H_{11}}) = 24.33$. This decreased residual is a validation in which we let the model interpretation and the fundamental details of the system guide our hypotheses generation. To verify this approach, we generated an alternative hypothesis, H_{12}, where IAA|AFB pairs with the same AFB, versus those with the same IAA (H_{11}), have equal k_1, k_2, k_3 and k_4. This hypothesis has the same cost function as Eq 13 but with the following optimization constraint,

$$\text{subject to} \qquad k_l^{(i,j)} = k_l^{(i',j)} \qquad \forall i, i' \in \mathcal{I}, \text{ and } l = 1, 2, 3, 4. \tag{14}$$

Note that H_{12} was not generated based on the model interpretation as H_{11}, but was proposed as a counter example to our approach. The resulting residual is $G(M_2, \theta_{H_{12}}) = 36.62$, where $\theta_{H_{12}}$ has 56 distinct parameters. The increased residual validates our approach. Comparing H_1, H_{11} and H_{12} suggests that 1) larger numbers of distinct parameters tend to decrease the residual, and 2) when constraining the parameters across a smaller subset of IAA|AFB pairs, the model interpretation serves as a helpful guide in generating reasonable hypotheses.

The higher residuals of H_1 hypotheses family also suggest that for any two IAA|AFB pairs, more than one parameter ought to be allowed to vary (increasing degrees-of-freedom in the parameter estimation) to fit both data sets. Therefore, we further investigate whether a specific grouping of experimental data and parameter reduction hypotheses is possible. Each case of varying parameter (in addition to k_5), k_1, k_2, k_3 or k_4, is denoted with H_{21}, H_{22}, H_{23} or H_{24}, respectively (the four hypotheses are elements of the set $H_{2\kappa}$, where $\kappa = 1, 2, 3,$ or 4). Each hypothesis, depending on the parameter allowed to vary, is associated with data grouping that are supported by the model interpretation.

1. For H_{21} and H_{22}, the additional parameter allowed to vary is dependent on the identity of AFB and independent of the identity of the IAA. Therefore, IAA|AFB pairs are grouped by their IAAs (each group containing two pairs, IAA_i|TIR1 and IAA_i|AFB2), resulting in 24 distinct groups. For each group, the parameters are estimated under the constraint,

$$\text{subject to} \qquad k_l^{(i,j)} = k_l^{(i,j')} \qquad \forall j, j' \in \mathcal{J},\ l \in \{1, 2, 3, 4\} \backslash \{\kappa\}, \text{ and } \kappa = 1, 2. \tag{15}$$

   These hypotheses imply that a group of IAA|AFB pairs that have the same IAA have the same basal synthesis and degradation rates (k_3 and k_4) of the output. Furthermore, they imply that the variations among each group can be captured by varying k_5 and k_1 for H_{21}, or k_5 and k_2 for H_{22}.

2. For H_{23} and H_{24}, the additional parameter allowed to vary is dependent on the identity of IAA and independent of the identity of the AFB. Therefore, IAA|AFB pairs are grouped by their AFBs (each group containing 24 pairs, IAA_i|AFB, where $i = [1, \cdots, 24]$), resulting in two groups. For each group, the parameters are estimated under the constraint,

$$\text{subject to} \qquad k_l^{(i,j)} = k_l^{(i',j)} \qquad \forall i, i' \in \mathcal{I},\ l \in \{1, 2, 3, 4\} \backslash \{\kappa\}, \text{ and } \kappa = 3, 4. \tag{16}$$

   The hypotheses imply that a group of IAA|AFB pairs that have the same AFB has the same synthesis and degradation rates of the internal state (k_1 and k_2). Furthermore, they imply that the variations among each group can be captured by varying k_5 and k_3 for H_{23}, or k_5 and k_4 for H_{24}.

Supplementary Table 3 shows the residuals and the number of distinct parameters for various hypotheses investigated. Compared to H_1 hypotheses, H_2 hypotheses tend to have lower residuals, owing to the larger degrees-of-freedom given in the estimation constraints. Additionally, H_{24} has the lowest residual even with the lowest number of distinct parameters. This suggests that for any two IAA|AFB pairs, the differential dynamics between the two can be captured through varying the basal rate parameters of IAA and the input-mediated degradation by the AFBs (k_5). These two dynamics, however, are independent of one another as discussed previously (Results, Figure 2). Also, single parameter variation studies suggests that a set of time-courses predicted by varying k_3 or k_4 have identical degradation profiles when normalized to their initial conditions (Supplementary Figure 11, Supplementary Table 7). The simulation study is also supported by experimental data of IAA1 and IAA1.1, where IAA1.1 is a codon-optimized version of IAA1. This results in higher expression level for IAA1.1 relative to IAA1, which under the model interpretation, is equivalent to increasing k_3 and leaving other parameters the same. When the two curves are normalized to their initial conditions (Supplementary Figure 9), the curves overlap closely. This is reflected by the close k_5 values of IAA1 and IAA1.1 (Supplementary Table 4 and 5).

The normalized degradation curves in Supplementary Figure 11 further provide two notable features of the model. First, they suggest that the two parameter k_3 and k_4 are, in fact, dependent parameters that can be consolidated into a single parameter by normalizing the output. The normalized version of M_2 is

$$\frac{dx(t)}{dt} = k_1\, u(t) - k_2\, x(t) \tag{17}$$

$$\frac{dz(t)}{dt} = k_4 - k_4\, z(t) - k_5\, x(t)\, z(t), \tag{18}$$

where $z = \frac{y}{y_0} = \frac{k_4}{k_3}\, y$, the output normalized to its initial value. This procedure further reduces the number of parameters to be estimated and decreases computational cost in estimation. The differences in the estimated values of k_5 are negligible between the two versions of model. A second notable feature of the model is that the range of degradation profiles in experimental data can be fitted just as well by varying k_1 instead of k_5. This feature is not surprising as varying k_1 increase the rate at which x increases, ultimately having the same effect on the output. However, because of the way we interpret the model parameters, k_1 is independent of the identity of IAA. This conflicts with our objective of identifying a degradation rate parameter that are unique to each IAA|AFB pair. Therefore, we choose k_5 as the single parameter that captures the differential degradation range we observe among the IAA|AFB pairs.

1.4 Summary

Through iterative searches in model discrimination and parameter reduction, we identified a single parameter that captures the differential degradation exhibited by the family of IAA|AFB pairs. The reasoning behind finding a single parameter is largely inspired by the engineering principles of modularity and composable parts. For example, an electric circuit is composed of individual modular parts, such as resistors and transistors. The function of the circuit is tunable by swapping out these modular parts, where the electrical functionality of each type of modular part is specified by a number (i.e. a resistor is specified by its resistance). Casting this principle on the auxin signaling pathway, we ask whether the IAA|AFB pair degradation module (in the larger scheme of the auxin signal pathway) is a modular part, and if so, whether the biological functionality of the module can be specified by a number. The functional feature of the IAA|AFB module, degradation, demonstrates a large range of responses. Therefore, we hypothesize that the number that specifies each IAA|AFB pair's unique biological functionality is its degradation rate (k_5).

Now that we have a data-sheet of k_5 for a large group of IAA|AFB pair, the hypothesis regarding the modularity of these pairs must be verified. It will require an auxin synthetic network containing an IAA|AFB pair, where the part can be easily replaced with another pair. Using a similar approach, a succinct mathematical representation of such a network can be devised, and preferably, the k_5 identified

in this work will be a part of such a model. If a coherent function that maps the differential degradation rates (caused by using different IAA|AFB pairs) and the differential outputs of the larger network can be identified, it will allow us to test to what extent and under what context these pairs are modular. And if this is not the case, the question remains whether there is another set of identifiable quantities for the IAA|AFB pairs that is a better specification of their biological functionality and predictors of the composite network output. Furthermore, the relationship between the k_5 and the output of the network will illuminate the core interactions within the network, aiding in increasingly accurate mathematical representations of the synthetic network. These approaches will not only answer questions regarding the engineerability of auxin signaling pathway, but also provide the basis for novel ways of system identification in biology.

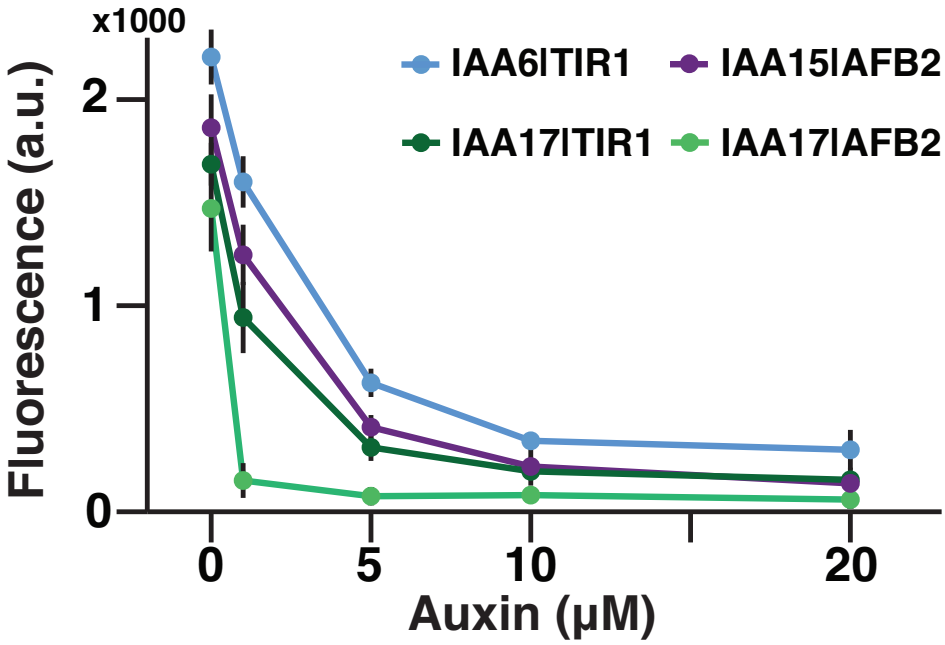

Supplementary Figure 1: Addition of 10μM auxin is sufficient for maximal degradation of IAAs. IAAs with the slowest and fastest degradation rates for TIR1 (IAA6 and IAA17, respectively) and AFB2 (IAA15 and IAA17, respectively) were treated with increasing concentrations of auxin. Fluorescence levels were measured two hours after auxin treatment. Doses of 10μM and 20μM resulted similar levels of degradation. Error bars represent $\pm$ one standard deviation between two experiments performed on different days.

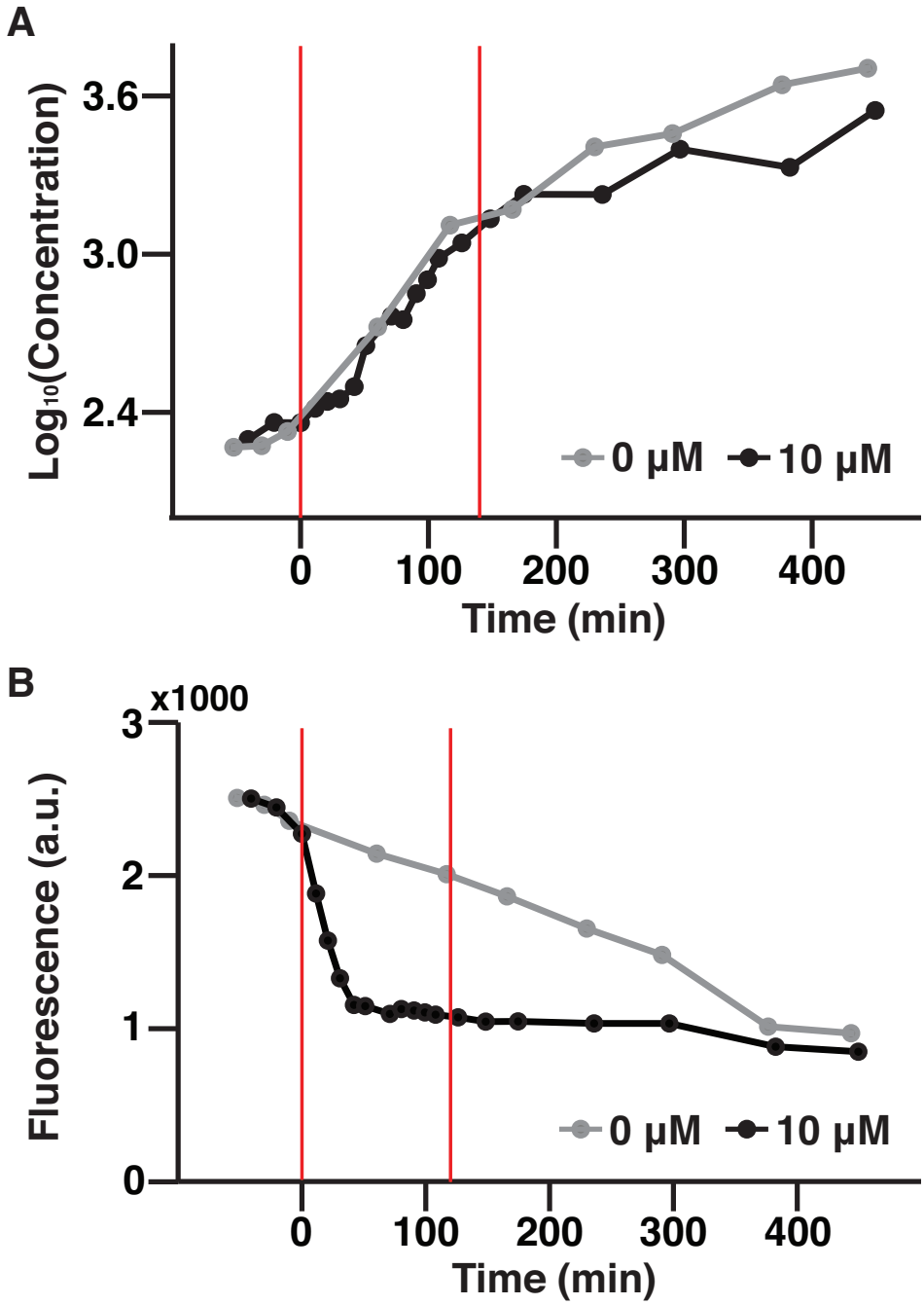

Supplementary Figure 2: Fluorescence levels decrease drastically as yeast cells enter stationary phase. (A) Representative graphs of yeast growth over time of cells containing IAA1|TIR1 treated with mock (grey) or with 10μM auxin (black). (B) Fluorescence in the same cells over time. Red lines demarcate window of experimental data collection.

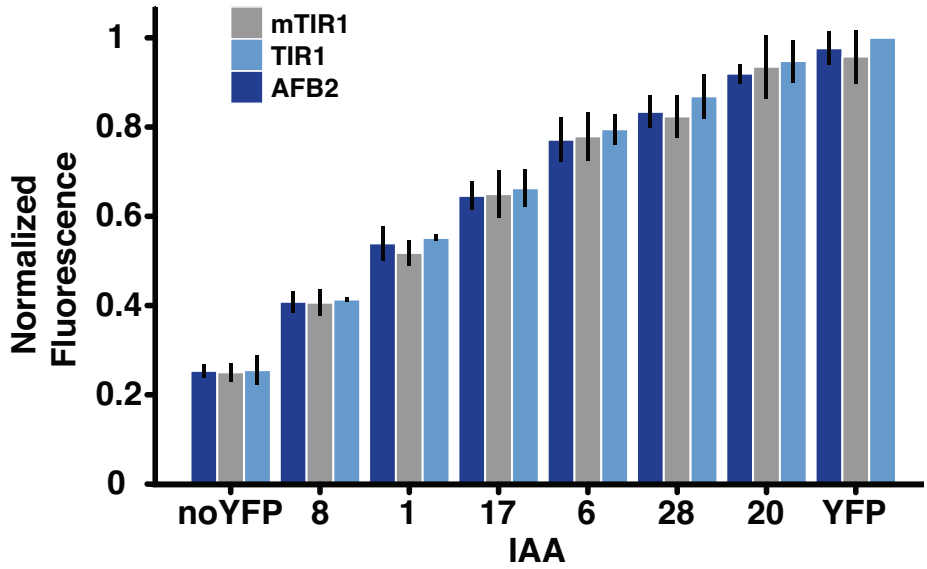

Supplementary Figure 3: AFBs do not have differential effects on basal degradation of IAAs. A sample set of IAAs was co-expressed with mTIR1, TIR1, or AFB2. Fluorescence at steady state, prior to auxin addition, was measured. These IAAs were chosen as they span the range of observed initial steady state intensity values. The noYFP strain expresses an allele of IAA17 without a YFP fusion. Regardless of AFB identity, initial fluorescence levels were indistinguishable for a given IAA. Strains were prepared as in Figure 1C. Each experiment was normalized to the YFP—TIR1 expression level. Error bars are ± one standard deviation between three experiments performed on different days.

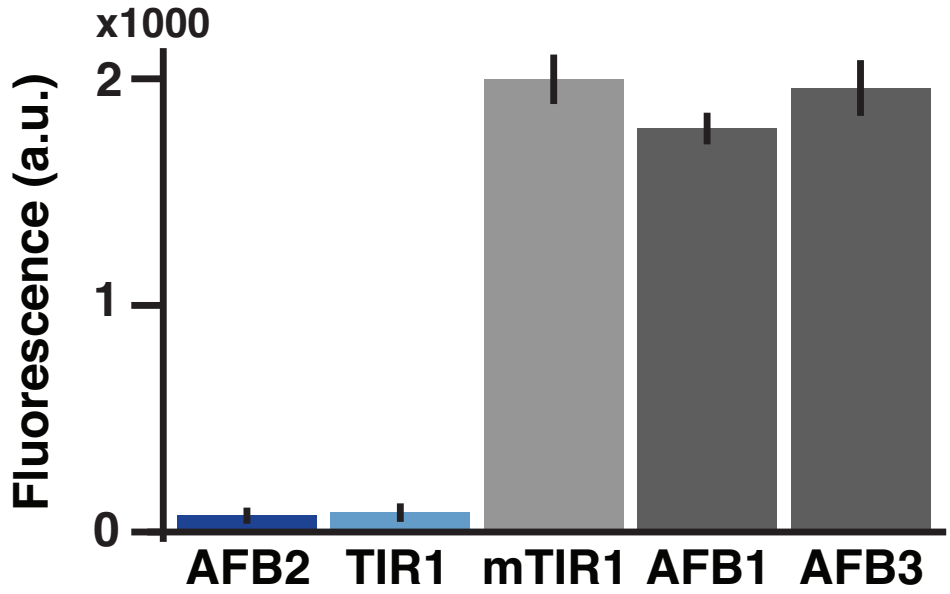

Supplementary Figure 4: AFB1 and AFB3 do not promote degradation of IAA2. IAA2 was co-expressed with each of five receptor types. Fluorescence levels were measured after a 3-hour treatment with 20μM auxin. Similar to mTIR1, AFB1 and AFB3 failed to exhibit degradation of IAA2. Error bars represent $\pm$ one standard deviation between two replicates.

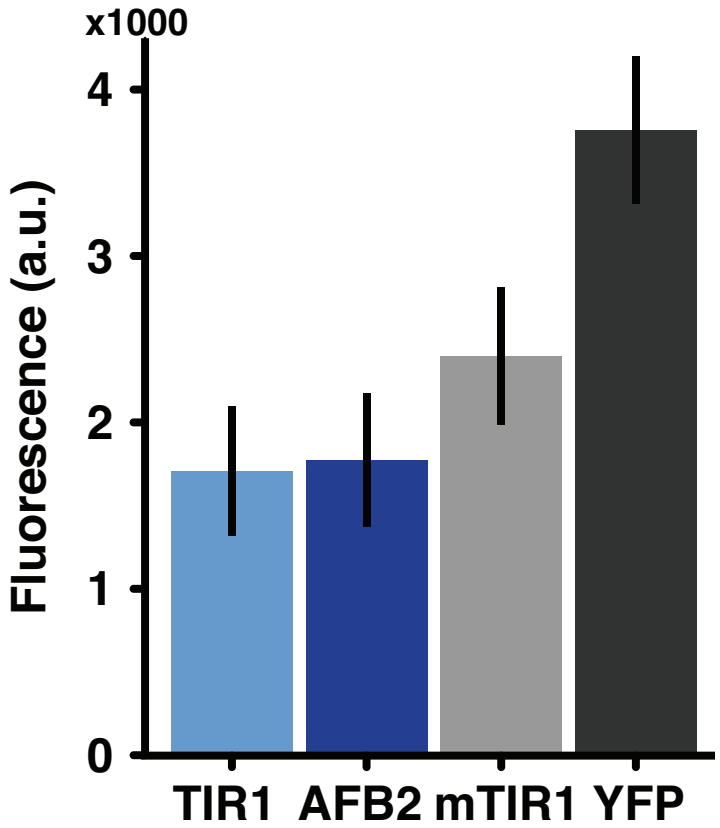

Supplementary Figure 5: TIR1 is expressed at a similar level to AFB2. AFB-YFP constructs were singly integrated into yeast, and their fluorescence intensities were compared using flow-cytometry. Error bars represent one standard deviation, between three replicates.

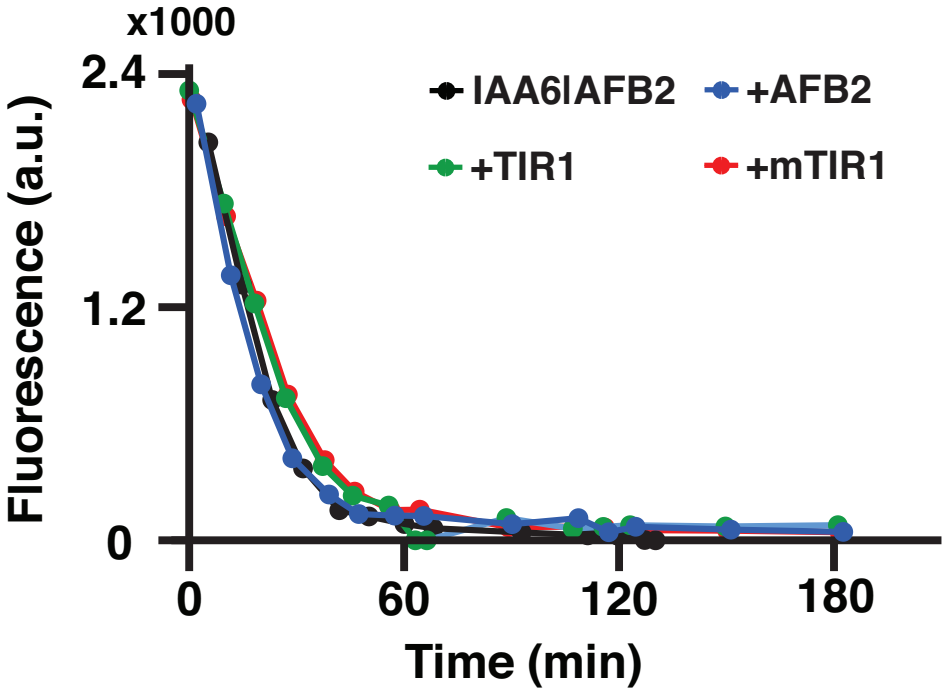

Supplementary Figure 6: AFB2 expression is not rate limiting. Additional copies of AFB (blue), TIR1 (green) or mTIR1 (red) were co-expressed with IAA6|AFB2 in diploid cells. These were compared to the original IAA6|AFB2 strain (black line). The overlapping curves indicate that the degradation rates are similar, implying that with IAA6, the effect of AFB2 is dominant relative to TIR1, and its activity is not increased with additional copies of the gene.

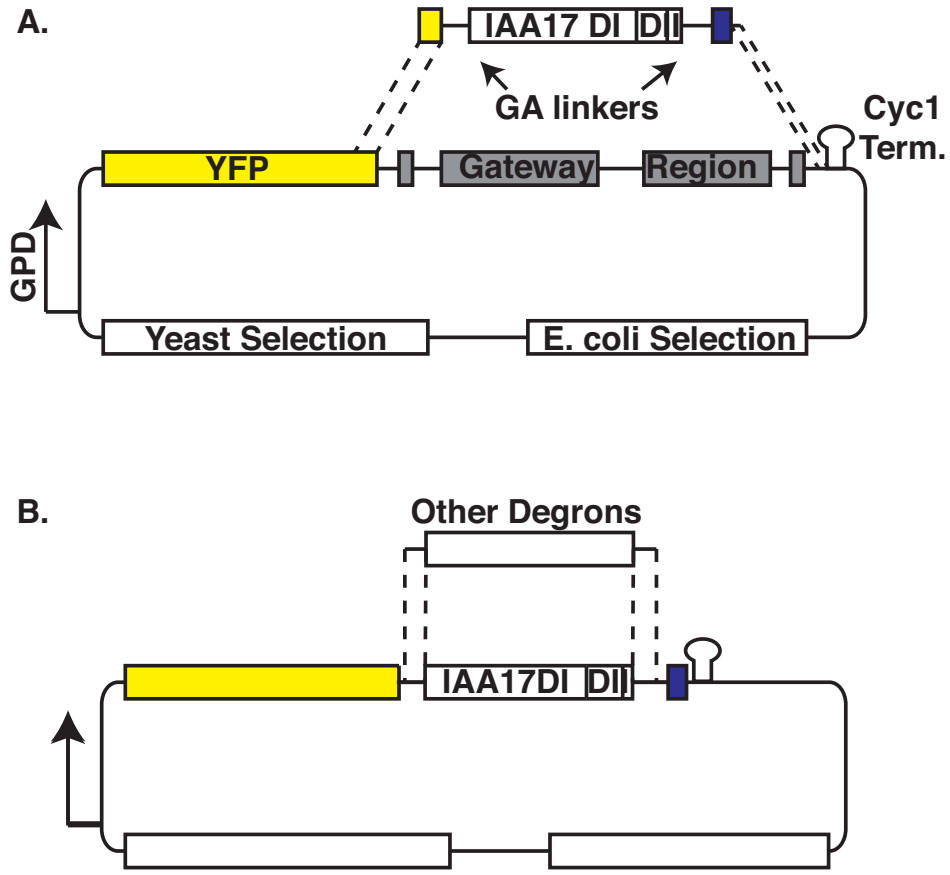

Supplementary Figure 7: Schematic of cloning strategy for domain II truncations. (A) IAA17.T1 was synthesized with Gly-Ala linkers and a 2XSV40-NLS at the C-terminus. This fragment was amplified with primers listed in Table S9 and cloned using Gibson assembly [3]. (B) Gibson assembly was then used to insert other IAA truncations into the same NLS-containing plasmid backbone.

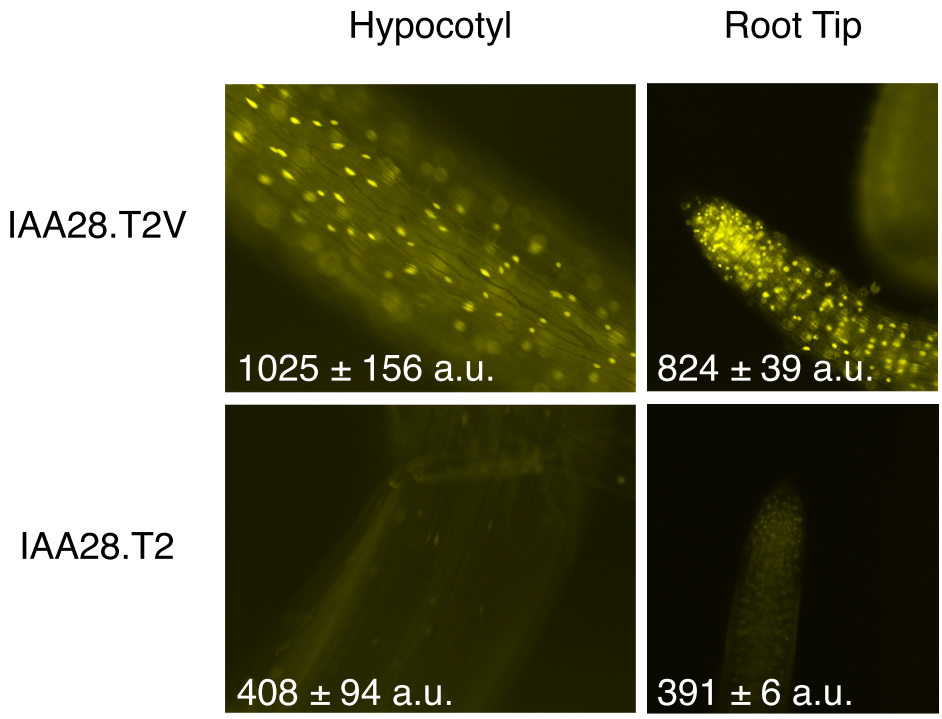

Supplementary Figure 8: Yeast degradation experiments predict relative degradation rates in plants. Consistent with the truncation degradation rates observed in yeast (Fig. 3B), hypocotyls and root tips of plants expressing IAA28.T2-VENUS accumulated lower fluorescence levels than those expressing DII-VENUS (identical to IAA28.T2V) [2]. Mean fluorescence intensity ± SEM values are shown with representative images.

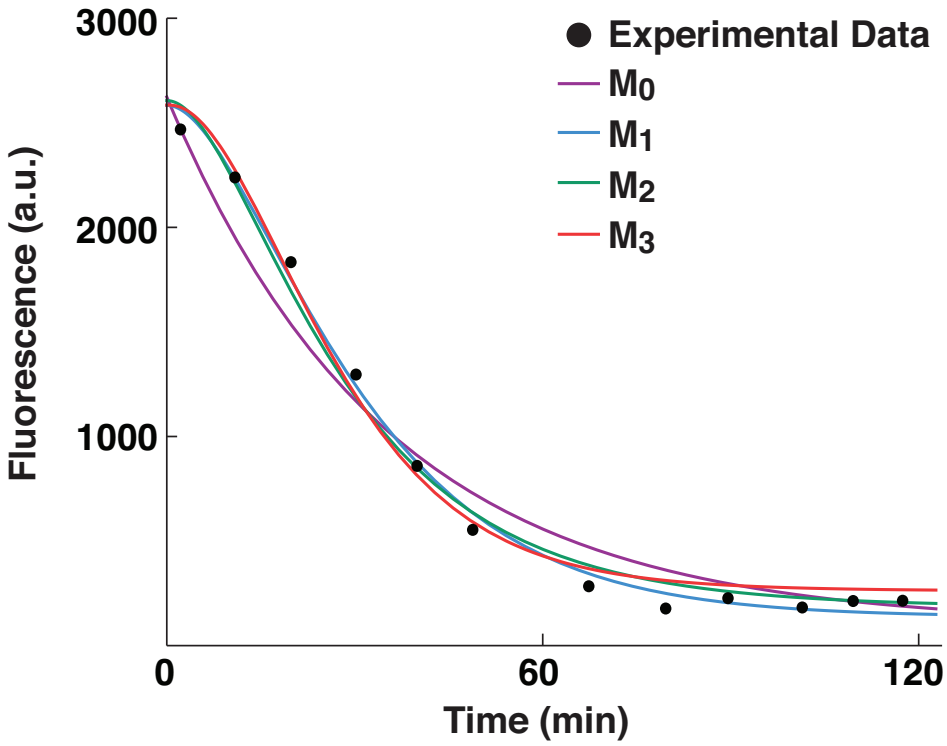

Supplementary Figure 9: Sample time-course IAA degradation data and model fits of IAA14|TIR1. Experimental data are shown in black circles, and the fits are shown in purple, blue, green and red for M_0, M_1, M_2 and M_3 models, respectively.

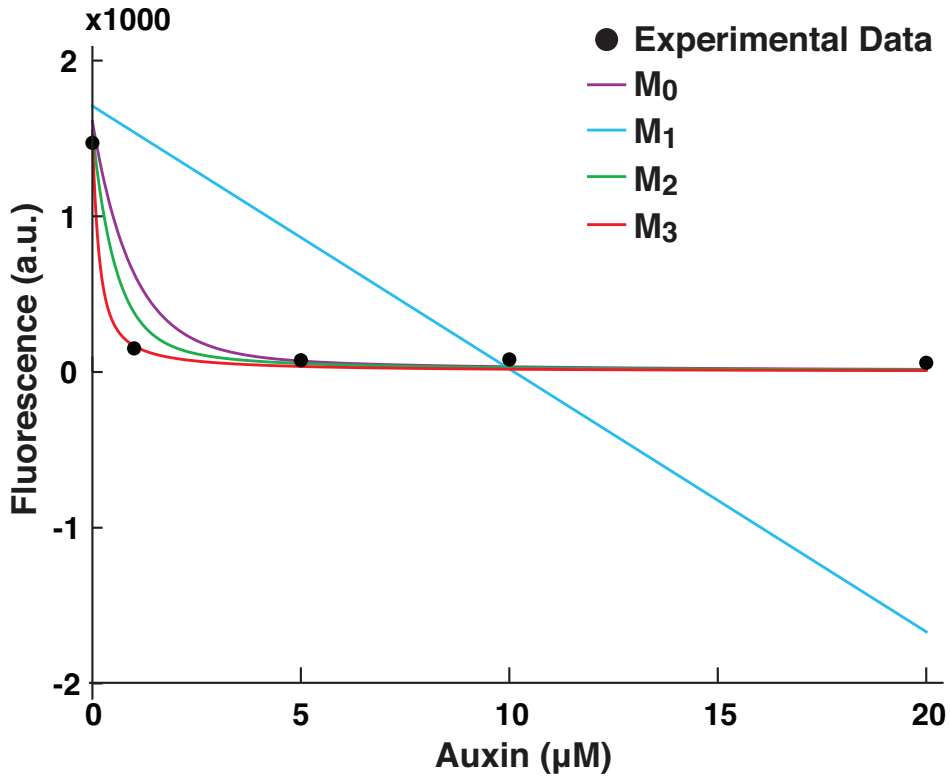

Supplementary Figure 10: Sample dose-response data and model predicted dose-response of IAA17|AFB2. Experimental data are shown in black circles, and the fits are shown in purple, blue, green and red for M_0, M_1, M_2, and M_3 models, respectively.

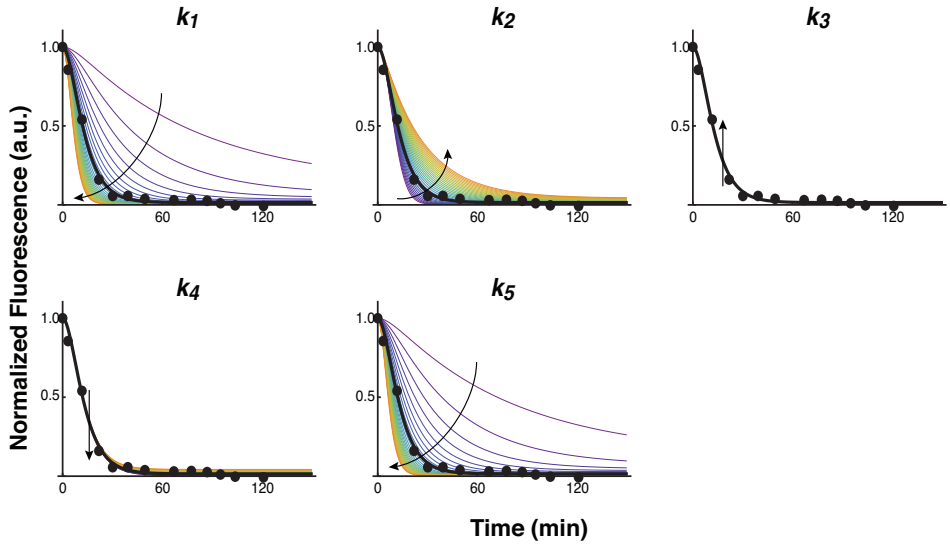

Supplementary Figure 11: Parameter variations study of M_2. Parameters of M_2 are varied from 10% to 300% of the nominal (estimated) values for IAA17|AFB2. The range was chosen based on the demonstrated range of estimated parameters shown in Supplementary Table 7. The trend demonstrated here is general for all IAA |AFB pairs. The resulting degradation curves are normalized to its initial condition. The experimental data are shown in black dots and the black arrows indicate the direction of parameter value increase.

Supplementary Table 1. A table of degradation rates, half-lives, and affinities from yeast, *in vitro* and plant studies.

AFB	IAA	Havens, 2012[1]		Calderon, 2012[2]	Dreher , 2006[3*]		Ramos, 2001[4*]	Quellet, 2001[5*]	Gray, 2001[6*]
		k5 mean	t 1/2 mean	Kd	basal half-life	auxin half-life	basal half-life	basal half-life	basal half-life
TIR1	1	3.94E-02	24.6	44.33	11.8	-	8	-	-
TIR1	1.1	3.49E-02	26.6	-	-	-	-	-	-
TIR1	2	3.84E-02	25.0	-	-	-	-	-	-
TIR1	3	2.90E-02	30.1	16.97	-	-	-	-	-
TIR1	4	2.59E-02	32.6	-	-	-	-	-	-
TIR1	6	2.01E-02	38.8	-	-	-	-	-	-
TIR1	7	3.52E-02	26.5	17	-	-	-	-	10.8
TIR1	8	4.10E-02	24.3	-	-	-	-	-	-
TIR1	9	3.70E-02	25.6	-	19	-	-	-	-
TIR1	10	2.65E-02	32.1	-	-	-	-	-	-
TIR1	11	1.24E-02	54.7	-	-	-	-	-	-
TIR1	12	3.06E-02	29.2	270	-	-	-	-	-
TIR1	13	3.81E-02	25.1	-	-	-	-	-	-
TIR1	14	3.11E-02	28.8	10.1	-	-	-	-	-
TIR1	15	2.02E-02	38.6	-	-	-	-	-	-
TIR1	17	3.63E-02	26.1	33	10.0	4.8	-	80.0	-
TIR1	18	3.20E-02	28.2	-	-	-	-	-	-
TIR1	19	2.82E-02	30.9	-	-	-	-	-	-
TIR1	20	2.88E-03	>>>	-	>>>	>>>	-	-	-
TIR1	26	2.75E-02	31.3	-	-	-	-	-	-
TIR1	27	3.48E-02	26.7	-	-	-	-	-	-
TIR1	28	2.55E-02	33.1	75	79.3	14.8	-	-	-
TIR1	31	5.55E-03	89.1	>1000	>20 hr	4 hr	-	-	-
TIR1	32	4.60E-03	>>>	-	-	-	-	-	

AFB	IAA	Havens, 2012[1]		Calderon, 2012[2]	Dreher , 2006[3*]		Ramos, 2001[4*]	Quellet, 2001[5*]	Gray, 2001[6*]
		k5 mean	t 1/2 mean	Kd	basal half-life	auxin half-life	basal half-life	basal half-life	basal half-life
AFB2	1	4.52E-02	19.3	-	-	-	-	-	-
AFB2	1.1	4.03E-02	20.9	-	-	-	-	-	-
AFB2	2	4.24E-02	20.3	-	-	-	-	-	-
AFB2	3	5.71E-02	16.8	-	-	-	-	-	-
AFB2	4	5.96E-02	16.3	-	-	-	-	-	-
AFB2	6	6.57E-02	15.4	-	-	-	-	-	-
AFB2	7	8.07E-02	13.6	-	-	-	-	-	-
AFB2	8	9.78E-02	12.2	-	-	-	-	-	-
AFB2	9	6.44E-02	15.7	-	-	-	-	-	-
AFB2	10	5.19E-02	17.7	-	-	-	-	-	-
AFB2	11	2.06E-02	31.8	-	-	-	-	-	-
AFB2	12	5.00E-02	18.1	-	-	-	-	-	-
AFB2	13	5.00E-02	18.3	-	-	-	-	-	-
AFB2	14	6.87E-02	15.0	-	-	-	-	-	-
AFB2	15	2.38E-02	29.0	-	-	-	-	-	-
AFB2	17	1.08E-01	11.5	-	-	-	-	-	-
AFB2	18	5.25E-02	17.7	-	-	-	-	-	-
AFB2	19	6.50E-02	15.6	-	-	-	-	-	-
AFB2	20	2.85E-03	>>>	-	-	-	-	-	-
AFB2	26	4.09E-02	20.7	-	-	-	-	-	-
AFB2	27	6.18E-02	15.9	-	-	-	-	-	-
AFB2	28	4.13E-02	20.5	-	-	-	-	-	-
AFB2	31	1.06E-02	48.9	-	-	-	-	-	-
AFB2	32	3.38E-03	>>>	-	-	-	-	-	-

[1] YFP-IAA|AFB pairs were co-expressed in yeast and YFP levels were monitored after the addition of 10 mM IAA. k5 and t 1/2 were calculated using data-driven model (Fig. 2)

[2] In vitro radio-labeled auxin binding assays were performed using purified ASK1-TIR1 complexes expressed in insect cells and GST-tagged IAAs expressed in *E.coli.*

[3] IAA:LUC transgenic seedlings were treated with cyclohexamide and LUC levels assayed at multiple time intervals. For auxin half-lives , seedlings were pretreated with 2,4-D for two hours prior to the addition of cyclohexamide The data was normalized to the mock treated samples and linearized by taking the natural log. The eqn of the linear best fit line was used to calc half-lives.

[4] IAA:LUC transgenic seedlings were treated with cyclohexamide and LUC levels assayed at multiple time intervals.

[5] Pulse-chase experiments were utlized to calculate the half-life of endogenous IAA17 in WT dark grown seedlings.

[6] Pulse-chase experiments were utlized to calculate the half-life of endogenous IAA7 in WT seedlings using the formula $t1/2 = 0.693t/\ln(N0/Nx)$, where t is time in minutes and N0 and Nx equal the amounts of AXR2 at t = 0 and t = 30min.

* Assays performed in whole seedlings: cannot distinguish receptor(s) responsible for degradation. Values are listed in the TIR1 category as TIR1 is presumed to be the dominant receptor *in planta,* though multiple receptors may play a role.

Supplementary Table 2: Table of amino acids included in each IAA truncation. The position of the conserved 13 amino acid domain II is included for comparison.

Truncation	Domains	Amino Acids		
		IAA1	IAA6	IAA28
Full Length (FL)	DI-DIV	1-168	1-189	1-175
T1	D1 and DII	1-75	1-94	1-81
T2	DII + additional aa	41-75	62-94	43-81
T2V	DII + additional aa	NA	NA	28-61
Conserved Core	DII alone	55-67	70-82	48-60

Supplementary Table 3: The residuals and the number of distinct parameters for M_0, M_1, M_2 (including its hypotheses), and M_3.

Hypothesis	$G(M)$	Number of distinct parameters for 48 IAA|Fbox pairs
H_0	49.31	144
H_1	81.68	240
H_2	24.54	240
H_{21}	32.29	168
H_{22}	46.32	168
H_{23}	48.11	102
H_{24}	27.44	102
H_3	30.63	336

Supplementary Table 4: Estimated parameters for IAA|TIR1 pairs using H_{23}.

Fbox	IAA	Replicate	k_1	k_2	k_3	k_4	k_5
TIR1	1	1	1.08E-01	9.22E-02	4.29E+00	3.14E-03	3.44E-02
TIR1	1.1	1	1.08E-01	9.22E-02	8.69E+00	3.14E-03	3.22E-02
TIR1	2	1	1.08E-01	9.22E-02	6.86E+00	3.14E-03	3.54E-02
TIR1	3	1	1.08E-01	9.22E-02	9.03E+00	3.14E-03	2.62E-02
TIR1	4	1	1.08E-01	9.22E-02	9.74E+00	3.14E-03	2.58E-02
TIR1	6	1	1.08E-01	9.22E-02	8.44E+00	3.14E-03	2.02E-02
TIR1	7	1	1.08E-01	9.22E-02	7.62E+00	3.14E-03	3.05E-02
TIR1	8	1	1.08E-01	9.22E-02	3.29E+00	3.14E-03	3.17E-02
TIR1	9	1	1.08E-01	9.22E-02	7.39E+00	3.14E-03	3.34E-02
TIR1	10	1	1.08E-01	9.22E-02	5.02E+00	3.14E-03	2.55E-02
TIR1	11	1	1.08E-01	9.22E-02	4.61E+00	3.14E-03	9.46E-03
TIR1	12	1	1.08E-01	9.22E-02	8.91E+00	3.14E-03	2.67E-02
TIR1	13	1	1.08E-01	9.22E-02	8.24E+00	3.14E-03	3.54E-02
TIR1	14	1	1.08E-01	9.22E-02	5.16E+00	3.14E-03	3.17E-02
TIR1	15	1	1.08E-01	9.22E-02	6.67E+00	3.14E-03	1.91E-02
TIR1	17	1	1.08E-01	9.22E-02	6.74E+00	3.14E-03	3.03E-02
TIR1	18	1	1.08E-01	9.22E-02	7.44E+00	3.14E-03	2.89E-02
TIR1	19	1	1.08E-01	9.22E-02	5.71E+00	3.14E-03	2.41E-02
TIR1	20	1	1.08E-01	9.22E-02	9.99E+00	3.14E-03	2.21E-03
TIR1	26	1	1.08E-01	9.22E-02	8.03E+00	3.14E-03	2.66E-02
TIR1	27	1	1.08E-01	9.22E-02	4.06E+00	3.14E-03	3.18E-02
TIR1	28	1	1.08E-01	9.22E-02	8.20E+00	3.14E-03	2.09E-02
TIR1	31	1	1.08E-01	9.22E-02	6.72E+00	3.14E-03	4.88E-03
TIR1	32	1	1.08E-01	9.22E-02	2.47E+00	3.14E-03	3.81E-03
TIR1	1	2	1.42E-01	1.72E-01	3.89E+00	3.19E-03	4.43E-02
TIR1	1.1	2	1.42E-01	1.72E-01	9.00E+00	3.19E-03	3.77E-02
TIR1	2	2	1.42E-01	1.72E-01	5.77E+00	3.19E-03	4.14E-02
TIR1	3	2	1.42E-01	1.72E-01	8.67E+00	3.19E-03	3.19E-02
TIR1	4	2	1.42E-01	1.72E-01	1.05E+01	3.19E-03	2.59E-02
TIR1	6	2	1.42E-01	1.72E-01	8.79E+00	3.19E-03	2.00E-02
TIR1	7	2	1.42E-01	1.72E-01	7.07E+00	3.19E-03	4.00E-02
TIR1	8	2	1.42E-01	1.72E-01	2.92E+00	3.19E-03	5.02E-02
TIR1	9	2	1.42E-01	1.72E-01	7.56E+00	3.19E-03	4.07E-02
TIR1	10	2	1.42E-01	1.72E-01	4.76E+00	3.19E-03	2.74E-02
TIR1	11	2	1.42E-01	1.72E-01	4.71E+00	3.19E-03	1.54E-02
TIR1	12	2	1.42E-01	1.72E-01	8.83E+00	3.19E-03	3.45E-02
TIR1	13	2	1.42E-01	1.72E-01	8.46E+00	3.19E-03	4.07E-02
TIR1	14	2	1.42E-01	1.72E-01	5.32E+00	3.19E-03	3.05E-02
TIR1	15	2	1.42E-01	1.72E-01	5.71E+00	3.19E-03	2.14E-02
TIR1	17	2	1.42E-01	1.72E-01	6.30E+00	3.19E-03	4.23E-02
TIR1	18	2	1.42E-01	1.72E-01	8.19E+00	3.19E-03	3.51E-02
TIR1	19	2	1.42E-01	1.72E-01	5.39E+00	3.19E-03	3.22E-02
TIR1	20	2	1.42E-01	1.72E-01	9.59E+00	3.19E-03	3.54E-03
TIR1	26	2	1.42E-01	1.72E-01	9.27E+00	3.19E-03	2.85E-02
TIR1	27	2	1.42E-01	1.72E-01	3.92E+00	3.19E-03	3.78E-02
TIR1	28	2	1.42E-01	1.72E-01	7.87E+00	3.19E-03	3.02E-02
TIR1	31	2	1.42E-01	1.72E-01	6.81E+00	3.19E-03	6.23E-03
TIR1	32	2	1.42E-01	1.72E-01	2.55E+00	3.19E-03	5.39E-03

Supplementary Table 5: Estimated parameters for IAA|AFB2 pairs using H_{23}.

Fbox	IAA	Replicate	k_1	k_2	k_3	k_4	k_5
AFB2	1	1	1.49E-01	1.18E-01	4.48E+00	3.63E-03	4.59E-02
AFB2	1.1	1	1.49E-01	1.18E-01	9.77E+00	3.63E-03	4.47E-02
AFB2	2	1	1.49E-01	1.18E-01	8.09E+00	3.63E-03	4.65E-02
AFB2	3	1	1.49E-01	1.18E-01	1.13E+01	3.63E-03	6.14E-02
AFB2	4	1	1.49E-01	1.18E-01	1.16E+01	3.63E-03	6.05E-02
AFB2	6	1	1.49E-01	1.18E-01	8.55E+00	3.63E-03	7.06E-02
AFB2	7	1	1.49E-01	1.18E-01	7.19E+00	3.63E-03	8.35E-02
AFB2	8	1	1.49E-01	1.18E-01	3.16E+00	3.63E-03	1.05E-01
AFB2	9	1	1.49E-01	1.18E-01	8.01E+00	3.63E-03	7.29E-02
AFB2	10	1	1.49E-01	1.18E-01	5.80E+00	3.63E-03	5.16E-02
AFB2	11	1	1.49E-01	1.18E-01	5.87E+00	3.63E-03	2.08E-02
AFB2	12	1	1.49E-01	1.18E-01	9.16E+00	3.63E-03	5.04E-02
AFB2	13	1	1.49E-01	1.18E-01	9.57E+00	3.63E-03	5.52E-02
AFB2	14	1	1.49E-01	1.18E-01	6.25E+00	3.63E-03	6.45E-02
AFB2	15	1	1.49E-01	1.18E-01	7.94E+00	3.63E-03	2.47E-02
AFB2	17	1	1.49E-01	1.18E-01	6.04E+00	3.63E-03	1.04E-01
AFB2	18	1	1.49E-01	1.18E-01	8.57E+00	3.63E-03	5.80E-02
AFB2	19	1	1.49E-01	1.18E-01	5.96E+00	3.63E-03	5.65E-02
AFB2	20	1	1.49E-01	1.18E-01	1.07E+01	3.63E-03	2.67E-03
AFB2	26	1	1.49E-01	1.18E-01	1.06E+01	3.63E-03	4.42E-02
AFB2	27	1	1.49E-01	1.18E-01	4.49E+00	3.63E-03	6.19E-02
AFB2	28	1	1.49E-01	1.18E-01	8.85E+00	3.63E-03	4.14E-02
AFB2	31	1	1.49E-01	1.18E-01	7.50E+00	3.63E-03	1.07E-02
AFB2	32	1	1.49E-01	1.18E-01	2.85E+00	3.63E-03	2.51E-03
AFB2	1	2	1.27E-01	8.77E-02	3.72E+00	3.25E-03	4.46E-02
AFB2	1.1	2	1.27E-01	8.77E-02	9.23E+00	3.25E-03	3.59E-02
AFB2	2	2	1.27E-01	8.77E-02	7.84E+00	3.25E-03	3.82E-02
AFB2	3	2	1.27E-01	8.77E-02	8.45E+00	3.25E-03	5.28E-02
AFB2	4	2	1.27E-01	8.77E-02	1.02E+01	3.25E-03	5.87E-02
AFB2	6	2	1.27E-01	8.77E-02	8.10E+00	3.25E-03	6.08E-02
AFB2	7	2	1.27E-01	8.77E-02	6.33E+00	3.25E-03	7.79E-02
AFB2	8	2	1.27E-01	8.77E-02	2.66E+00	3.25E-03	9.07E-02
AFB2	9	2	1.27E-01	8.77E-02	7.16E+00	3.25E-03	5.58E-02
AFB2	10	2	1.27E-01	8.77E-02	5.49E+00	3.25E-03	5.23E-02
AFB2	11	2	1.27E-01	8.77E-02	5.63E+00	3.25E-03	2.04E-02
AFB2	12	2	1.27E-01	8.77E-02	8.07E+00	3.25E-03	4.96E-02
AFB2	13	2	1.27E-01	8.77E-02	8.90E+00	3.25E-03	4.47E-02
AFB2	14	2	1.27E-01	8.77E-02	5.43E+00	3.25E-03	7.30E-02
AFB2	15	2	1.27E-01	8.77E-02	7.37E+00	3.25E-03	2.29E-02
AFB2	17	2	1.27E-01	8.77E-02	5.05E+00	3.25E-03	1.12E-01
AFB2	18	2	1.27E-01	8.77E-02	8.16E+00	3.25E-03	4.71E-02
AFB2	19	2	1.27E-01	8.77E-02	4.67E+00	3.25E-03	7.35E-02
AFB2	20	2	1.27E-01	8.77E-02	9.29E+00	3.25E-03	3.03E-03
AFB2	26	2	1.27E-01	8.77E-02	9.99E+00	3.25E-03	3.77E-02
AFB2	27	2	1.27E-01	8.77E-02	3.93E+00	3.25E-03	6.17E-02
AFB2	28	2	1.27E-01	8.77E-02	7.56E+00	3.25E-03	4.12E-02
AFB2	31	2	1.27E-01	8.77E-02	6.90E+00	3.25E-03	1.06E-02
AFB2	32	2	1.27E-01	8.77E-02	2.68E+00	3.25E-03	4.25E-03

Supplementary Table 6: Estimated parameters for Degron comparison study using H_{23}.

Fbox	IAA	Degron	Replicate	k_1	k_2	k_3	k_4	k_5
TIR1	1	FL	1	1.08E-01	9.22E-02	6.51E+00	3.14E-03	3.98E-02
TIR1	1	T1	1	1.08E-01	9.22E-02	2.80E+00	3.14E-03	3.41E-02
TIR1	1	T2	1	1.08E-01	9.22E-02	4.92E+00	3.14E-03	1.10E-02
TIR1	6	FL	1	1.08E-01	9.22E-02	6.89E+00	3.14E-03	3.59E-02
TIR1	6	T1	1	1.08E-01	9.22E-02	5.53E+00	3.14E-03	3.22E-02
TIR1	6	T2	1	1.08E-01	9.22E-02	6.06E+00	3.14E-03	1.32E-02
TIR1	28	FL	1	1.08E-01	9.22E-02	5.81E+00	3.14E-03	1.70E-02
TIR1	28	T1	1	1.08E-01	9.22E-02	5.94E+00	3.14E-03	2.96E-02
TIR1	28	T2	1	1.08E-01	9.22E-02	7.22E+00	3.14E-03	3.16E-02
TIR1	28	T2V	1	1.08E-01	9.22E-02	8.39E+00	3.14E-03	6.79E-03
TIR1	1	FL	2	1.42E-01	1.72E-01	6.70E+00	3.19E-03	4.55E-02
TIR1	1	T1	2	1.42E-01	1.72E-01	2.82E+00	3.19E-03	4.44E-02
TIR1	1	T2	2	1.42E-01	1.72E-01	4.76E+00	3.19E-03	1.24E-02
TIR1	6	FL	2	1.42E-01	1.72E-01	7.73E+00	3.19E-03	4.62E-02
TIR1	6	T1	2	1.42E-01	1.72E-01	5.97E+00	3.19E-03	4.45E-02
TIR1	6	T2	2	1.42E-01	1.72E-01	6.57E+00	3.19E-03	1.81E-02
TIR1	28	FL	2	1.42E-01	1.72E-01	5.84E+00	3.19E-03	1.98E-02
TIR1	28	T1	2	1.42E-01	1.72E-01	5.99E+00	3.19E-03	3.50E-02
TIR1	28	T2	2	1.42E-01	1.72E-01	7.28E+00	3.19E-03	3.59E-02
TIR1	28	T2V	2	1.42E-01	1.72E-01	8.14E+00	3.19E-03	7.51E-03
AFB2	1	FL	1	1.49E-01	1.18E-01	7.13E+00	3.63E-03	9.16E-02
AFB2	1	T1	1	1.49E-01	1.18E-01	3.21E+00	3.63E-03	1.05E-01
AFB2	1	T2	1	1.49E-01	1.18E-01	4.91E+00	3.63E-03	2.35E-02
AFB2	6	FL	1	1.49E-01	1.18E-01	7.43E+00	3.63E-03	1.25E-01
AFB2	6	T1	1	1.49E-01	1.18E-01	6.03E+00	3.63E-03	1.82E-01
AFB2	6	T2	1	1.49E-01	1.18E-01	6.32E+00	3.63E-03	6.81E-02
AFB2	28	FL	1	1.49E-01	1.18E-01	6.21E+00	3.63E-03	4.02E-02
AFB2	28	T1	1	1.49E-01	1.18E-01	6.70E+00	3.63E-03	7.67E-02
AFB2	28	T2	1	1.49E-01	1.18E-01	7.84E+00	3.63E-03	7.03E-02
AFB2	28	T2V	1	1.49E-01	1.18E-01	8.97E+00	3.63E-03	1.97E-02
AFB2	1	FL	2	1.27E-01	8.77E-02	7.63E+00	3.25E-03	7.44E-02
AFB2	1	T1	2	1.27E-01	8.77E-02	3.15E+00	3.25E-03	8.17E-02
AFB2	1	T2	2	1.27E-01	8.77E-02	4.88E+00	3.25E-03	1.69E-02
AFB2	6	FL	2	1.27E-01	8.77E-02	7.14E+00	3.25E-03	1.30E-01
AFB2	6	T1	2	1.27E-01	8.77E-02	5.83E+00	3.25E-03	1.87E-01
AFB2	6	T2	2	1.27E-01	8.77E-02	6.10E+00	3.25E-03	7.32E-02
AFB2	28	FL	2	1.27E-01	8.77E-02	5.83E+00	3.25E-03	2.91E-02
AFB2	28	T1	2	1.27E-01	8.77E-02	6.68E+00	3.25E-03	5.88E-02
AFB2	28	T2	2	1.27E-01	8.77E-02	7.65E+00	3.25E-03	5.35E-02
AFB2	28	T2V	2	1.27E-01	8.77E-02	8.64E+00	3.25E-03	1.39E-02

Supplementary Table 7: Average, minimum and maximum values of the estimated parameters in Supplementary Tables 4 and 5.

	average	min (% of average)	max (% of average)
k_1	0.13	0.11 (82)	0.15 (138)
k_2	0.12	8.8E-2 (74)	0.17 (195)
k_3	6.98	2.47 (35)	11.6 (468)
k_4	3.3E-3	3.1E-3 (95)	3.6E-3 (116)
k_5	3.87E-2	2.2-3 (5.7)	0.11 (51)

Supplemental Table 8: Oligonucleotides used in this study

ORF	Forward primer	Reverse primer
IAA1	ATGGAAGTCACCAATGGGCTTAACCTTAAG	TCATAAGGCAGTAGGAGCTTCGGATCC
IAA2	ATGGCGTACGAGAAAGTCAACGAGCTTAAC	TCATAAGGAAGAGTCTAGAGCAGGAGCGTC
IAA3	ATGGATGAGTTTGTTAACCTCA	TTATCATACACCACAGCCTAAAC
IAA4	ATGGAAAAAGTTGATGTTTATGATGAGCTTGTTAACCTAAAG	TTAAAGACCACCACAACCTAAACCTTTAACTTCAGATC
IAA5	ATGGCGAATGAGAGTAATAATCTTGGACTCG	TCATCCTCTGTTACATGATCTCTTCATAATCCTTAACC
IAA6	ATGGCAAAGGAAGGTCTAGCACTCGAG	TTAATCTTGCTGGAGACCAAAACCAGTTG
IAA7	ATGATCGGCCAACTTATGAACCTCAAG	TCAAGATCTGTTCTTGCAGTACTTCTCCATTG
IAA8	ATGAGTTCTGGGAACGATAAGATAAAACAAGTCC	TCAAACCCGCTCTTTGTTCTTCGATTTC
IAA9	ATGTCCCCGGAAGAGGAGCTACAGAG	TTAAGCTCTCATCTTCGATTTCTCCATTGC
IAA10	ATGAATGGTTTGCAAGAAGTTTGTTCGTC	CTACTTACCTACTCCAGCTCCAATTGATGTCTTCATG
IAA11	ATGGAAGGCGGTTCCGCTAGTG	TCATAATATCATCTGAGCTTTACCAGTAGCCTCC
IAA12	ATGCGTGGTGTGTCAGAATTGGAG	CTAAACAGGGTTGTTTCTTTGTCTATCCTTCTGC
IAA13	ATGATTACTGAACTTGAGATGGGGAAAGGTG	CTAAACCGGCTGCTTTCGCTGTC
IAA14	ATGAACCTTAAGGAGACGG	TTATCATGATCTGTTCTTGAACTTC
IAA15	ATGTCACCGGAGGAATACGTTAGGGTTTG	CTATAATCCAATAGCATCTCCGGTTTTCATTAACCTC
IAA17	ATGATGGGCAGTGTCGAGCTGAATC	TCAAGCTCTGCTCTTGCACTTCTCCATC
IAA18	ATGGAGGGTTATTCAAGAAAC	TTATCATCTTCTCATTTTCTCTTGC
IAA19	ATGGAGAAGGAAGGACTC	TTATCACTCGTCTACTCCTCTAGG
IAA20	ATGGGAAGAGGGAGAAGTTCATCGTC	TCAGTAGTGGTAATTAGCTCTTGAAATCTTCAGTCTTCTC
IAA26	ATGGAAGGTTGTCCAAGAAACAGAGAAATC	TCAGTGCATCATCTTCTCTTGCTTACTGC
IAA27	ATGTCTGTATCTGTAGCAGCAGAGCATGATTACATAG	CTAGTTCCTGCTTCTGCACTTCTCCATCAC
IAA28	ATGGAAGAAGAAAAGAGATTGG	TTACTATTCCTTGCCATGTTTTC
IAA31	ATGGAGGTCTCTAACTCTTGTTCTTCATTTTCTTCATC	TTAATACCTCTCCGGTCTCGTGATCTTTAGTCTTC
IAA32	ATGGACCCAAACACACCTGCAGAC	TTAAAAGGGAAGAAGAGCATCGTTTCTTCTTG
TIR1	ATGCAGAAGCGAATAGCCTTGTCG	TTATAATCCGTTAGTAGTAATGATTTGCCTGGAAAACC
AFB2	ATGAATTATTTCCCAGATGAAGTAATAGAGCATGTATTC	TTAGAGAATCCACACAAATGGCGG
mTIR1	ATGGTCTTCATCGGGAACTGCTACGC	TTATAATCCGTTAGTAGTAATGATTTGCCTGGAAAACC
AFB1	ATGGGTCTCCGATTCCCACCTAAG	TTACTTTATGGCTAGATGTGAAACTCCATTCTCAG
AFB3	ATGAATTATTTCCCAGACGAGGTTATAGAGCAC	CTAAAGAATCCTAACATATGGTGGTGCATCTTTTC

*all forward primers had AAAAAGCAGGCTTCAAA appended to the 5' end

**all reverse primers had AGAAAGCTGGGTG appended to the 5' end

Sequencing Primers

All Coding - M13F	GTAAAACGACGGCCAGT
All Coding - M13R	GGAAACAGCTATGACCATG
TIR1, mTIR1 (bp 663-682)	TGTTCCACTTGAAAAATTGG
TIR1, mTIR1 (bp 751-734)	GTCGCACTTCTGCAGTGT
AFB2	CTGATGGTCTTGCCTCTATTG
AFB1 (bp 478-501)	CGAGAGTGTATTGTTGAAGATTTA
AFB3 (bp 404-424)	GTGAAGGGTTTACCACTGATG

Primers used for Gibson Assembly of truncations

Template or construct	Forward	Reverse
YFP-IAA17.T1-NLS	ATCACTCTCGGCATGGACGAG	AGCGTGACATAACTAATTACATGACATCGATT
pGP4GY	GTTATGTCACGCTTACATTCACGCCC	GAGAGTGATCCCGGCGGC
IAA1.FL	TGCCGGGCCCATGGAAGTCACCAATGGGCTTAACC	GGGGGCGCCAGCACCTAAGGCAGTAGGAGCTTCGGATCCT
pGP4GY:IAA1.FL	GGTGCTGGCGCCCCCA	CCATTGGTGACTTCCATGGGCCCGGCACCC
IAA1.T1	TGCCGGGCCCATGGAAGTCACCAATGGGCTTAACC	AGCACCACTCACGTTTTTGTTGTTGTTGTTCTTACG
pGP4GY:IAA1.T1	AACAAAAACGTGAGTGGTGCTGGCGCCCC	CCATTGGTGACTTCCATGGGCCCGGCACCC
IAA1.T2	CCGGGCCCAACGACTCAACAGAAGAATCTGCTCCTC	AGCACCACTCACGTTTTTGTTGTTGTTGTTCTTACG
pGP4GY:IAA1.T2	AACAAAAACGTGAGTGGTGCTGGCGCCCC	TCTTCTGTTGAGTCGTTGGGCCCGGCACCC
IAA6.FL	TGCCGGGCCCATGGCAAAGGAAGGTCTAGCACTCG	GGGGGCGCCAGCACCATCTTGCTGGAGACCAAAACCAGTT
pGP4GY:IAA6.FL	GGTGCTGGCGCCCCCA	AGACCTTCCTTTGCCATGGGCCCGGCACCC
IAA6.T1	TGCCGGGCCCATGGCAAAGGAAGGTCTAGCACTCG	CCAGCACCGCCTATAGCTTTCGATGCTTCCTCATTG
pGP4GY:IAA6.T1	TCGAAAGCTATAGGCGGTGCTGGCGCCCC	AGACCTTCCTTTGCCATGGGCCCGGCACCC
IAA6.T2	TGCCGGGCCCGAATCACTGCCGGTTGTGAAGAGTC	CCAGCACCGCCTATAGCTTTCGATGCTTCCTCATTG
pGP4GY:IAA6T2	TCGAAAGCTATAGGCGGTGCTGGCGCCCC	ACAACCGGCAGTGATTCGGGCCCGGCACCC
IAA28.FL	GGCCCATGGAAGAAGAAAAGAGATTGGAGCTAAGGC	GGGGGCGCCAGCACCTTCCTTGCCATGTTTTCTAGGTGAGA
pGP4GY:IAA28.FL	GGTGCTGGCGCCCCCA	CTCTTTTCTTCTTCCATGGGCCCGGCACCC
IAA28.T1	GGCCCATGGAAGAAGAAAAGAGATTGGAGCTAAGGC	GCACCCAATTCCTTCTCTTCATCACTCTCCTTCTTC
pGP4GY:IAA28.T1	GAAGAGAAGGAATTGGGTGCTGGCGCCCC	CTCTTTTCTTCTTCCATGGGCCCGGCACCC
IAA28.T2	GTGCCGGGCCCAGGGTTGAGGTAGCTCCAGTGGTG	GCACCCAATTCCTTCTCTTCATCACTCTCCTTCTTC
pGP4GY:IAA28.T2	GAAGAGAAGGAATTGGGTGCTGGCGCCCC	GGAGCTACCTCAACCCTGGGCCCGGCACCC
IAA28.T2V	TGCCGGGCCCAAACAAAAAAGCTCGACCAAAGAAACA	GCGCCAGCACCGTTTCTCCGGGATGATCTCACCG
pGP4GY:IAA28.T2V	ATCATCCCGGAGAAACGGTGCTGGCGCCCC	GTCGAGCTTTTTTGTTTGGGCCCGGCACCC

Primers used for Gibson Assembly of the plant expression vector

IAA28.T2:DII-VENUS	TGTACAAAAAAGCAGGCTATGAGGGTTGAGGTAGCTCCAGTGG	GCAGCTGCCGCACAATTCCTTCTCTTCATCACTCTCCTT
DII-VENUS	TGCGGCAGCTGCGACCC	CATAGCCTGCTTTTTTGTACAAACTTGACTAGTGG

*primer names = annealing template sequence name:overlap for homologous assembly

**undelined regions anneal to the template, while the non-underlined are the additional sequence for homologous assembly

Supplementary Table 9: Yeast strains used in this study

Strain Name	Relevant Genotype
W303-1A	*MAT***a** *leu2-3,112 trp1-1 can1-100 ura3-1 ade2-1 his3-11,15*
W303-1B	*MATα leu2-3,112 trp1-1 can1-100 ura3-1 ade2-1 his3-11,15*
TIR1|IAA1	*MAT***a***/MATα LEU2:pGPD-TIR1/leu2-3,112 trp1-1/TRP1:pGPD-YFP-IAA1*
TIR1|IAA2	*MAT***a***/MATα LEU2:pGPD-TIR1/leu2-3,112 trp1-1/TRP1:pGPD-YFP-IAA2*
TIR1|IAA3	*MAT***a***/MATα LEU2:pGPD-TIR1/leu2-3,112 trp1-1/TRP1:pGPD-YFP-IAA3*
TIR1|IAA4	*MAT***a***/MATα LEU2:pGPD-TIR1/leu2-3,112 trp1-1/TRP1:pGPD-YFP-IAA4*
TIR1|IAA5	*MAT***a***/MATα LEU2:pGPD-TIR1/leu2-3,112 trp1-1/TRP1:pGPD-YFP-IAA5*
TIR1|IAA6	*MAT***a***/MATα LEU2:pGPD-TIR1/leu2-3,112 trp1-1/TRP1:pGPD-YFP-IAA6*
TIR1|IAA7	*MAT***a***/MATα LEU2:pGPD-TIR1/leu2-3,112 trp1-1/TRP1:pGPD-YFP-IAA7*
TIR1|IAA8	*MAT***a***/MATα LEU2:pGPD-TIR1/leu2-3,112 trp1-1/TRP1:pGPD-YFP-IAA8*
TIR1|IAA9	*MAT***a***/MATα LEU2:pGPD-TIR1/leu2-3,112 trp1-1/TRP1:pGPD-YFP-IAA9*
TIR1|IAA10	*MAT***a***/MATα LEU2:pGPD-TIR1/leu2-3,112 trp1-1/TRP1:pGPD-YFP-IAA10*
TIR1|IAA11	*MAT***a***/MATα LEU2:pGPD-TIR1/leu2-3,112 trp1-1/TRP1:pGPD-YFP-IAA11*
TIR1|IAA12	*MAT***a***/MATα LEU2:pGPD-TIR1/leu2-3,112 trp1-1/TRP1:pGPD-YFP-IAA12*
TIR1|IAA13	*MAT***a***/MATα LEU2:pGPD-TIR1/leu2-3,112 trp1-1/TRP1:pGPD-YFP-IAA13*
TIR1|IAA14	*MAT***a***/MATα LEU2:pGPD-TIR1/leu2-3,112 trp1-1/TRP1:pGPD-YFP-IAA14*
TIR1|IAA15	*MAT***a***/MATα LEU2:pGPD-TIR1/leu2-3,112 trp1-1/TRP1:pGPD-YFP-IAA15*
TIR1|IAA17	*MAT***a***/MATα LEU2:pGPD-TIR1/leu2-3,112 trp1-1/TRP1:pGPD-YFP-IAA17*
TIR1|IAA18	*MAT***a***/MATα LEU2:pGPD-TIR1/leu2-3,112 trp1-1/TRP1:pGPD-YFP-IAA18*
TIR1|IAA19	*MAT***a***/MATα LEU2:pGPD-TIR1/leu2-3,112 trp1-1/TRP1:pGPD-YFP-IAA19*
TIR1|IAA20	*MAT***a***/MATα LEU2:pGPD-TIR1/leu2-3,112 trp1-1/TRP1:pGPD-YFP-IAA20*
TIR1|IAA26	*MAT***a***/MATα LEU2:pGPD-TIR1/leu2-3,112 trp1-1/TRP1:pGPD-YFP-IAA26*
TIR1|IAA27	*MAT***a***/MATα LEU2:pGPD-TIR1/leu2-3,112 trp1-1/TRP1:pGPD-YFP-IAA27*
TIR1|IAA28	*MAT***a***/MATα LEU2:pGPD-TIR1/leu2-3,112 trp1-1/TRP1:pGPD-YFP-IAA28*
TIR1|IAA29	*MAT***a***/MATα LEU2:pGPD-TIR1/leu2-3,112 trp1-1/TRP1:pGPD-YFP-IAA29*
TIR1|IAA31	*MAT***a***/MATα LEU2:pGPD-TIR1/leu2-3,112 trp1-1/TRP1:pGPD-YFP-IAA31*
TIR1|IAA32	*MAT***a***/MATα LEU2:pGPD-TIR1/leu2-3,112 trp1-1/TRP1:pGPD-YFP-IAA32*
AFB2|IAA1	*MAT***a***/MATα LEU2:pGPD-AFB2/leu2-3,112 trp1-1/TRP1:pGPD-YFP-IAA1*

Strain Name	Relevant Genotype
AFB2|IAA2	*MAT**a**/MATα LEU2:pGPD-AFB2/leu2-3,112 trp1-1/TRP1:pGPD-YFP-IAA2*
AFB2|IAA3	*MAT**a**/MATα LEU2:pGPD-AFB2/leu2-3,112 trp1-1/TRP1:pGPD-YFP-IAA3*
AFB2|IAA4	*MAT**a**/MATα LEU2:pGPD-AFB2/leu2-3,112 trp1-1/TRP1:pGPD-YFP-IAA4*
AFB2|IAA5	*MAT**a**/MATα LEU2:pGPD-AFB2/leu2-3,112 trp1-1/TRP1:pGPD-YFP-IAA5*
AFB2|IAA6	*MAT**a**/MATα LEU2:pGPD-AFB2/leu2-3,112 trp1-1/TRP1:pGPD-YFP-IAA6*
AFB2|IAA7	*MAT**a**/MATα LEU2:pGPD-AFB2/leu2-3,112 trp1-1/TRP1:pGPD-YFP-IAA7*
AFB2|IAA8	*MAT**a**/MATα LEU2:pGPD-AFB2/leu2-3,112 trp1-1/TRP1:pGPD-YFP-IAA8*
AFB2|IAA9	*MAT**a**/MATα LEU2:pGPD-AFB2/leu2-3,112 trp1-1/TRP1:pGPD-YFP-IAA9*
AFB2|IAA10	*MAT**a**/MATα LEU2:pGPD-AFB2/leu2-3,112 trp1-1/TRP1:pGPD-YFP-IAA10*
AFB2|IAA11	*MAT**a**/MATα LEU2:pGPD-AFB2/leu2-3,112 trp1-1/TRP1:pGPD-YFP-IAA11*
AFB2|IAA12	*MAT**a**/MATα LEU2:pGPD-AFB2/leu2-3,112 trp1-1/TRP1:pGPD-YFP-IAA12*
AFB2|IAA13	*MAT**a**/MATα LEU2:pGPD-AFB2/leu2-3,112 trp1-1/TRP1:pGPD-YFP-IAA13*
AFB2|IAA14	*MAT**a**/MATα LEU2:pGPD-AFB2/leu2-3,112 trp1-1/TRP1:pGPD-YFP-IAA14*
AFB2|IAA15	*MAT**a**/MATα LEU2:pGPD-AFB2/leu2-3,112 trp1-1/TRP1:pGPD-YFP-IAA15*
AFB2|IAA17	*MAT**a**/MATα LEU2:pGPD-AFB2/leu2-3,112 trp1-1/TRP1:pGPD-YFP-IAA17*
AFB2|IAA18	*MAT**a**/MATα LEU2:pGPD-AFB2/leu2-3,112 trp1-1/TRP1:pGPD-YFP-IAA18*
AFB2|IAA19	*MAT**a**/MATα LEU2:pGPD-AFB2/leu2-3,112 trp1-1/TRP1:pGPD-YFP-IAA19*
AFB2|IAA20	*MAT**a**/MATα LEU2:pGPD-AFB2/leu2-3,112 trp1-1/TRP1:pGPD-YFP-IAA20*
AFB2|IAA26	*MAT**a**/MATα LEU2:pGPD-AFB2/leu2-3,112 trp1-1/TRP1:pGPD-YFP-IAA26*
AFB2|IAA27	*MAT**a**/MATα LEU2:pGPD-AFB2/leu2-3,112 trp1-1/TRP1:pGPD-YFP-IAA27*
AFB2|IAA28	*MAT**a**/MATα LEU2:pGPD-AFB2/leu2-3,112 trp1-1/TRP1:pGPD-YFP-IAA28*
AFB2|IAA29	*MAT**a**/MATα LEU2:pGPD-AFB2/leu2-3,112 trp1-1/TRP1:pGPD-YFP-IAA29*
AFB2|IAA31	*MAT**a**/MATα LEU2:pGPD-AFB2/leu2-3,112 trp1-1/TRP1:pGPD-YFP-IAA31*
AFB2|IAA32	*MAT**a**/MATα LEU2:pGPD-AFB2/leu2-3,112 trp1-1/TRP1:pGPD-YFP-IAA32*
TIR1|IAA1.FL-NLS	*MAT**a**/MATα LEU2:pGPD-TIR1/leu2-3,112 trp1-1/TRP1:pGPD-YFP-IAA1-NLS*
TIR1|IAA1.T1-NLS	*MAT**a**/MATα LEU2:pGPD-TIR1/leu2-3,112 trp1-1/TRP1:pGPD-YFP-IAA1.T1-NLS*
TIR1|IAA1.T2-NLS	*MAT**a**/MATα LEU2:pGPD-TIR1/leu2-3,112 trp1-1/TRP1:pGPD-YFP-IAA1.T2-NLS*
TIR1|IAA6.FL-NLS	*MAT**a**/MATα LEU2:pGPD-TIR1/leu2-3,112 trp1-1/TRP1:pGPD-YFP-IAA6-NLS*
TIR1|IAA6.T1-NLS	*MAT**a**/MATα LEU2:pGPD-TIR1/leu2-3,112 trp1-1/TRP1:pGPD-YFP-IAA6.T1-NLS*
TIR1|IAA6.T2-NLS	*MAT**a**/MATα LEU2:pGPD-TIR1/leu2-3,112 trp1-1/TRP1:pGPD-YFP-IAA6.T2-NLS*

Strain Name	Relevant Genotype
TIR1|IAA28.FL-NLS	*MAT**a**/MATα LEU2:pGPD-TIR1/leu2-3,112 trp1-1/TRP1:pGPD-YFP-IAA28-NLS*
TIR1|IAA28.T1-NLS	*MAT**a**/MATα LEU2:pGPD-TIR1/leu2-3,112 trp1-1/TRP1:pGPD-YFP-IAA28.T1-NLS*
TIR1|IAA28.T2-NLS	*MAT**a**/MATα LEU2:pGPD-TIR1/leu2-3,112 trp1-1/TRP1:pGPD-YFP-IAA28.T2-NLS*
TIR1|IAA28.T2V-NLS	*MAT**a**/MATα LEU2:pGPD-TIR1/leu2-3,112 trp1-1/TRP1:pGPD-YFP-IAA28.T2V-NLS*
AFB2|IAA1.FL-NLS	*MAT**a**/MATα LEU2:pGPD-AFB2/leu2-3,112 trp1-1/TRP1:pGPD-YFP-IAA1-NLS*
AFB2|IAA1.T1-NLS	*MAT**a**/MATα LEU2:pGPD-AFB2/leu2-3,112 trp1-1/TRP1:pGPD-YFP-IAA1.T1-NLS*
AFB2|IAA1.T2-NLS	*MAT**a**/MATα LEU2:pGPD-AFB2/leu2-3,112 trp1-1/TRP1:pGPD-YFP-IAA1.T2-NLS*
AFB2|IAA6.FL-NLS	*MAT**a**/MATα LEU2:pGPD-AFB2/leu2-3,112 trp1-1/TRP1:pGPD-YFP-IAA6-NLS*
AFB2|IAA6.T1-NLS	*MAT**a**/MATα LEU2:pGPD-AFB2/leu2-3,112 trp1-1/TRP1:pGPD-YFP-IAA6.T1-NLS*
AFB2|IAA6.T2-NLS	*MAT**a**/MATα LEU2:pGPD-AFB2/leu2-3,112 trp1-1/TRP1:pGPD-YFP-IAA6.T2-NLS*
AFB2|IAA28.FL-NLS	*MAT**a**/MATα LEU2:pGPD-AFB2/leu2-3,112 trp1-1/TRP1:pGPD-YFP-IAA28-NLS*
AFB2|IAA28.T1-NLS	*MAT**a**/MATα LEU2:pGPD-AFB2/leu2-3,112 trp1-1/TRP1:pGPD-YFP-IAA28.T1-NLS*
AFB2|IAA28.T2-NLS	*MAT**a**/MATα LEU2:pGPD-AFB2/leu2-3,112 trp1-1/TRP1:pGPD-YFP-IAA28.T2-NLS*
AFB2|IAA28.T2V-NLS	*MAT**a**/MATα LEU2:pGPD-AFB2/leu2-3,112 trp1-1/TRP1:pGPD-YFP-IAA28.T2V-NLS*

References

[1] Caldern-Villalobos LIA, Lee S, Oliveira CD, Ivetac A, Brandt W, Armitage L, Sheard LB, Tan X, Parry G, Mao H, Zheng N, Napier R, Kepinski S & Estelle M (2012) A combinatorial TIR1/AFB-Aux/IAA co-receptor system for differential sensing of auxin. Nat Chem Biol 8: 477-485

[2] Brunoud G, Wells DM, Oliva M, Larrieu A, Mirabet V, Burrow AH, Beeckman T, Kepinski S, Traas J, Bennett MJ & Vernoux T (2012) A novel sensor to map auxin response and distribution at high spatio-temporal resolution. Nature 482: 103-6

[3] Gibson DG, Young L, Chuang R-Y, Venter JC, Hutchison CA & Smith HO (2009) Enzymatic assembly of DNA molecules up to several hundred kilobases. Nat Methods 6: 343-345

[4] Dreher KA, Brown J, Saw RE & Callis J (2006) The Arabidopsis Aux / IAA Protein Family Has Diversified in Degradation and Auxin Responsiveness. Plant Cell 18: 699-714

[5] Ramos J, Zenser N, Leyser O & Callis J (2001) Rapid degradation of auxin/indoleacetic acid proteins requires conserved amino acids of domain II and is proteasome dependent. Plant Cell 13: 2349-2360

[6] Ouellet F, Overvoorde PJ & Theologis A (2001) IAA17/AXR3: biochemical insight into an auxin mutant phenotype. Plant Cell. 13: 829-41.

[7] Gray WM, Kepinski S, Rouse D, Leyser O & Estelle M (2001) Auxin regulates SCF(TIR1)-dependent degradation of AUX/IAA proteins. Nature 414: 271-6.

Recapitulation of the forward nuclear auxin response pathway in yeast

Edith Pierre-Jerome[a,1], Seunghee S. Jang[b,1], Kyle A. Havens[b,1], Jennifer L. Nemhauser[a,2], and Eric Klavins[b,2]

Departments of [a]Biology and [b]Electrical Engineering, University of Washington, Seattle, WA 98195

Edited by Mark Estelle, University of California, San Diego, La Jolla, CA, and approved May 7, 2014 (received for review December 27, 2013)

Auxin influences nearly every aspect of plant biology through a simple signaling pathway; however, it remains unclear how much of the diversity in auxin effects is explained by variation in the core signaling components and which properties of these components may contribute to diversification in response dynamics. Here, we recapitulated the entire *Arabidopsis thaliana* forward nuclear auxin signal transduction pathway in *Saccharomyces cerevisiae* to test whether signaling module composition enables tuning of the dynamic response. Sensitivity analysis guided by a small mathematical model revealed the centrality of auxin/indole-3-acetic acid (Aux/IAA) transcriptional corepressors in controlling response dynamics and highlighted the strong influence of natural variation in Aux/IAA degradation rates on circuit performance. When the basic auxin response circuit was expanded to include multiple Aux/IAAs, we found that dominance relationships between coexpressed Aux/IAAs were sufficient to generate distinct response modules similar to those seen during plant development. Our work provides a new method for dissecting auxin signaling and demonstrates the key role of Aux/IAAs in tuning auxin response dynamics.

synthetic biology | signaling dynamics

Evolution depends on the plasticity of existing signaling pathways. The small molecule auxin is linked to signaling modules that allowed plants to move to land, develop new organs, and respond to the environment (1, 2). Despite the wide range of auxin responses, the core auxin signal transduction pathway is quite simple, involving a small number of components from perception through transcription (Fig. 1*A*). Auxin triggers the rapid turnover of Aux/IAA (IAA) proteins, which repress the activity of auxin response factor (ARF) transcription factors through recruitment of TOPLESS (TPL) corepressors (3, 4). Auxin receptors, auxin signaling F-box (AFB) proteins, act as part of an E3 ubiquitin ligase to catalyze the ubiquitination and subsequent degradation of IAAs when auxin is present (5, 6). ARFs bound to auxin-responsive *cis*-regulatory elements (AuxREs) are then free to regulate the expression of auxin target genes, which include the IAAs themselves (7–9).

How such a simple pathway can orchestrate the large number of context-specific responses regulated by auxin is a long-standing question. Notably, each component in the auxin signaling pathway belongs to a large gene family (2, 10, 11). In *Arabidopsis*, there are 6 AFBs, 23 ARFs, and 29 IAAs. Functional divergence between component family members could provide variation in response to a generic auxin signal (12). Members of the ARF family can be classified as transcriptional activators or repressors (7, 8), and the role of repressor ARFs in regulating auxin signaling is still a matter of debate (13). In addition, expression studies of auxin-signaling gene families support the idea of an "auxin pre-pattern" where certain combinations of coexpressed components generate auxin circuits with distinct auxin response capabilities (14, 15). However, owing to the high level of redundancy and coexpression of auxin signaling component family members, feedback, and interference from other signaling pathways (16), the contributions of individual components to auxin circuit behavior have remained elusive.

Here, we ported several variations of the auxin transcriptional response pathway from *Arabidopsis thaliana* to *Saccharomyces cerevisiae*. In so doing, we defined a minimal auxin response circuit (ARC) sufficient to recapitulate auxin-induced transcription in a heterologous context. Because no feedback was engineered into these ARCs, they captured the dynamic potential of the simplest forward response architecture. The ARC consists of five plant components: an AFB, an IAA, TPL, an activating ARF transcription factor, and an auxin-responsive plant promoter (Fig. 1). The implementation of ARCs in yeast (ARC^{Sc}) relied on successful interfacing of the ARC with other essential elements of the yeast degradation and transcriptional machinery (Fig. 1*B*). This modular, plug-in nature of the ARC, similar to what was observed with auxin-induced degradation (17), highlights the likelihood that the ARC could be implemented in a variety of other eukaryotic contexts. The suite of ARC variants represented in the ARC^{Sc} collection presented an opportunity to quantitatively investigate the dynamic capabilities of the auxin response in isolation.

Auxin response pivots on relief of transcriptional repression, yet neither expression of an IAA alone nor coexpression with TPL repressed induction of the IAA19 promoter by activator ARFs (Fig. 1*C* and *SI Appendix*, Fig. S1). A fusion of full-length TPL with the ARF-interaction domain of IAA12 is able to fully recapitulate the stabilized IAA12 mutant phenotype (3). Following this logic, we identified two TPL truncations (TPL-N100 and TPL-N300) that conferred repression in yeast when fused to a full-length IAA. However, only repression by TPL-N100 (hereafter referred to as TPL) was relieved by auxin treatment (Fig. 1*C*). In a yeast strain where we could simultaneously monitor degradation of the TPL:IAA fusion and reporter activation, we observed reporter activation dynamics similar to those observed in

Significance

Auxin is a simple small molecule, yet it elicits an enormous variety of responses. How a single molecule can encode such diverse and context-specific information is a long-standing question. One hypothesis is that variation in auxin response components generates diversity in local auxin responses. To test this, we transplanted the forward nuclear auxin signal transduction pathway from plants into yeast. We found that auxin circuit composition can tune the dynamic response, and we identified which properties of auxin response components had the largest impact on circuit performance. Reconstitution of eukaryotic pathways in novel contexts can inform our understanding of the pathways themselves and can generate tools for engineering novel cellular behaviors.

Author contributions: E.P.-J., K.A.H., J.L.N., and E.K. designed research; E.P.-J. and K.A.H. performed research; S.S.J. designed and performed quantitative analyses; E.K. designed quantitative analyses; and E.P.-J., S.S.J., J.L.N., and E.K. wrote the paper.

The authors declare no conflict of interest.

This article is a PNAS Direct Submission.

[1]E.P.-J., S.S.J., and K.A.H. contributed equally to this work.

[2]To whom correspondence may be addressed. E-mail: jn7@uw.edu or klavins@uw.edu.

This article contains supporting information online at www.pnas.org/lookup/suppl/doi:10.1073/pnas.1324147111/-/DCSupplemental.

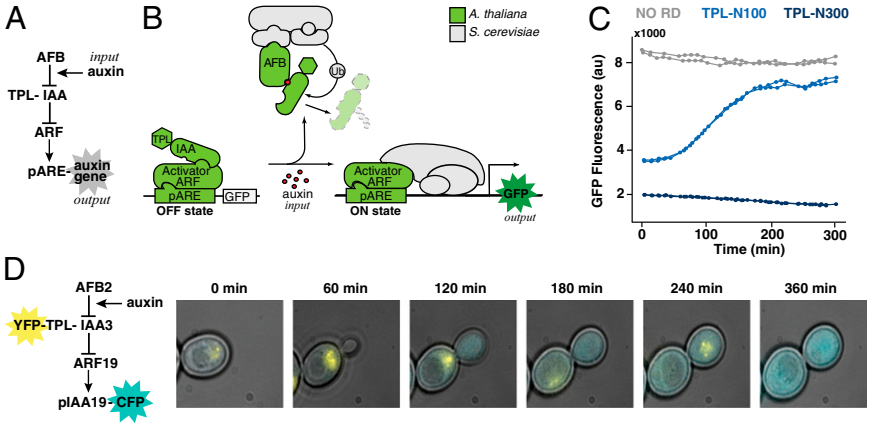

Fig. 1. Auxin-induced transcription in yeast. (*A*) Network diagram of the forward auxin response pathway in yeast. An auxin input increases association of a member of the TIR1/AFB family of F-box proteins (AFB) and an IAA protein fused to the first 100 aa of the TPL corepressor (TPL-IAA). Auxin-induced association of an AFB and a TPL-IAA leads to degradation of the TPL-IAA, thereby freeing a transcriptional activator in the ARF family to induce expression of an output gene driven by a promoter containing an auxin response element (pARE). (*B*) The five *A. thaliana* components needed to recapitulate auxin response in *S. cerevisiae* are shown in light green. They were an AFB F-box receptor, an IAA, a TPL corepressor, an ARF transcription factor, and an auxin-responsive promoter. The remaining cellular machinery (gray) was supplied by yeast. Fluorescence from a GFP reporter was used as a quantitative output. (*C*) Synthetic auxin-reversible repression required fusion of a specific TPL truncation to the IAA protein. Flow cytometry was used to monitor the induction of a GFP reporter following auxin treatment in circuits containing either IAA14 with no repression domain (NO RD), shown in gray, or two different C-terminal TPL truncations fused to IAA14. Auxin was added at time 0. TPL-N300 (dark blue) includes the first 300 aa of TPL and excludes the multiple C-terminal WD repeats. Fusion of TPL-N300 to IAA proteins results in reporter repression that is largely auxin-insensitive. TPL-N100 (light blue) includes only the first 100 aa of TPL. When fused to an IAA, TPL-N100 provides auxin-reversible repression. Two replicate induction curves are shown for each circuit. (*D*) Auxin-induced IAA degradation and subsequent transcriptional activation could be simultaneously monitored in dual-labeled yeast strains. YFP-TPL-IAA3 and a Cerulean reporter driven by the auxin-responsive IAA19 promoter (pIAA19-CFP) were monitored following auxin treatment using time-lapse microscopy and a microfluidic chamber.

cells where the TPL:IAA fusion was not labeled (Fig. 1*D*). Thus, performance of ARC^{Sc} is consistent with the established model of plant auxin signaling, with the exception that the TPL and IAA components are acting as a single protein.

The expansion of the IAA gene family has been linked to the increase in auxin signal complexity of land plants (2), suggesting IAAs play an essential role in tuning the auxin response. To explore the range of behaviors possible in a basic ARC configuration, we therefore took advantage of the large number of naturally evolved variants in the IAA gene family. We tested the impact of different IAAs on response dynamics of ARC^{Sc} variants containing either ARF19 or ARF7 using time-lapse flow cytometry (Fig. 2 and

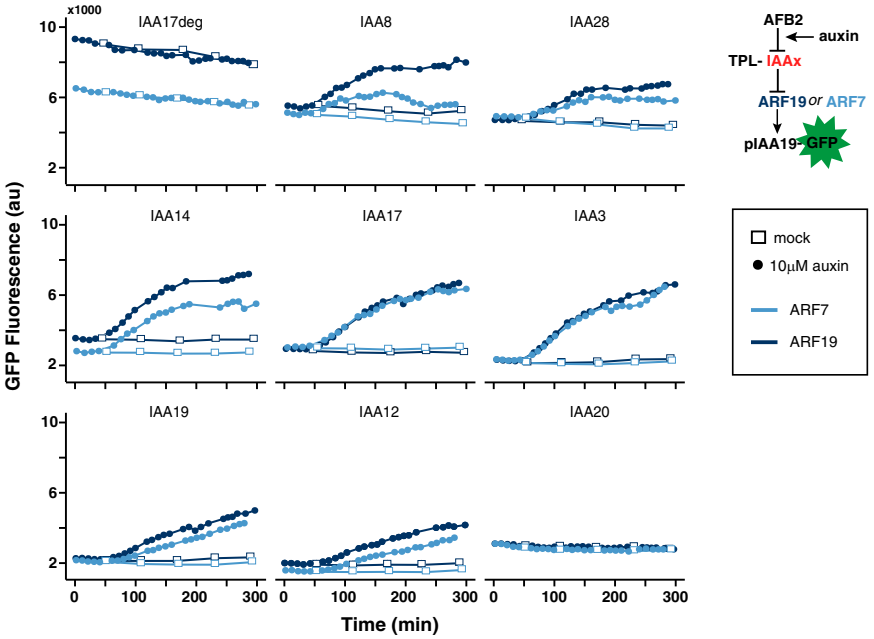

Fig. 2. IAAs drive auxin response dynamics. Representative auxin-induced reporter fluorescence curves are shown for ARCs with ARF7 (light blue) or ARF19 (dark blue) in the context of different IAAs. Auxin was added at time 0 in all graphs. ARF7 and ARF19 showed qualitatively similar patterns of auxin response, whereas the identity of the IAA had a dramatic effect on ARC dynamics. ARC^{Sc} recapitulated regulatory features of plant ARC function. Transcriptional repression required the known ARF–IAA interaction domain, because an IAA lacking this domain (IAA17deg) had no effect on ARF activity. In addition, auxin response was mediated by IAA degradation, because a naturally occurring IAA lacking a degron (IAA20) rendered the circuit insensitive to auxin treatment.

SI Appendix, Fig. S2). Our analysis focused primarily on IAAs that display strong mutant phenotypes when stabilized by point mutations that disrupt formation of the AFB–auxin–IAA complex (18–23). Additional IAAs found in distinct subgroups in the IAA family tree were also included (10). Circuits containing an IAA missing the ARF interaction domain (IAA17deg) failed to repress ARF activity, and thus indicated the maximum potential for reporter activation (Fig. 2). Yeast expressing IAA20, an IAA with a substantially diverged degron sequence rendering it insensitive to auxin, showed no reporter activation. Circuits with other IAAs exhibited substantial differences in the initial repressed state, as well as in the magnitude and rate of GFP reporter induction. The induction curves for a given IAA with either ARF19 or ARF7 were qualitatively quite similar, suggesting that ARF7 and ARF19 have similar or overlapping functions. This interpretation is supported by genetic and phylogenetic analysis in plants (24–26). This does not exclude the possibility that other ARF–IAA combinations, or higher-order interactions between multiple components from the ARF and IAA families, could generate additional diversity.

To quantify the differences in the behavior of ARC^{Sc} IAA variants, we developed a small model that expands upon the model used to quantify our degradation system (27). The present model captures the overall flow of information while avoiding reference to specific molecules and kinetic parameters that cannot be measured and limiting the potential for overfitting (28, 29). In our model the variable u represents the concentration of the applied auxin input and the variable g represents the GFP output of the reporter (Fig. 3*A*). A lumped internal state, which combines multiple reactions including the binding of auxin to the AFB receptor and related molecular machinery, is represented by x. IAA protein levels are represented by y. The model has eight parameters ($k_{1–8}$) that intuitively correspond to the biological processes listed in Table 1. We tested the validity of this interpretation numerically by evaluating fits of the data using different assumptions about which parameters change when different ARFs or IAAs are used in the circuit (*SI Appendix*). Our analysis, and the interpretation in Table 1, suggests varying the IAA corresponds to tuning three parameters: expression level (k_3), auxin-induced degradation (k_5), and ARF affinity (k_8) of each IAA. The rest of the parameters are independent of the changing components in the circuit except for k_7, which depends on which ARF is present.

To identify how IAA features influence the observed differences in response behavior, we defined two performance metrics: the preauxin steady state g_0 and the activation time ΔT (Fig. 3B). The metrics were plotted against the estimated IAA dependent parameter values for each variant to quantify the sensitivity of the pathway to these parameters. The preauxin steady state g_0 was accurately predicted by k_3 (expression level) and to a lesser extent by k_8 (ARF affinity), whereas, as the model suggests, k_5 did not reliably affect g_0 (Fig. 3*C* and *SI Appendix*). In other words, the "OFF" state of the circuit before auxin treatment is largely determined by the amount of IAA present and only modestly affected by the affinity of the IAA for the ARF. Experimentally, we also confirmed that ARCs containing the high-expressing IAA1.1, encoded by a yeast codon-optimized *IAA1* (27), had a much lower preauxin steady state than those with IAA1 (*SI Appendix*, Fig. S3). In contrast, activation time ΔT was predicted with high accuracy by k_5 alone (Fig. 3*D*). This result indicates that natural variation in IAA degradation rates—and not similar levels of variation in the other parameters tested here—is sufficient to dramatically alter the dynamics of auxin response.

We next engineered ARC^{Sc} variants with pairs of IAAs to test the impact of competition between IAAs on auxin response (Fig. 4*A*). This architecture was inspired by work suggesting that sequential modules of ARF–IAA partners drive discrete stages in the development of lateral roots (30–32). IAA28, IAA14, IAA12, and IAA3 have all been implicated in lateral root development (Fig. 4*B*). IAA28 regulates founder-cell specification (33) and IAA14 subsequently drives the initial cell divisions (22). IAA12 is involved in later divisions and outgrowth (30), and IAA3 has been shown to be involved in emergence as well as negative regulation of the IAA14 module (34). Limited expression studies available

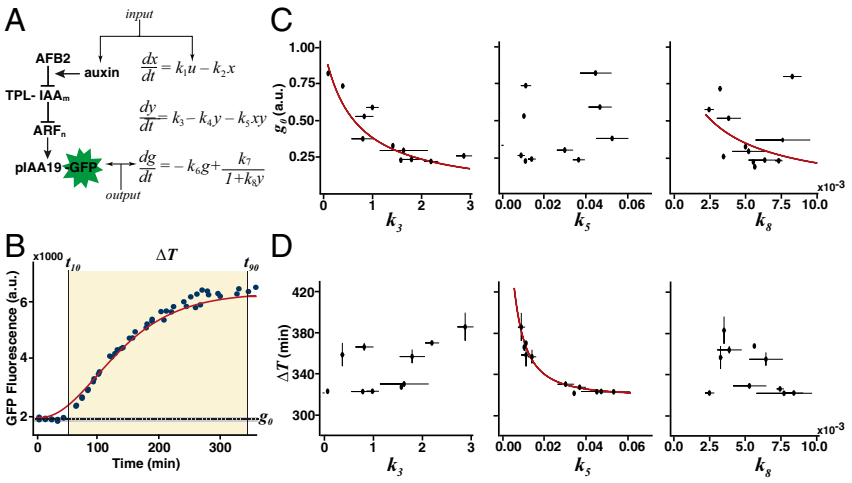

Fig. 3. Model selection and sensitivity analysis of the auxin response pathway. (*A*) Gray-box model of the auxin response pathway. The auxin input is represented by the variable u and the GFP output of the reporter is represented by the variable g. The variable x represents a lumped internal state, which combines multiple reactions including the binding of auxin to the AFB receptor, and the variable y represents IAA protein levels. The model has eight parameters ($k_{1–8}$) that intuitively correspond to the biological processes listed in Table 1. We focused on three parameters with strong effect on ARC dynamics: IAA expression level (k_3), rate of auxin-induced IAA degradation (k_5), and ARF-IAA affinity (k_8). (*B*) A graphical representation of the two performance metrics used for sensitivity analysis: the preauxin steady state g_0 and the activation time ΔT (t_{90}–t_{10}). Sample data from one ARC is shown as blue dots with a sample model fit in red. (*C* and *D*) Sensitivity analysis of preauxin steady state g_0 (*C*) and activation time ΔT (*D*) to model parameter values of k_3, k_5, and k_8 for each IAA. Each parameter was varied across its entire range of estimated values derived from our experimental dataset, and all other parameters were held constant. Each IAA is plotted as a single point, and the red line indicates the sensitivity curve computed from the model. The preauxin steady state g_0 was accurately predicted by k_3 (expression level) and to a lesser extent by k_8 (ARF affinity), with k_5 having little effect. In contrast, activation time ΔT was predicted with high accuracy by k_5 (auxin-induced degradation) alone. Error bars represent SD ($n = 2$). More details can be found in *SI Appendix*.

Table 1. Parameter interpretations

Parameter	Biological interpretation
k_1	Assembly of auxin-primed AFB receptor
k_2	Basal degradation/dissociation of auxin-primed AFB receptor
k_3	IAA expression
k_4	Basal degradation/dilution of IAA
k_5	Auxin-induced degradation of IAA
k_6	Basal degradation/dilution of GFP
k_7	GFP expression
k_8	ARF affinity of IAA

for IAA and ARF family members indicate that multiple family members are often coexpressed in plant cells, raising the question of how specificity or ordering is encoded (14, 15). Our data and those of others suggest that multiple IAAs can interact with and repress the same activator ARF (15). One attractive hypothesis is that a hierarchy of ARC function is encoded by a hierarchy of function within the IAAs themselves.

Although it was not possible to experimentally determine a mechanism for this potential for hierarchical action, we were able to test whether such a pattern can be simulated in a minimal synthetic context. Toward that end, we generated ARC^{Sc} variants expressing pairwise combinations of IAA3, IAA12, IAA14, and IAA28. These competition strains made it possible to characterize the impact of an additional IAA on the dynamics of an ARC. Induction curves of ARC^{Sc} competition strains indicated that transcriptional dynamics were largely biased toward the IAA that acts in later developmental modules (Fig. 4*C*). The 12+14 and 12+3 circuits exhibited response dynamics similar to that of a 12+12 circuit, whereas transcriptional dynamics of 14+28 circuits were nearly identical to a 14+14 circuit. The 14+3 transcriptional dynamics showed a high degree of variation from one experiment to another, following response dynamics of either 14+14 or 3+3 circuits. This leads to a dominance hierarchy of 28 < 14, 3 < 12, which matches the proposed sequence of roles in lateral root development.

The preferential response to one of the two coexpressed IAAs suggests dominance relationships between IAAs could play a role in the generation of sequential auxin responses. Novel dynamics created by heterodimers may also be a factor in some cases, although the strong dominance of one IAA over another makes this less likely for most of the examples tested here. The dominance relationships uncovered here could explain how transcriptional dynamics could be switched from one regime to another over time. IAAs are among the earliest auxin response genes (9), suggesting that differences in synthesis and degradation rates among family members could lead to a dramatic change in the cellular complement of IAAs after exposure to auxin. In this way, IAAs may tune the intensity and duration of downstream transcriptional outputs similar to IκB repressors in the mammalian NF-κB pathway (35, 36).

We hypothesized that dominance between IAAs could reflect competition for two key interactions in the transmission of an auxin signal: binding to the AFB and binding to the ARF (Fig. 4*A*). These interactions are approximately captured by the parameters k_5 (auxin-induced degradation rate) and k_8 (ARF affinity). In plants, where IAAs are strongly and differentially auxin-induced, IAA expression level is also likely to play a critical role in determining which IAA drives transcriptional dynamics. However, because both IAAs in the yeast strains tested here are expressed from the same strong constitutive yeast promoters, we predicted that k_3 (expression level) was unlikely to have a significant role in determining dominance in our assays. Indeed, we found only minor differences in expression levels between coexpressed IAAs, and these small differences had no correlation to dominance (*SI Appendix*, Fig. S4). Because all of our rate estimates were obtained from experiments where only a single IAA is expressed, these estimates cannot be directly applied to predict competition outcomes in the more complex setting of multiple coexpressed IAAs. Instead, we modified our model to introduce two new parameters, α and β (*SI Appendix*), which represent the relative contributions of the two competing IAAs to the parameters k_5 and k_8, respectively. Thus, α and β

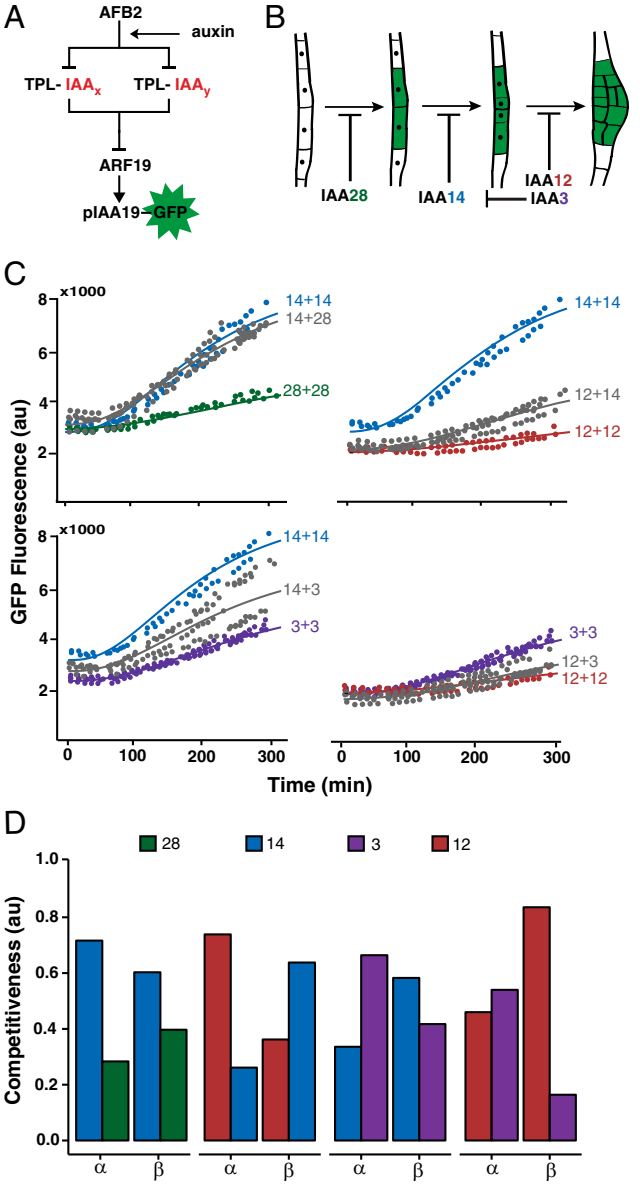

Fig. 4. IAA coexpression reveals dominance relationships between IAAs. (*A*) Modified ARF19 circuits were built that contained pairs of IAAs (IAAx and IAAy). (*B*) Schematic showing the simplified sequence of lateral root development: founder cell specification, first cell division and patterning/outgrowth. Auxin response modules are proposed to be sequentially triggered by degradation of the indicated IAAs. (*C*) One IAA could dictate the auxin response dynamics of yeast cells expressing multiple IAAs. Comparisons are shown between circuits containing two copies of the same IAA (colored points) or one copy of each IAA (gray points). Model fits are shown as solid lines. (*D*) α (AFB binding competiveness) or β (ARF binding competitiveness) can affect the contribution of an IAA to ARC dynamics. Estimated α and β values from the modified model are shown for each of the IAAs tested here. More details can be found in *SI Appendix*.

describe which IAA is dominant in terms of its affinity to either the AFB (α) or the ARF (β). IAAs that demonstrated clear dominance in the behavior of the induction curve in mixed IAA circuits had a higher α and/or β than the other coexpressed IAA (Fig. 4*D*). It is worth noting that each of the original parameters, as well as the derived α and β, encompass multiple rates controlled by distinct biochemical mechanisms. Given the current limits for experimental measurement of each of the constituent rates within these composite parameters, it is impossible to predict the dominance relationship of any IAA pair or to explain observed dominance by an explicit molecular mechanism. Instead, these competition experiments serve to underline the striking complexity possible with even relatively simple circuits and generate a new hypothesis for sequential auxin circuit function during development.

By transplanting auxin response into yeast and defining a small mathematical model able to explain ARC dynamics, we were able to rigorously test how auxin response is controlled and tuned using only the core ARC components. When combined with feedback and interactions with other pathways, such tuning knobs likely have even more dramatic effects. By finding the ARC tuning knobs, this approach generated hypotheses about the evolution of natural ARC variants in plants, as well as showing a path to engineer novel circuit behaviors in synthetic contexts. The inherent modularity of the ARC lends itself to adding additional layers of complexity and quantitative analysis of other challenging features of auxin response, such as feedback or higher-order complexes between ARFs and IAAs. Indeed, recent structural studies indicate the potential for higher-order ARF–IAA complexes than previously suspected (37–39). ARC^{Sc} may be a useful tool for quantifying the impact of this structural complexity on response dynamics. In addition, incorporation of additional auxin-responsive promoters could expand the functionality of our system and allow incorporation of combinatorial control by multiple transcription factors. More generally, ARC^{Sc} demonstrates how the reconstitution of eukaryotic pathways can serve as a powerful companion to systems biology-driven studies that generate predictions about functional signaling modules.

Materials and Methods

Strain Construction. A library of IAAs was cloned downstream of a GPD promoter in *TRP1* integration vectors using a standard Gateway LR reaction (LRClonase II; Life Technologies) and transformed into W814-29B *MATa* strains (YKL381) containing pGP5G-AFB2 [AFB2 integration at *LEU2*, expression from the GPD promoter (27)]. ARFs were amplified from *Arabidopsis* cDNA and subcloned into the Gateway pDONR221 plasmid using a standard Gateway BP reaction (BP Clonase II; Life Technologies). Each ARF was then subsequently cloned into pGP8A-ccdB (integration at *HIS3,* expression from the *ADH1* promoter) and transformed into a W303-1A *MATa* strain containing the pIAA19-GFP reporter integrated at *URA3* (YKL12). Strains containing AFB2 and an IAA were then mated to strains containing the reporter and an ARF to generate the library of ARC^{Sc} variants. See *SI Appendix*, Table S1 for strains used in this study.

Plasmid Construction. *Arabidopsis* genes were inserted into single integrating derivatives of pAG Gateway vectors (27, 40) (*SI Appendix*, Fig. S5 and Table S2). *TRP1* targeting single integrating Gateway vectors (27) were further modified to contain an N-terminal TPL repression domain (RD) for auxin response assays, or an N-terminal YFP-RD tag to monitor the degradation of RD–IAA fusions. Repression domains TPL-N100 and TPL-N300 were amplified from *A. thaliana* Columbia ecotype cDNA. For the GFP auxin induction reporter plasmid, 300 bp immediately upstream of the IAA19 start codon was amplified from *Arabidopsis* gDNA and inserted upstream of GFP in the pAG306 (*URA3*, multiply inserting) targeting vector.

Yeast Methods. Standard yeast drop-out and yeast extract–peptone–dextrose plus adenine (YPAD) media were used, with care taken to use the same batch of synthetic complete (SC) media for related experiments. A standard lithium acetate protocol (41) was used for transformations of digested plasmids. All cultures were grown at 30 °C with shaking at 220 rpm.

Flow Cytometry. Fluorescence measurements were taken with a BD Accuri C6 flow cytometer and CSampler plate adapter using an excitation wavelength of 488 and an emission detection filter at 533 nm. A total of 10,000 events above a 400,000 FSC-H threshold (to exclude debris) were measured for each sample and data exported as FCS 3.0 files for processing using the flowCore R software package and custom R scripts (27).

Induction Assays. A freshly grown colony for each strain was inoculated in SC and the cell density (in events per microliter) was estimated using cytometry data gated for yeast by a custom R script (27). Each culture was then diluted to 0.25 events per microliter in 12 mL of SC. This dilution was split into duplicate 5-mL aliquots and incubated for 16 h. At 16 h, duplicate aliquots were combined, mixed, and resplit into two tubes and initial measurements taken in the cytometer (starting density was ∼200 events per microliter). For each strain, one replicate was mock-treated [95% (vol/vol) ethanol] and one replicate was treated with 10 μM indole-3-acetic acid. Immediately after auxin addition, fluorescence for the 0-min time point was recorded and subsequent measurements acquired at 10-min intervals for 5 h. Up to 12 strains were measured in parallel.

Steady-State Expression Measurements. A freshly grown colony was inoculated into 1 mL of SC in a 96-well plate and grown to stationary overnight. The next morning each culture was diluted into fresh SC and fluorescence measurements taken ∼6 h later.

Microscopy. Yeast cells grown overnight in SC at 30 °C were diluted 1:100 in SC, incubated for 4–5 h, and then diluted 1:20 before loading onto a Y04D plate (CellASIC). Using the CellASIC-ONIX microfluidic system and associated software, cells were treated with 10 μM auxin in SC medium. An inverted Nikon Eclipse Ti microscope with a 60×, numerical aperture and 1.4 oil objective was used to image the yeast cells at 1-h intervals using a YFP-HYQ and CFP bandpass filter (Nikon) with a CoolSNAP HQ2 14-bit camera.

Expression Analysis. Yeast cells were grown in YPAD and collected at an OD of 0.9. RNA was extracted using the RiboPure RNA purification kit (Life Technologies). One microgram of RNA was used for cDNA synthesis using the iScript cDNA Synthesis kit (Bio-Rad). Samples were analyzed using the iQ SYBR Green Supermix (Biorad) reactions in a C100 Thermal Cycler fitted with a CFX96 Real-Time Detection System (Biorad). Relative expression levels were calculated using the formula $(E_{target})^{-CPtarget}/(E_{ref})^{-CPref}$ (42) and normalized to the *ACT1* reference gene.

Quantitative Analysis. A gray-box modeling approach was used to identify a minimal mathematical model for the auxin response characterized by ARC^{Sc} variants. A more detailed description of the modeling and quantitative analysis is found in *SI Appendix*. The annotated code and supporting data are available for download at http://klavinslab.org/data.html.

ACKNOWLEDGMENTS. We thank Takato Imaizumi, Ben Kerr, Georg Seelig, and Tom Daniel for careful reading of our manuscript; Nick Bolten for work on optimizing plasmid construction; Miles Gander for technical assistance; and members of the J.L.N. and E.K. groups for helpful discussions. This work was supported by the Paul G. Allen Family Foundation (J.L.N. and E.K.) and National Science Foundation (NSF) Grant CISE-0832773 (to E.K.). E.P.J. was supported by an NSF Graduate Research Fellowship and the Seattle Chapter of the Achievement Rewards for College Scientists Foundation.

1. Finet C, Berne-Dedieu A, Scutt CP, Marlétaz F (2013) Evolution of the ARF gene family in land plants: Old domains, new tricks. *Mol Biol Evol* 30(1):45–56.
2. Paponov IA, et al. (2009) The evolution of nuclear auxin signalling. *BMC Evol Biol* 9:126.
3. Szemenyei H, Hannon M, Long JA (2008) TOPLESS mediates auxin-dependent transcriptional repression during Arabidopsis embryogenesis. *Science* 319(5868):1384–1386.
4. Ulmasov T, Murfett J, Hagen G, Guilfoyle TJ (1997) Aux/IAA proteins repress expression of reporter genes containing natural and highly active synthetic auxin response elements. *Plant Cell* 9(11):1963–1971.
5. Dharmasiri N, Dharmasiri S, Estelle M (2005) The F-box protein TIR1 is an auxin receptor. *Nature* 435(7041):441–445.
6. Kepinski S, Leyser O (2005) The Arabidopsis F-box protein TIR1 is an auxin receptor. *Nature* 435(7041):446–451.
7. Ulmasov T, Hagen G, Guilfoyle TJ (1999) Activation and repression of transcription by auxin-response factors. *Proc Natl Acad Sci USA* 96(10):5844–5849.
8. Tiwari SB, Hagen G, Guilfoyle T (2003) The roles of auxin response factor domains in auxin-responsive transcription. *Plant Cell* 15(2):533–543.

9. Abel S, Nguyen MD, Theologis A (1995) The PS-IAA4/5-like family of early auxin-inducible mRNAs in Arabidopsis thaliana. *J Mol Biol* 251(4):533–549.
10. Remington DL, Vision TJ, Guilfoyle TJ, Reed JW (2004) Contrasting modes of diversification in the Aux/IAA and ARF gene families. *Plant Physiol* 135(3):1738–1752.
11. Dharmasiri N, et al. (2005) Plant development is regulated by a family of auxin receptor F box proteins. *Dev Cell* 9(1):109–119.
12. Lokerse AS, Weijers D (2009) Auxin enters the matrix—assembly of response machineries for specific outputs. *Curr Opin Plant Biol* 12(5):520–526.
13. Pierre-Jerome E, Moss BL, Nemhauser JL (2013) Tuning the auxin transcriptional response. *J Exp Bot* 64(9):2557–2563.
14. Rademacher EH, et al. (2012) Different auxin response machineries control distinct cell fates in the early plant embryo. *Dev Cell* 22(1):211–222.
15. Vernoux T, et al. (2011) The auxin signalling network translates dynamic input into robust patterning at the shoot apex. *Mol Syst Biol* 7:508.
16. Del Bianco M, Kepinski S (2011) Context, specificity, and self-organization in auxin response. *Cold Spring Harb Perspect Biol* 3(1):a001578.
17. Nishimura K, Fukagawa T, Takisawa H, Kakimoto T, Kanemaki M (2009) An auxin-based degron system for the rapid depletion of proteins in nonplant cells. *Nat Methods* 6(12):917–922.
18. Tian Q, Reed JW (1999) Control of auxin-regulated root development by the Arabidopsis thaliana SHY2/IAA3 gene. *Development* 126(4):711–721.
19. Nagpal P, et al. (2000) AXR2 encodes a member of the Aux/IAA protein family. *Plant Physiol* 123(2):563–574.
20. Ouellet F, Overvoorde PJ, Theologis A (2001) IAA17/AXR3: Biochemical insight into an auxin mutant phenotype. *Plant Cell* 13(4):829–841.
21. Rogg LE, Lasswell J, Bartel B (2001) A gain-of-function mutation in IAA28 suppresses lateral root development. *Plant Cell* 13(3):465–480.
22. Fukaki H, Tameda S, Masuda H, Tasaka M (2002) Lateral root formation is blocked by a gain-of-function mutation in the SOLITARY-ROOT/IAA14 gene of Arabidopsis. *Plant J* 29(2):153–168.
23. Hamann T, Benkova E, Bäurle I, Kientz M, Jürgens G (2002) The Arabidopsis BODENLOS gene encodes an auxin response protein inhibiting MONOPTEROS-mediated embryo patterning. *Genes Dev* 16(13):1610–1615.
24. Fukaki H, Taniguchi N, Tasaka M (2006) PICKLE is required for SOLITARY-ROOT/IAA14-mediated repression of ARF7 and ARF19 activity during Arabidopsis lateral root initiation. *Plant J* 48(3):380–389.
25. Okushima Y, Fukaki H, Onoda M, Theologis A, Tasaka M (2007) ARF7 and ARF19 regulate lateral root formation via direct activation of LBD/ASL genes in Arabidopsis. *Plant Cell* 19(1):118–130.
26. Wilmoth JC, et al. (2005) NPH4/ARF7 and ARF19 promote leaf expansion and auxin-induced lateral root formation. *Plant J* 43(1):118–130.
27. Havens KA, et al. (2012) A synthetic approach reveals extensive tunability of auxin signaling. *Plant Physiol* 160(1):135–142.
28. Ljung L (1999) *System Identification: Theory for the User* (Prentice Hall, Upper Saddle River, NJ), 2nd Ed.
29. Neuert G, et al. (2013) Systematic identification of signal-activated stochastic gene regulation. *Science* 339(6119):584–587.
30. De Smet I, et al. (2010) Bimodular auxin response controls organogenesis in Arabidopsis. *Proc Natl Acad Sci USA* 107(6):2705–2710.
31. De Smet I (2012) Lateral root initiation: One step at a time. *New Phytol* 193(4): 867–873.
32. Lavenus J, et al. (2013) Lateral root development in Arabidopsis: Fifty shades of auxin. *Trends Plant Sci* 18(8):450–458.
33. De Rybel B, et al. (2010) A novel aux/IAA28 signaling cascade activates GATA23-dependent specification of lateral root founder cell identity. *Curr Biol* 20(19): 1697–1706.
34. Goh T, Kasahara H, Mimura T, Kamiya Y, Fukaki H (2012) Multiple AUX/IAA-ARF modules regulate lateral root formation: The role of Arabidopsis SHY2/IAA3-mediated auxin signalling. *Philos Trans R Soc Lond B Biol Sci* 367(1595):1461–1468.
35. Kearns JD, Basak S, Werner SL, Huang CS, Hoffmann A (2006) IkappaBepsilon provides negative feedback to control NF-kappaB oscillations, signaling dynamics, and inflammatory gene expression. *J Cell Biol* 173(5):659–664.
36. Tian B, Nowak DE, Brasier AR (2005) A TNF-induced gene expression program under oscillatory NF-kappaB control. *BMC Genomics* 6:137.
37. Boer DR, et al. (2014) Structural basis for DNA binding specificity by the auxin-dependent ARF transcription factors. *Cell* 156(3):577–589.
38. Korasick DA, et al. (2014) Molecular basis for AUXIN RESPONSE FACTOR protein interaction and the control of auxin response repression. *Proc Natl Acad Sci USA* 111(14):5427–5432.
39. Nanao MH, et al. (2014) Structural basis for oligomerization of auxin transcriptional regulators. *Nat Commun* 5:3617.
40. Alberti S, Gitler AD, Lindquist S (2007) A suite of Gateway cloning vectors for high-throughput genetic analysis in Saccharomyces cerevisiae. *Yeast* 24(10):913–919.
41. Gietz RD, Woods RA (2002) Transformation of yeast by lithium acetate/single-stranded carrier DNA/polyethylene glycol method. *Methods Enzymol* 350:87–96.
42. Pfaffl MW (2001) A new mathematical model for relative quantification in real-time RT-PCR. *Nucleic Acids Res* 29(9):e45.

Contents

1 Quantitative Analysis **2**

Supplementary Figures

1 TPL co-expression with IAA14 does not inhibit ARF activation. 9

2 Flow cytometry data for all ARC^{Sc} strains tested. 10

3 Preauxin steady state GFP reporter activity of IAA 1.1 is lower than that of IAA1 in ARF19 circuits. 11

4 IAA expression levels do not correlate with dominance behavior in ARC^{Sc} competition strains. . . . 12

5 Assembly of pGP4GY-ccdB. 13

6 The block diagram of the ARC^{Sc} and its model. 14

7 Model-fit residual decreases with fewer constraints on parameter estimation. 15

8 Preauxin steady state values of ARC variants. 16

9 k_3 and k_8 are not correlated. 17

Supplementary Tables

1 List of strains. 18

2 List of primers. 20

3 Estimated parameter values of the 21 ARC^{Sc} variants and the replicates. 21

4 Estimated parameter values of the competition ARC^{Sc} variants and the replicates. 22

1 Quantitative Analysis

Model identification. The model mirrors the construction of the ARC^{Sc} (Supplementary Figure 6): Just as an ARF and a promoter were added to the previously engineered AFB|IAA system, an additional equation for GFP (represented by g) was added to the previously identified mathematical model of the AFB|IAA system [1] to obtain the following.

$$\begin{aligned} \dot{x} &= k_1 u - k_2 x \\ \dot{y} &= k_3 - k_4 y - k_5 x y \\ \dot{g} &= -k_6 g + \frac{k_7}{1 + k_8 y}. \end{aligned} \tag{1}$$

The time-dependent variables u, x, y and g represent the concentration of auxin input, a lumped internal state (combining the intermediate reactions involving the binding of auxin to the AFB receptor and related molecular machinery), the IAA levels, and the GFP reporter, respectively. The parameters describe the synthesis of the internal state (k_1), the degradation and dilution of the internal state (k_2), expression of IAA (k_3), degradation and dilution of IAA (k_4), auxin-induced degradation of IAA (k_5), degradation and dilution of GFP (k_6), non-repressed expression of the reporter (k_7), and the repression on the reporter (k_8). The first two equations in the model are identical to the model of the AFB|IAA system reported previously [1]. The third equation captures the dynamics of GFP output – the basal degradation and dilution rate, and the IAA dependent expression rate. Because IAAs bind with ARF and inhibit the activation of GFP expression, the GFP expression rate is inversely proportional to the amount of IAA. The model is not intended to be mechanistic. Nevertheless, even without additional terms modeling ARF dynamics, for example by directly modeling the inhibitory effect of IAA on GFP expression, the model fits the wide range of GFP induction responses (Figure 2). In fact, the addition of a species representing the concentration of ARF introduces uncertainty to the parameter estimation that cannot be resolved because of the low number of observable outputs.

Parameter-Component dependency. The main question we answer in our analysis of the model is: which of the parameters k_1 through k_8 are tuned by the choice of AFB or IAA. We call the proteins that make up the circuit,

and in particular the ARF and IAA, *components*. As can be seen from the data, the auxin response clearly depends on the choice of components. For those aspects of the dynamics that are independent of the changing components, we expect that the model parameters associated with the components remain constant across ARC^{Sc} variants. For example, k_1 is a parameter associated with the choice of AFB [1] and when estimating the parameters of ARC^{Sc} circuits, all with the same AFB variant, the value for k_1 is constant for all members of the set. However, k_3 is associated with the choice of IAA; therefore, when estimating the parameters of ARC^{Sc} circuits with different IAAs, we expect the parameter values to be different for each variant. This dependency implies that every dependent parameter becomes a variable unique to an ARC^{Sc} variant (made up of unique constituent components), and the set of these unique variables add to the dimension in which we compare ARC^{Sc} variants with one another. Since we seek a small set of quantitative features for simpler comparison across ARC^{Sc} variants for parsimonious representation, we aim to keep the number of dependencies small.

We use a matrix to represent the relationship between parameters (k_1 through k_8) and components (the ARFs and IAAs). In particular, we define the $m \times n$ Boolean matrix A for m-parameters and n-components. Note that n refers to the number of component types that compose the system, and not the number of interchangeable variants for a given component type. Here $m = 8$ and $n = 2$. The entry $a_{i,j}$ is 1 if the i-th parameter is dependent on the choice of the j-th component, and is 0, otherwise.

To validate our interpretation of the parameters k_1 through k_8, we estimate A using pooled experimental data. Note that there exist $2^{m \times n}$ candidates for A and each candidate is a hypothesis regarding the parameter-component dependency. Some hypotheses perform better than others with respect to how well they fits the range of divergent system behaviors across a set of system variants. These candidates tend to have more non-zero entries because each non-zero entry effectively allows another degree-of-freedom for fitting experimental data. At the same time, the candidates with more non-zero entries ultimately result in more unique variables per system variant. Therefore, we search for an A that results in a low model-fit residual with small number of non-zero entries.

We implemented the model fitting and parameter-component matrix search in *Mathematica*. The code and supporting data are available for download at http://klavinslab.org/data.html. Given that there are 2^{16} possible

candidate matrices for the 2-component ARC^{Sc} circuits and the 8-parameter model, directly examining all of the candidates is prohibitively expensive in computational cost (approximately 2 hours per matrix using the *NMinimize* function in *Mathematica*). Instead, we selectively choose and evaluate candidate matrices using a greedy search algorithm (Supplementary Figure 7). The algorithm begins with 0-matrix (*parent* matrix) and searches a set of candidate matrices that are generated by adding an additional 1 to each of the available positions (previously where it was 0) (a set of *child* matrices). Among the set, the matrix with the lowest model-fit residual is chosen. The process is iterated by updating the parent matrix with the best performer and generating a next set of matrices. Though efficient, this approach sometimes fails to consider other candidate matrices that are nearly equivalent in model-fit residual to the lowest value. Repeated searches from different initial conditions, however, gave the same results in this case. Additionally, we observed a trend where the model-fit residual monotonically decreases with increasing number of non-zero entries. We conjecture that this behavior will be observed in general, but no analytical proof yet exists. Finally, it is notable that because of various uncertainties in measurement/experimental noise and estimation errors, the residual eventually saturates at some low value and further addition of non-zero entries do not decrease it further. We defined an arbitrary threshold at which point the iterative search for optimal A halts.

The optimal matrix A^* (Supplementary Figure 7) suggests the following interpretations regarding the ARC^{Sc} and the model parameter.

- The expression strength of IAA (k_3) is one of the strongest determinants of the ARC^{Sc} response dynamics as it was consistently chosen as the first non-zero entry in multiple iterations of greedy search algorithm. Additionally, the parameter is dependent on the choice of IAA alone, and is independent of the ARF.

- The basal expression of GFP (k_7) is dependent on the choice of ARF, but independent of the choice of IAA.

- Somewhat unexpectedly, the auxin-mediated IAA degradation (k_5) is dependent on the choice of both IAA and ARF. One hypothesis is that ARF and AFB compete for binding with IAA and when IAA is bound to ARF, AFB cannot bind – inhibiting auxin-mediated IAA degradation.

- The affinity of IAA to ARF (k_8) is dependent on the choices of IAA and ARF, which is consistent with the

model interpretation.

The findings of parameter-component dependency identified here could have been obtained, to some degree, through qualitative observation of ARC^{Sc} responses (e.g. The minimal dependency of k_3 on the choice of ARF could have been elicited from noticing that the preauxin steady state of ARC^{Sc} remains constant when a different ARF is used). However, by using the approach discussed here, we investigated different hypotheses and determined that not all of the model parameters need be varied to account for the range of dynamic responses in ARC^{Sc}. Using the approach, we have identified a minimal set of quantities that identify the biological functions of ARC^{Sc}. Furthermore, these values may be tuned by choosing the appropriate ARF and IAA.

Sensitivity Analysis. We defined two performance metrics to capture the overall behavior of the system: The preauxin steady state and the activation time. These metrics enable quantitative comparisons among the ARC^{Sc} variants (and may guide later rational engineering of synthetic gene networks using the synthetic system analyzed here).

The preauxin steady state. The analytical expression for the preauxin steady state with $u = 0$ is

$$g_0 = \frac{k_7 k_4}{k_6 (k_4 + k_3 k_8)}. \tag{2}$$

Experimentally, it was shown that the maximal GFP intensity is dependent on the choice of ARF. Therefore, to fairly compare preauxin steady states of GFP among the ARC^{Sc} variants with different ARFs, the values were normalized by k_7/k_6, which corresponds to the maximal GFP expression rate when y is zero. Thus the normalized value represents the relative fraction of the preauxin steady states of GFP with respect to the maximal GFP intensity possible for the given ARF. Note that the relative rankings of IAAs in ARF19 and ARF7 are conserved for this metric (Supplementary Figure 8).

Sensitivity analysis reveals how the preauxin steady state changes with a change in the model parameters (Figure 3C) – specifically k_3, k_5, and k_8. Each parameter was varied one at a time from the minimum and the maximum estimated values. The preauxin steady state depends on the synthesis rate of IAA and the affinity of IAA to ARF. At the same time, because the preauxin steady state is measured before auxin is added to the system, the quantity

is independent of the auxin-induced IAA degradation (k_5). Therefore, the preauxin steady state does not vary as k_5 is changed, and the sensitivity analysis consistently predicts this behavior. The effect of varying k_3 and k_8 is qualitatively equivalent – when either of the value is decreased, the preauxin steady state increases, and vice versa.

The activation time, ΔTt. We define the *activation time* as the difference in time between when 10% GFP expression intensity (t_{10}) and 90% GFP expression (t_{90}) are reached. We set the initial state (refers to the preauxin steady state GFP intensity) as the 0% and the final state (refers to the post-auxin steady state GFP intensity) as 100%. The ODEs are solved to numerically approximate the activation time, because there is no analytical solution to the model. As in the sensitivity analysis of the preauxin steady state, each parameter was varied between the minimum and the maximum of the estimated parameter values from the data, while the other parameters are held constant (Figure 3D). The most striking trend is that the activation time is predicted with high accuracy by k_5 alone and that k_3 or k_8 are poor predictors of the activation time. This suggests that when engineering a synthetic gene network using the ARC^{Sc} circuit which requires faster/slower activation rate, it is far more advantageous to select an IAA with a higher/lower k_5 than one with a different k_3 or k_8.

The sensitivity analysis also suggests that varying k_3 and k_8 have similar effect on the ΔT. This raises the possibility that these parameters are indistinguishable when the output measurement is limited to the variable g. However, the ambiguity is resolved if the output measurements are extended to the variable y, because it allows us to estimate k_3 – the expression rate of IAA – independently of the k_8. To achieve a similar effect, we pooled two data sets - GFP induction data and YFP-IAA degradation data. Though the YFP-IAA degradation data is collected from a variation of ARC^{Sc} circuit that lacks the plant promoter, it is a close approximation of the standard ARC^{Sc} circuit. This condition allowed us to deduce the approximate range of k_3 for ARC^{Sc} circuits. Though mathematically indistinguishable in sensitivity, different IAAs with different k_3 and k_8 values have varying effects on the circuit performance. In particular, the scatter plot of k_3 and k_8 shows little correlation, suggesting that the two parameters are controlled independently within the IAA sequence and have partially independent roles in output dynamics (Supplementary Figure 9). We hypothesize that k_3 is determined by the transcriptional and translational efficiency of the IAA in question, whereas k_8 is determined by the affinity of the IAA for its target ARF.

Competition of multiple IAAs. Instead of modifying the model structure and introducing new variables and parameters to represent the secondary IAA, we reinterpret the standard model[1]. Specifically, the variable y was interpreted as the *effective* IAA. This is because without engineering the multiple-IAA ARC^{Sc} to measure either or both of the IAA dynamics, it is difficult to decouple the effects of individual IAAs. Therefore, we assume that there exists a lumped species whose behavior is a combination of behaviors of the two IAAs.

As discussed, the characteristic features of an IAA in ARC^{Sc} are quantified by k_3, k_5 and k_8. Similarly, we assume the characteristic features of the effective IAA species of a mixed-IAA ARC^{Sc} are quantified by the same parameters. We further hypothesize that k_5 and k_8 of the mixed IAA circuit are linear combinations of the parametric values of each individual IAA with the weighting coefficient parametrized by α and β, respectively. These parameters approximate the relative competitiveness in AFB- and ARF-binding of one of the two IAA in a mixed ARC^{Sc} system. This relationship is written as follows.

$$k_{5,\text{mixed-IAA}} = \alpha k_{5,\text{IAA}_x} + (1-\alpha) k_{5,\text{IAA}_y} \tag{3}$$

$$k_{8,\text{mixed-IAA}} = \beta k_{8,\text{IAA}_x} + (1-\beta) k_{8,\text{IAA}_y}. \tag{4}$$

It was shown that mixed-IAA response dynamics often mimic the response of one of the individual IAA ARC^{Sc} circuit more closer than the other. To determine whether this trend is bolstered by either a strong relative competitiveness of AFB- or ARF-binding of a given IAA, we simulated the effect of varying α and β simultaneously. To examine the preferential response dynamics of a mixed ARC^{Sc} system, we define a metric ω, that quantifies how closely the mixed ARC^{Sc} mimics the IAA$_x$ behavior, as follows.

$$\omega = \frac{\int |g(\theta_{xy}) - g(\theta_y)| dt}{\int |g(\theta_x) - g(\theta_y)| dt}, \tag{5}$$

where $g(\theta_{xy})$ is the response dynamics of a mixed ARC^{Sc} that co-expresses IAA$_x$ and IAA$_y$. IAA$_x$ has near 0 dominance, when α and β are both zeros, and complete dominance when they are both ones. With a low β (e.g. $\beta =$

[1]The estimated parameters for the IAA-competition ARC^{Sc} variants are shown in the Supplementary Table 4.

0, IAA_x entirely loses the competition over ARF-binding to IAA_y), IAA_x can still dominate the response by having a high relative competitiveness in AFB-binding (α). With a low α, IAA_x cannot dominate even with maximum β value. It is not surprising that competitiveness is better captured by α since α corresponds to k_5 which affects the auxin response much more than k_8. Note that one cannot conclude from this analysis that a faster or slower k_5 predicts competition. Rather, we simply use α to describe which of two IAAs dominate by showing which effective k_5 results from the competition.

References

[1] K. Havens *et al.*, A synthetic approach reveals extensive tunability of auxin signaling. *Plant Physiology*. **160**(1) 135-142 (2012).

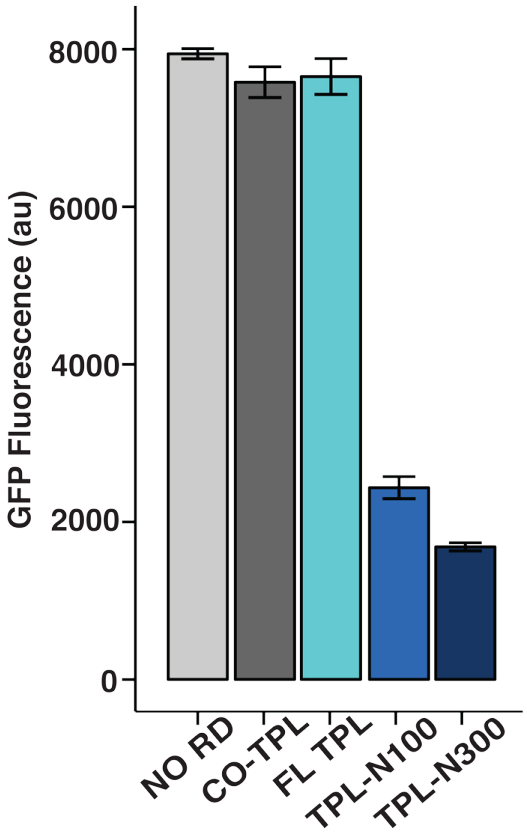

Supplementary Figure 1: TPL co-expression with IAA14 does not inhibit ARF activation. Full length (FL) TPL was either co-expressed with IAA14 (dark grey) or fused to IAA14 (light blue). Both constructs exhibited similar levels of preauxin steady state GFP reporter activity as ARC strains with IAA14 alone (NO RD). The other RD constructs are shown for reference. Error bars represent standard deviation (n=2).

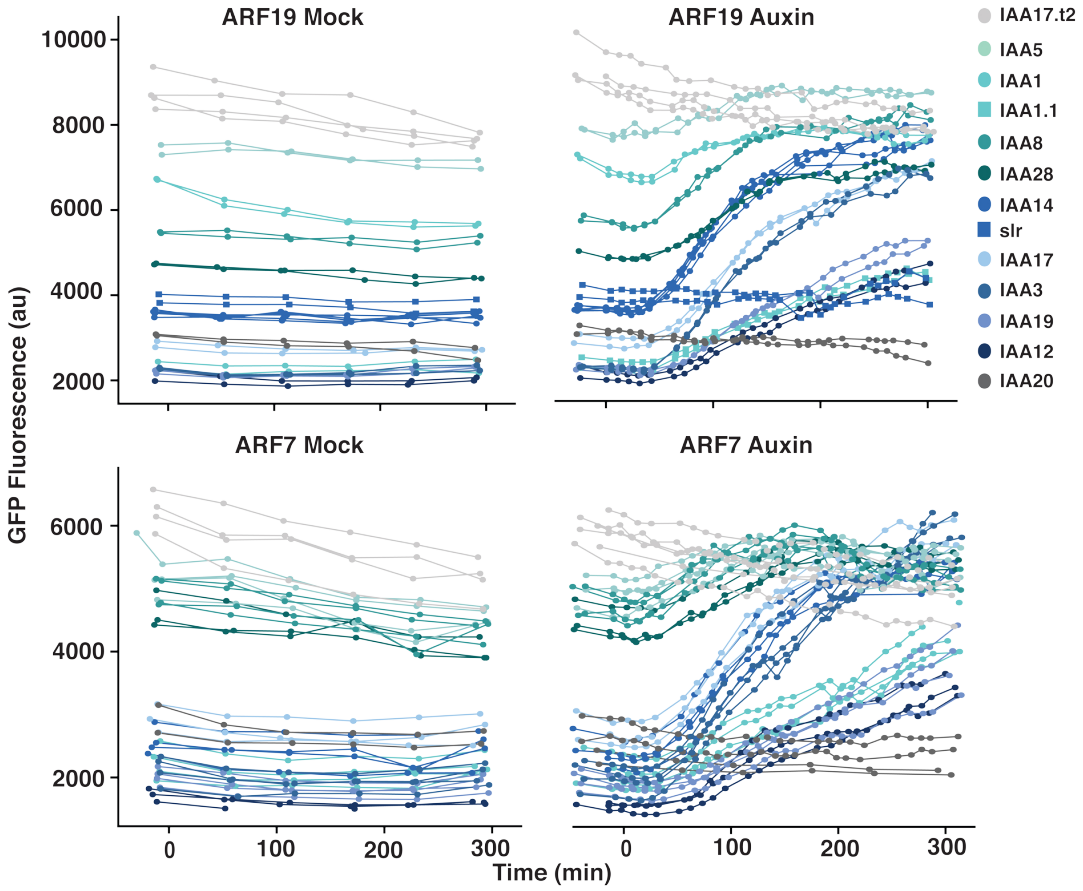

Supplementary Figure 2: Flow cytometry data for all ARC^{Sc} strains tested. In addition, data is shown for IAA17.t2 (grey), which lacks the ARF interaction domain, IAA1.1 (light blue square), which is a yeast codon-optimized version of IAA1 and slr (blue square), which is an auxin-insensitive form of IAA14. The top panels show mock and auxin treated data for each IAA in the presence of ARF19, while the bottom panels show the same IAAs in the presence of ARF7.

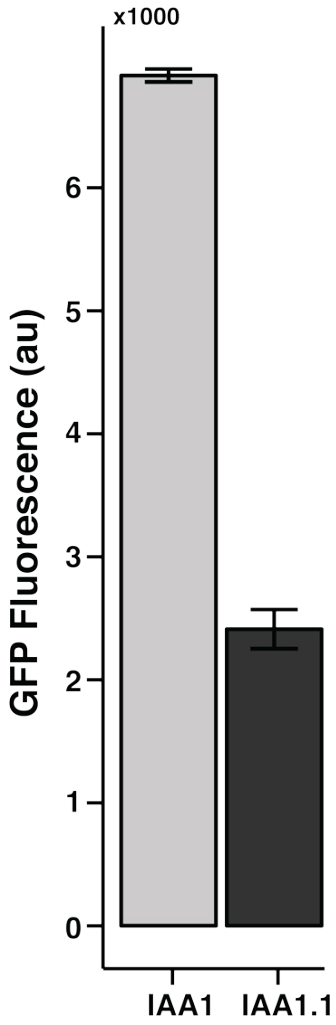

Supplementary Figure 3: Preauxin steady state GFP reporter activity of IAA 1.1 is lower than that of IAA1 in ARF19 circuits. IAA1.1 is codon optimized for yeast. It has a higher expression level than IAA1, while maintaining a similar rate of auxin-induced degradation [1]. Error bars represent standard deviation (n=2).

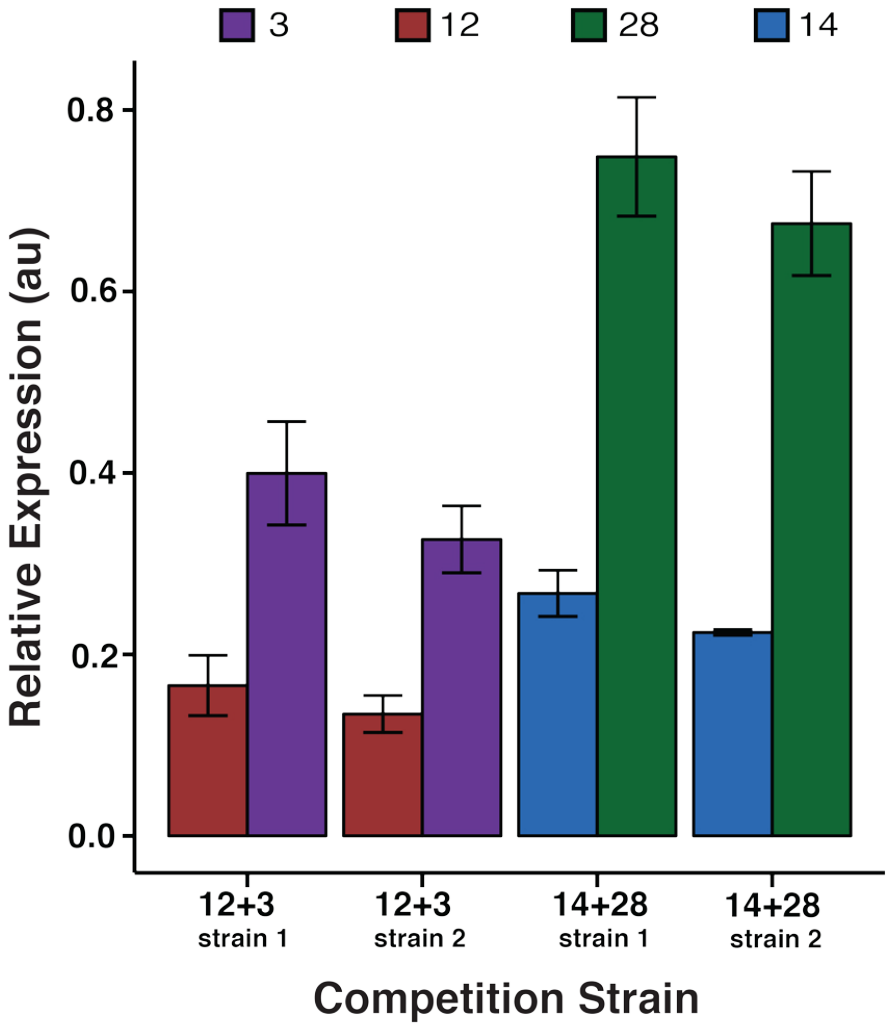

Supplementary Figure 4: IAA expression levels do not correlate with dominance behavior in ARC^{Sc} competition strains. qPCR was used to measure expression of each IAA present in replicate 12+3 or 14+28 strains. In both circuits, there were only modest differences in expression between the IAAs found in each strain. Notably, the dominant IAA in each of these competition circuits is not the IAA expressed at the highest level. Error bars represent standard error (n=3).

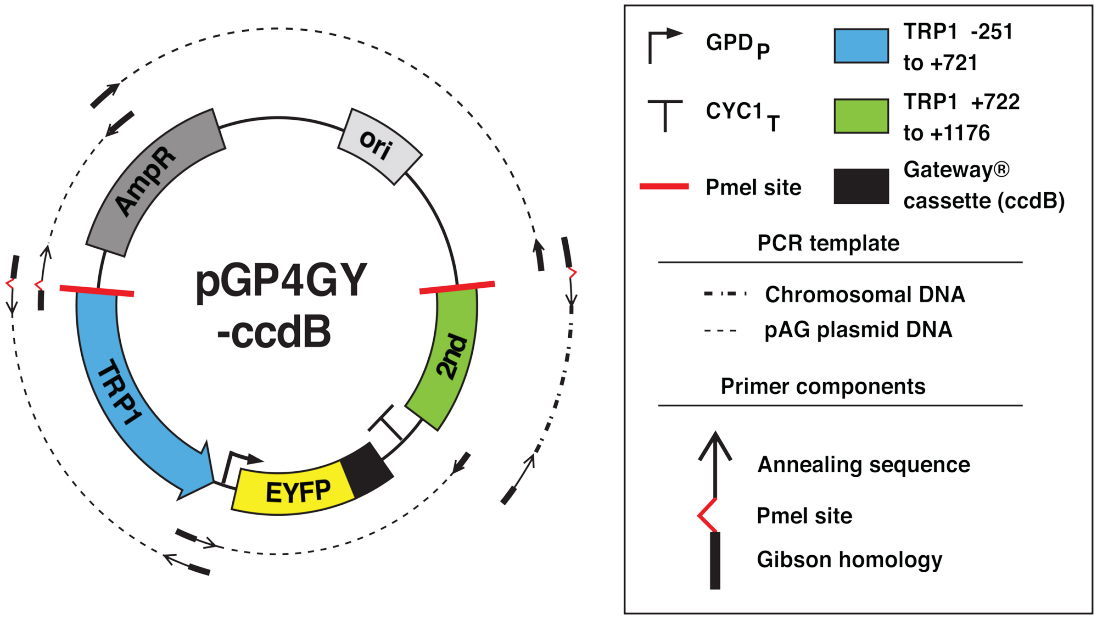

Supplementary Figure 5: Assembly of pGP4GY-ccdB. The construction of pG4GY-ccdB illustrates the minimum modifications needed to generate a single integrating derivative of a pAG vector. pG4GY-ccdB was generated in a single Gibson reaction using four PCR products from a pAG template (pAG304GPD-EYFP-ccdB) and one from a yeast chromosomal template. PmeI sites were inserted via PCR primer overhangs. The Gateway® expression cassette region (black) contains the ccdB counter-selectable marker and chloramphenicol resistance cassette flanked by attR recombination sites to facilitate Gateway® LR reactions. The second targeting domain (green) begins at the first bp on the chromosome following the sequence homologous to the TRP1 selectable marker cassette (blue); the TRP1 coding region starts at bp +1. This figure is not to scale.

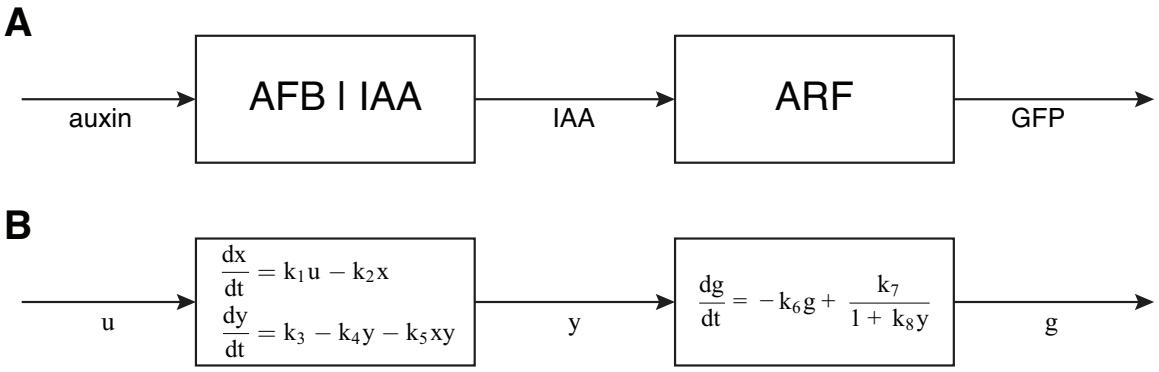

Supplementary Figure 6: The block diagram of the ARC^{Sc} and its model. (A) The subcomponent, AFB|IAA, was characterized previously. The ARF and GFP components were added here. The output of the first component (IAA), interacts with the ARF and affects the system output (GFP). (B) The mathematical model is extended to encompass the dynamics of the ARC^{Sc} by adding a third equation for the GFP dynamics. The block diagram illustrates the analogous composition of both the physical system and the mathematical model identification presented.

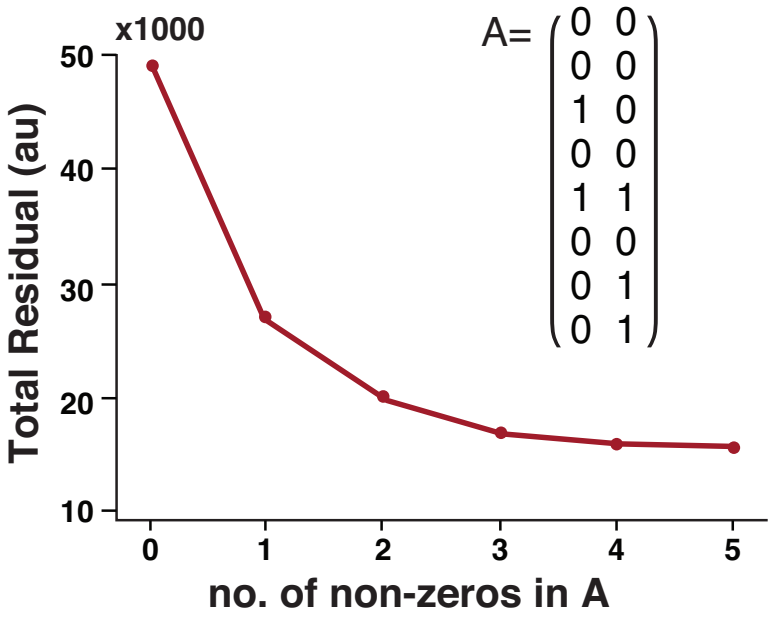

Supplementary Figure 7: Model-fit residual decreases with fewer constraints on parameter estimation. The increasing number of non-zero entries in the Parameter-Component dependency matrix corresponds to fewer constraints on the optimization of parameters to fit experimental data. The figure shows an instance of the greedy search algorithm, where monotonically decreasing behavior is observed. We conjecture that this behavior will be observed in general, but no analytical proof yet exists.

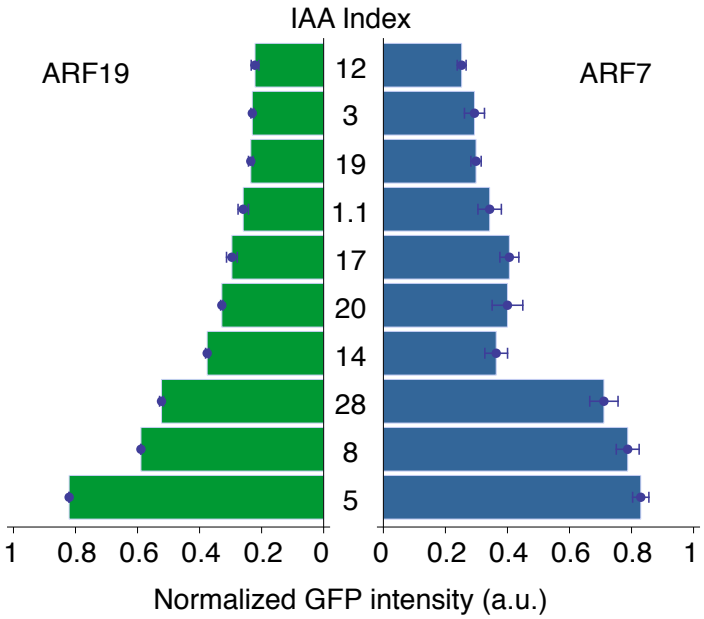

Supplementary Figure 8: Preauxin steady state values of ARC variants. A total of 20 different ARCs – 2 different ARFs in combination with 10 different IAAs – were evaluated. They are ordered according to GFP intensity in the ARF19 ARCs. For each ARC^{Sc}, two to four replicates were analyzed and the error bar shows one standard deviation among the replicates.

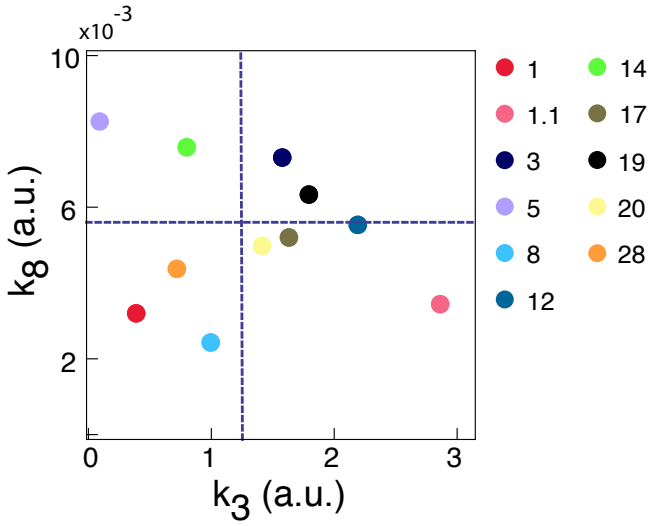

Supplementary Figure 9: k_3 and k_8 are not correlated. Scatter plot of k_3 and k_8 values are plotted for the 11 IAAs assayed with ARF19. Two to four biological replicates were analyzed per ARC, and each point represents the mean of the estimated parameter across replicates. The dashed lines indicate the mean of k_3 and k_8 across all IAAs.

Supplementary Table 1: Yeast strains used in this study

Strain	Genotype	Figure
W303-1A	MATa leu2-3,112 trp1-1 can1-100 ura3-1 his3-1,115 ybp1-1	
W814-29B	MATα ade2-1 trp1-1 can1-100 ura3-1 leu2-3,112 his3-1,115	
YKL381	MATα LEU2:pGPD-AFB2	
YKL388	MATa HIS3:pADH1-ARF19 URA3:pIAA19-GFP	
YKL714	MATa HIS3:pADH1-ARF7 URA3:pIAA19-GFP	
NY477	MATa HIS3:pADH1-ARF19 URA3:pIAA19-Cerulean-stop	
NY1205	MATa/MATα leu2-3,112/LEU2:pGPD-AFB2 trp1-1/TRP1:pGPD-TPL-N100-IAA3 his3-1,115/HIS3:pADH1-ARF19 ura3-1/URA3:pIAA19-Cerulean-stop	Figure 1
YKL1808	MATa/MATα leu2-3,112/LEU2:pGPD-AFB2 trp1-1/TRP1:pGPD-YFP-TPL-N100-IAA3 his3-1,115/HIS3:pADH1-ARF19	Figure 1
YKL1718	MATa/MATα leu2-3,112/LEU2:pGPD-AFB2 his3-1,115/HIS3:pADH1-ARF19 ura3-1/URA3:pIAA19-GFP trp1-1/TRP1:pGPD-IAA14	Figure 1,S1
YKL1717	MATa/MATα leu2-3,112/LEU2:pGPD-AFB2 his3-1,115/HIS3:pADH1-ARF19 ura3-1/URA3:pIAA19-GFP trp1-1/TRP1:pGPD-TPL-N300-IAA14	Figure 1,S1
YKL 1706	MATa/MATα leu2-3,112/LEU2:pGPD-AFB2 trp1-1/TRP1:pGPD-TPL-N100-IAA14 his3-1,115/HIS3:pADH1-ARF19 ura3-1/URA3:pIAA19-GFP	Figure 1, 2, S2
YKL1560	MATa/MATα leu2-3,112/LEU2:pGPD-AFB2 trp1-1/TRP1:pGPD-TPL-N100-IAA12 his3-1,115/HIS3:pADH1-ARF19 ura3-1/URA3:pIAA19-GFP	Figure 2, S2
YKL1564	MATa/MATα leu2-3,112/LEU2:pGPD-AFB2 trp1-1/TRP1:pGPD-TPL-N100-IAA28 his3-1,115/HIS3:pADH1-ARF19 ura3-1/URA3:pIAA19-GFP	Figure 2, S2
YKL1562	MATa/MATα leu2-3,112/LEU2:pGPD-AFB2 trp1-1/TRP1:pGPD-TPL-N100-IAA3 his3-1,115/HIS3:pADH1-ARF19 ura3-1/URA3:pIAA19-GFP	Figure 1, 2, S2
YKL1563	MATa/MATα leu2-3,112/LEU2:pGPD-AFB2 trp1-1/TRP1:pGPD-TPL-N100-IAA19 his3-1,115/HIS3:pADH1-ARF19 ura3-1/URA3:pIAA19-GFP	Figure 2, S2
YKL1567	MATa/MATα leu2-3,112/LEU2:pGPD-AFB2 trp1-1/TRP1:pGPD-TPL-N100-IAA20 his3-1,115/HIS3:pADH1-ARF19 ura3-1/URA3:pIAA19-GFP	Figure 2, S2
YKL1561	MATa/MATα leu2-3,112/LEU2:pGPD-AFB2 trp1-1/TRP1:pGPD-TPL-N100-IAA1 his3-1,115/HIS3:pADH1-ARF19 ura3-1/URA3:pIAA19-GFP	Figure S2,S3
YKL1568	MATa/MATα leu2-3,112/LEU2:pGPD-AFB2 trp1-1/TRP1:pGPD-TPL-N100-IAA1.1 his3-1,115/HIS3:pADH1-ARF19 ura3-1/URA3:pIAA19-GFP	Figure S2,S3
YKL1566	MATa/MATα leu2-3,112/LEU2:pGPD-AFB2 trp1-1/TRP1:pGPD-TPL-N100-IAA17.T2 his3-1,115/HIS3:pADH1-ARF19 ura3-1/URA3:pIAA19-GFP	Figure 2, S2
YKL1720	MATa/MATα leu2-3,112/LEU2:pGPD-AFB2 trp1-1/TRP1:pGPD-TPL-N100-IAA5 his3-1,115/HIS3:pADH1-ARF19 ura3-1/URA3:pIAA19-GFP	Figure S2
YKL1722	MATa/MATα leu2-3,112/LEU2:pGPD-AFB2 trp1-1/TRP1:pGPD-TPL-N100-IAA8 his3-1,115/HIS3:pADH1-ARF19 ura3-1/URA3:pIAA19-GFP	Figure 2, S2
YKL1707	MATa/MATα leu2-3,112/LEU2:pGPD-AFB2 trp1-1/TRP1:pGPD-TPL-N100-IAA17 his3-1,115/HIS3:pADH1-ARF19 ura3-1/URA3:pIAA19-GFP	Figure 2, S2
YKL1565	MATa/MATα leu2-3,112/LEU2:pGPD-AFB2 trp1-1/TRP1:pGPD-TPL-IAA14.SLR his3-1,115/HIS3:pADH1-ARF19 ura3-1/URA3:pIAA19-GFP	Figure S2
NY520	MATa/MATα his3-1,115/HIS3:pADH1-ARF7 ura3-1/URA3:pIAA19-GFP leu2-3,112/LEU2:pGPD-AFB2 trp1-1/TRP1:pGPD-TPL-N100-IAA14	Figure 2, S2
YKL1569	MATa/MATα leu2-3,112/LEU2:pGPD-AFB2 trp1-1/TRP1:pGPD-TPL-IAA12 his3-1,115/HIS3:pADH1-ARF7 ura3-1/URA3:pIAA19-GFP	Figure 2, S2
YKL1573	MATa/MATα leu2-3,112/LEU2:pGPD-AFB2 trp1-1/TRP1:pGPD-TPL-IAA28 his3-1,115/HIS3:pADH1-ARF7 ura3-1/URA3:pIAA19-GFP	Figure 2, S2
YKL1571	MATa/MATα leu2-3,112/LEU2:pGPD-AFB2 trp1-1/TRP1:pGPD-TPL-IAA3 his3-1,115/HIS3:pADH1-ARF7 ura3-1/URA3:pIAA19-GFP	Figure 2, S2
YKL1572	MATa/MATα leu2-3,112/LEU2:pGPD-AFB2 trp1-1/TRP1:pGPD-TPL-IAA19 his3-1,115/HIS3:pADH1-ARF7 ura3-1/URA3:pIAA19-GFP	Figure 2, S2
YKL1576	MATa/MATα leu2-3,112/LEU2:pGPD-AFB2 trp1-1/TRP1:pGPD-TPL-IAA20 his3-1,115/HIS3:pADH1-ARF7 ura3-1/URA3:pIAA19-GFP	Figure 2, S2
YKL1570	MATa/MATα leu2-3,112/LEU2:pGPD-AFB2 trp1-1/TRP1:pGPD-TPL-IAA1 his3-1,115/HIS3:pADH1-ARF7 ura3-1/URA3:pIAA19-GFP	Figure S2

YKL1577	MATa/MATα leu2-3,112/LEU2:pGPD-AFB2 trp1-1/TRP1:pGPD-TPL-IAA1.1 his3-1,115/HIS3:pADH1-ARF7 ura3-1/URA3:pIAA19-GFP	Figure S2
YKL1574	MATa/MATα leu2-3,112/LEU2:pGPD-AFB2 trp1-1/TRP1:pGPD-TPL-IAA14.SLR his3-1,115/HIS3:pADH1-ARF7 ura3-1/URA3:pIAA19-GFP	Figure S2
YKL1723	MATa/MATα leu2-3,112/LEU2:pGPD-AFB2 trp1-1/TRP1:pGPD-TPL-N100-IAA5 his3-1,115/HIS3:pADH1-ARF7 ura3-1/URA3:pIAA19-GFP	Figure S2
YKL1725	MATa/MATα leu2-3,112/LEU2:pGPD-AFB2 trp1-1/TRP1:pGPD-TPL-N100-IAA8 his3-1,115/HIS3:pADH1-ARF7 ura3-1/URA3:pIAA19-GFP	Figure 2, S2
NY524	MATa/MATα his3-1,115/HIS3:pADH1-ARF7 ura3-1/URA3:pIAA19-GFP leu2-3,112/LEU2:pGPD-AFB2 trp1-1/TRP1:pGPD-TPL-N100-IAA17	Figure 2, S2
YKL1575	MATa/MATα leu2-3,112/LEU2:pGPD-AFB2 trp1-1/TRP1:pGPD-TPL-IAA17.T2 his3-1,115/HIS3:pADH1-ARF7 ura3-1/URA3:pIAA19-GFP	Figure 2, S2
NY653	MATa/MATα leu2-3,112/LEU2:pGPD-AFB2 TRP1:pGPD-TPL-N100-IAA14/TRP1:pGPD-TPL-N100-IAA14 HIS3:pADH1-ARF19 URA3:pIAA19-GFP	Figure 4
NY665	MATa/MATα leu2-3,112/LEU2:pGPD-AFB2 TRP1:pGPD-TPL-N100-IAA28/TRP1:pGPD-TPL-N100-IAA28 HIS3:pADH1-ARF19 URA3:pIAA19-GFP	Figure 4
NY659	MATa/MATα leu2-3,112/LEU2:pGPD-AFB2 TRP1:pGPD-TPL-N100-IAA12/TRP1:pGPD-TPL-N100-IAA12 HIS3:pADH1-ARF19 URA3:pIAA19-GFP	Figure 4
NY897	MATa/MATα leu2-3,112/LEU2:pGPD-AFB2 TRP1:pGPD-TPL-N100-IAA3/TRP1:pGPD-TPL-N100-IAA3 HIS3:pADH1-ARF19 URA3:pIAA19-GFP	Figure 4
NY654	MATa/MATα leu2-3,112/LEU2:pGPD-AFB2 TRP1:pGPD-TPL-N100-IAA12/TRP1:pGPD-TPL-N100-IAA14 HIS3:pADH1-ARF19 URA3:pIAA19-GFP	Figure 4
NY658	MATa/MATα leu2-3,112/LEU2:pGPD-AFB2 TRP1:pGPD-TPL-N100-IAA14/TRP1:pGPD-TPL-N100-IAA12 HIS3:pADH1-ARF19 URA3:pIAA19-GFP	Figure 4
NY655	MATa/MATα leu2-3,112/LEU2:pGPD-AFB2 TRP1:pGPD-TPL-N100-IAA28/TRP1:pGPD-TPL-N100-IAA14 HIS3:pADH1-ARF19 URA3:pIAA19-GFP	Figure 4, S4
NY663	MATa/MATα leu2-3,112/LEU2:pGPD-AFB2 TRP1:pGPD-TPL-N100-IAA14/TRP1:pGPD-TPL-N100-IAA28 HIS3:pADH1-ARF19 URA3:pIAA19-GFP	Figure 4, S4
NY657	MATa/MATα leu2-3,112/LEU2:pGPD-AFB2 TRP1:pGPD-TPL-N100-IAA3/TRP1:pGPD-TPL-N100-IAA14 HIS3:pADH1-ARF19 URA3:pIAA19-GFP	Figure 4
NY893	MATa/MATα leu2-3,112/LEU2:pGPD-AFB2 TRP1:pGPD-TPL-N100-IAA14/TRP1:pGPD-TPL-N100-IAA3 HIS3:pADH1-ARF19 URA3:pIAA19-GFP	Figure 4
NY662	MATa/MATα leu2-3,112/LEU2:pGPD-AFB2 TRP1:pGPD-TPL-N100-IAA3/TRP1:pGPD-TPL-N100-IAA12 HIS3:pADH1-ARF19 URA3:pIAA19-GFP	Figure 4, S4
NY894	MATa/MATα leu2-3,112/LEU2:pGPD-AFB2 TRP1:pGPD-TPL-N100-IAA12/TRP1:pGPD-TPL-N100-IAA3 HIS3:pADH1-ARF19 URA3:pIAA19-GFP	Figure 4, S4
NY551	MATa/MATα his3-1,115/HIS3:pADH1-ARF19 ura3-1/URA3:pIAA19-GFP trp1-1/TRP1:pGPD-TPL leu2-3,112/LEU2:pGPD-AFB2 trp1-1/TRP1:pGPD-IAA14	Figure S1
NY903	MATa/MATα leu2-3,112/LEU2:pGPD-AFB2 trp1-1/TRP1:pGPD-TPL-IAA14 his3-1,115/HIS3:pADH1-ARF19 ura3-1/URA3:pIAA19-GFP	Figure S1

Supplementary Table 2: Primers used in this study

Primers to clone ARFs into pDONR	
prKL419: ARF7 F	AAAAAGCAGGCTTCAAAATGAAAGCTCCTTCATCAAATGG
prKL268: ARF7 R	AGAAAGCTGGGTGTCACCGGTTAAACGAAGTGG
prKL437: ARF19FW	AAAAAGCAGGCTTCAAAATGAAAGCTCCATCAAATG
prKL438: ARF19RV	AGAAAGCTGGGTGTTACTATCTGTTGAAAGAAGCTGC

Adapter primers used to increase the att sites on cloned ARF PCR product	
prKL52: adapter attB1 F	GGGGACAAGTTTGTACAAAAAAGCAGGCT
prKL53: adapter attB2 R	GGGGACCACTTTGTACAAGAAAGCTGGGT

Primers for Gibson assembly of pGP4G-TPL-N100-ccdB	
prNL1386:	tctagaactagtggatccccgggacaaaATGTCTTCTCTTAGTAGAGAGCTCG
prNL1376: TPLRD1_R_adapt	AGAAAGCTGGGTGTTAATCCTTCACTAGTATATCCACAGC
prNL1481: eYFPspacer_F	GGTGGACCAGGTGGTGGACATC
prKL771:Ampr_split_F	GTTCGCCAGTTAATAGTTTGCGCAACG
GPD+pBlueScript_R	gatccactagttctagaatccgtcgaaactaagttctggtg
prKL559:Ampr_split_R	ATCGGAGGACCGAAGGAGCTAACC

PCRs fused in Gibson
prNL1386 with prNL1376 using A.t. cDNA as template
prNL1481 with prKL559 using pGP4G-ccdB as template
prKL1390 with prKL771 using pGP4G-ccdB as template

Primers for Gibson assembly of pGP4G-TPL-N300-ccdB	
prNL1386:	tctagaactagtggatccccgggacaaaATGTCTTCTCTTAGTAGAGAGCTCG
prNL1377: TPLRD2_R_adapt	AGAAAGCTGGGTGTTAAGAATCTGCTGACGGGTAGTCTAAAGAA GCATT
prNL1481: eYFPspacer_F	GGTGGACCAGGTGGTGGACATC
prKL771:Ampr_split_F	GTTCGCCAGTTAATAGTTTGCGCAACG
prNL1390: GPD+pBlueScript_R	gatccactagttctagaatccgtcgaaactaagttctggtg
prKL559:Ampr_split_R	ATCGGAGGACCGAAGGAGCTAACC

PCRs fused in Gibson
prNL1386 with prNL1377 using A.t. cDNA as template
prNL1481 with prKL559 using pGP4G-ccdB as template
prKL1390 with prKL771 using pGP4G-ccdB as template

Supplementary Table 3. Estimated parameters of Auxin Response Circuits

IAA	RD	ARF	rep	k1	k2	k3	k4	k5	k6	k7	k8	
1.1	TPLRD1	7	1	0.138	0.103	1.320	0.003	0.011	0.007	43.294	0.004	
1.1	TPLRD1	7	2	0.138	0.103	1.945	0.003	0.012	0.007	43.294	0.004	
1.1	TPLRD1	7	3	0.138	0.103	1.348	0.003	0.013	0.007	43.294	0.005	
1.1	TPLRD1	7	4	0.138	0.103	1.542	0.003	0.013	0.007	43.294	0.005	
3	TPLRD1	7	1	0.138	0.103	0.801	0.003	0.083	0.007	43.294	0.009	
3	TPLRD1	7	2	0.138	0.103	1.332	0.003	0.056	0.007	43.294	0.006	
3	TPLRD1	7	3	0.138	0.103	1.307	0.003	0.082	0.007	43.294	0.006	
3	TPLRD1	7	4	0.138	0.103	2.527	0.003	0.069	0.007	43.294	0.004	
5	TPLRD1	7	1	0.138	0.103	0.070	0.003	0.032	0.007	43.294	0.007	
5	TPLRD1	7	2	0.138	0.103	0.107	0.003	0.046	0.007	43.294	0.007	
5	TPLRD1	7	3	0.138	0.103	0.146	0.003	0.012	0.007	43.294	0.004	
5	TPLRD1	7	4	0.138	0.103	0.102	0.003	0.006	0.007	43.294	0.008	
8	TPLRD1	7	1	0.138	0.103	0.120	0.003	0.063	0.007	43.294	0.006	
8	TPLRD1	7	2	0.138	0.103	0.122	0.003	0.047	0.007	43.294	0.009	
8	TPLRD1	7	3	0.138	0.103	0.192	0.003	0.024	0.007	43.294	0.004	
8	TPLRD1	7	4	0.138	0.103	0.078	0.003	0.056	0.007	43.294	0.013	
12	TPLRD1	7	1	0.138	0.103	1.608	0.003	0.012	0.007	43.294	0.007	
12	TPLRD1	7	2	0.138	0.103	1.531	0.003	0.017	0.007	43.294	0.006	
12	TPLRD1	7	3	0.138	0.103	1.546	0.003	0.012	0.007	43.294	0.006	
14	TPLRD1	7	1	0.138	0.103	1.033	0.003	0.127	0.007	43.294	0.005	
14	TPLRD1	7	2	0.138	0.103	0.669	0.003	0.055	0.007	43.294	0.009	
14	TPLRD1	7	3	0.138	0.103	1.158	0.003	0.078	0.007	43.294	0.006	
14	TPLRD1	7	4	0.138	0.103	1.011	0.003	0.109	0.007	43.294	0.006	
17	TPLRD1	7	1	0.138	0.103	0.771	0.003	0.042	0.007	43.294	0.005	
17	TPLRD1	7	2	0.138	0.103	1.308	0.003	0.046	0.007	43.294	0.004	
17	TPLRD1	7	3	0.138	0.103	0.843	0.003	0.023	0.007	43.294	0.005	
19	TPLRD1	7	1	0.138	0.103	1.728	0.003	0.013	0.007	43.294	0.004	
19	TPLRD1	7	2	0.138	0.103	2.656	0.003	0.011	0.007	43.294	0.003	
19	TPLRD1	7	3	0.138	0.103	1.820	0.003	0.011	0.007	43.294	0.004	
19	TPLRD1	7	4	0.138	0.103	1.617	0.003	0.009	0.007	43.294	0.006	
20	TPLRD1	7	1	0.138	0.103	0.575	0.003	0.000	0.007	43.294	0.007	
20	TPLRD1	7	2	0.138	0.103	1.122	0.003	0.000	0.007	43.294	0.004	
20	TPLRD1	7	3	0.138	0.103	1.043	0.003	0.000	0.007	43.294	0.006	
20	TPLRD1	7	4	0.138	0.103	1.008	0.003	0.000	0.007	43.294	0.006	
28	TPLRD1	7	1	0.138	0.103	0.363	0.003	0.025	0.007	43.294	0.003	
28	TPLRD1	7	2	0.138	0.103	0.419	0.003	0.047	0.007	43.294	0.004	
28	TPLRD1	7	3	0.138	0.103	0.361	0.003	0.025	0.007	43.294	0.004	
1	TPLRD1	19	1	0.138	0.103	0.413	0.003	0.013	0.007	62.284	0.003	
1	TPLRD1	19	2	0.138	0.103	0.364	0.003	0.010	0.007	62.284	0.003	
1.1	TPLRD1	19	1	0.138	0.103	2.750	0.003	0.008	0.007	62.284	0.003	
1.1	TPLRD1	19	2	0.138	0.103	2.974	0.003	0.010	0.007	62.284	0.004	
3	TPLRD1	19	1	0.138	0.103	1.584	0.003	0.035	0.007	62.284	0.007	
3	TPLRD1	19	2	0.138	0.103	1.570	0.003	0.038	0.007	62.284	0.007	
5	TPLRD1	19	1	0.138	0.103	0.096	0.003	0.050	0.007	62.284	0.008	
5	TPLRD1	19	2	0.138	0.103	0.087	0.003	0.039	0.007	62.284	0.009	
8	TPLRD1	19	1	0.138	0.103	1.080	0.003	0.050	0.007	62.284	0.002	
8	TPLRD1	19	2	0.138	0.103	0.909	0.003	0.043	0.007	62.284	0.003	
12	TPLRD1	19	1	0.138	0.103	2.096	0.003	0.011	0.007	62.284	0.005	
12	TPLRD1	19	2	0.138	0.103	2.288	0.003	0.011	0.007	62.284	0.006	
14	TPLRD1	19	1	0.138	0.103	1.185	0.003	0.040	0.007	62.284	0.005	
14	TPLRD1	19	2	0.138	0.103	0.680	0.003	0.060	0.007	62.284	0.009	
14	TPLRD1	19	3	0.138	0.103	0.587	0.003	0.053	0.007	62.284	0.010	
14	TPLRD1	19	4	0.138	0.103	0.820	0.003	0.055	0.007	62.284	0.007	
14	TPLRD1	19	5	0.138	0.103	0.725	0.003	0.054	0.007	62.284	0.008	
17	TPLRD1	19	1	0.138	0.103	1.288	0.003	0.027	0.007	62.284	0.006	
17	TPLRD1	19	2	0.138	0.103	1.975	0.003	0.033	0.007	62.284	0.004	
19	TPLRD1	19	1	0.138	0.103	1.970	0.003	0.013	0.007	62.284	0.006	
19	TPLRD1	19	2	0.138	0.103	1.617	0.003	0.015	0.007	62.284	0.007	
20	TPLRD1	19	1	0.138	0.103	1.412	0.003	0.000	0.007	62.284	0.005	
20	TPLRD1	19	2	0.138	0.103	1.415	0.003	0.000	0.007	62.284	0.005	
28	TPLRD1	19	1	0.138	0.103	0.955	0.003	0.011	0.007	62.284	0.003	
28	TPLRD1	19	2	0.138	0.103	0.703	0.003	0.010	0.007	62.284	0.004	

Supplementary Table 4. Estimated parameters of competition Auxin Response Circuits

Primary IAA	Secondary IAA	ARF	rep	k1	k2	k3	k4	k5	k6	k7	k8	
3	3	19	1	0.138	0.103	4.670	0.003	0.007	0.007	99.1	0.005	
3	3	19	2	0.138	0.103	4.636	0.003	0.007	0.007	99.1	0.005	
3	3	19	3	0.138	0.103	5.273	0.003	0.005	0.007	99.1	0.004	
3	3	19	4	0.138	0.103	5.701	0.003	0.008	0.007	99.1	0.004	
3	12	19	1	0.138	0.103	7.068	0.003	0.005	0.007	99.1	0.003	
3	12	19	2	0.138	0.103	5.841	0.003	0.006	0.007	99.1	0.005	
3	12	19	3	0.138	0.103	8.371	0.003	0.004	0.007	99.1	0.003	
3	12	19	4	0.138	0.103	8.754	0.003	0.004	0.007	99.1	0.003	
3	14	19	1	0.138	0.103	3.985	0.003	0.011	0.007	99.1	0.004	
3	14	19	2	0.138	0.103	7.883	0.003	0.012	0.007	99.1	0.002	
3	14	19	3	0.138	0.103	5.368	0.003	0.006	0.007	99.1	0.003	
3	14	19	4	0.138	0.103	3.874	0.003	0.009	0.007	99.1	0.005	
3	28	19	1	0.138	0.103	6.198	0.003	0.008	0.007	99.1	0.003	
3	28	19	2	0.138	0.103	6.621	0.003	0.007	0.007	99.1	0.003	
3	28	19	3	0.138	0.103	6.211	0.003	0.007	0.007	99.1	0.003	
3	28	19	4	0.138	0.103	6.236	0.003	0.008	0.007	99.1	0.003	
12	12	19	1	0.138	0.103	6.024	0.003	0.003	0.007	99.1	0.003	
12	12	19	2	0.138	0.103	6.762	0.003	0.002	0.007	99.1	0.003	
12	14	19	1	0.138	0.103	6.736	0.003	0.007	0.007	99.1	0.003	
12	14	19	2	0.138	0.103	6.501	0.003	0.007	0.007	99.1	0.003	
12	14	19	3	0.138	0.103	5.094	0.003	0.004	0.007	99.1	0.003	
12	14	19	4	0.138	0.103	6.984	0.003	0.005	0.007	99.1	0.003	
12	28	19	1	0.138	0.103	8.364	0.003	0.005	0.007	99.1	0.002	
12	28	19	2	0.138	0.103	3.474	0.003	0.004	0.007	99.1	0.003	
12	28	19	3	0.138	0.103	5.068	0.003	0.005	0.007	99.1	0.003	
12	28	19	4	0.138	0.103	5.128	0.003	0.004	0.007	99.1	0.003	
12	28	19	5	0.138	0.103	6.171	0.003	0.004	0.007	99.1	0.003	
14	14	19	1	0.138	0.103	3.718	0.003	0.014	0.007	99.1	0.004	
14	14	19	2	0.138	0.103	5.717	0.003	0.016	0.007	99.1	0.003	
14	28	19	1	0.138	0.103	4.869	0.003	0.011	0.007	99.1	0.002	
14	28	19	2	0.138	0.103	3.423	0.003	0.014	0.007	99.1	0.004	
14	28	19	3	0.138	0.103	3.412	0.003	0.009	0.007	99.1	0.003	
14	28	19	4	0.138	0.103	3.237	0.003	0.012	0.007	99.1	0.004	
28	28	19	1	0.138	0.103	6.099	0.003	0.003	0.007	99.1	0.002	
28	28	19	2	0.138	0.103	2.369	0.003	0.004	0.007	99.1	0.006	

Chapter 4

Molecular Basis of Auxin Nuclear Signaling

Edith Pierre-Jerome, Britney L. Moss, Amy Lanctot, Amber Hageman and

Jennifer L. Nemhauser

Abstract

Auxin regulated transcription pivots on the interaction between the AUXIN/INDOLE-3-ACETIC ACID (Aux/IAA) repressor proteins and the AUXIN RESPONSE FACTOR (ARF) transcription factors. Recent structural analyses of ARFs and Aux/IAAs have raised fundamental questions about the nature of the functional complexes driving auxin transcriptional responses. To parse the nature and significance of ARF-DNA and ARF-Aux/IAA interactions, we analyzed structure-guided variants of synthetic Auxin Response Circuits (ARCs) in the budding yeast *Saccharomyces cerevisiae*. Among our key findings was that ARFs exhibit promoter-specific activity and require dimerization at two distinct domains for full transcriptional activation. We also found that monomeric Aux/IAAs can repress ARF activity in both yeast and plants, and that there may be a bias in the orientation of these interactions. This type of systematic, quantitative structure-function analysis is not currently possible in plants, and was critical for discrimination between the multiple competing models currently proposed for auxin response.

Introduction

The plant hormone auxin regulates critical events in development, defense and metabolism, largely by orchestrating transcriptional changes. AUXIN RESPONSE FACTOR (ARF) transcription factors can be activated by auxin-induced degradation of AUXIN/INDOLE-3-ACETIC ACID repressors (Aux/IAAs, hereafter referred to as IAAs)[1]. Across flowering plants, ARFs and IAAs belong to large protein families [2]. Differences in the spatial distribution throughout the plant [3, 4] and the intrinsic function [5-8] across members of both families have led to a model where ARF-IAA complex composition defines context-specific auxin responses [9, 10]. However, the large size of both protein families, co-expression of multiple ARFs and IAAs within a cell, and numerous possible homo- and heterotypic interactions [1] have made testing this model quite challenging.

Recent structural studies have led to new models for ARF-IAA interactions and guided the engineering of critical genetic tools for probing the functional relevance of ARF-IAA complex composition. ARFs and IAAs interact through a conserved C-terminal domain shared by most members of each family [11]. This fold, originally called the III/IV domain, has been re-classified as a Phox and Bem1p (PB1) domain based on its structure [12-14]. The PB1 domain facilitates ARF-ARF and IAA-IAA interactions in yeast two-hybrid (Y2H) and *in vitro* assays [4, 15, 16], though the functional relevance of these homotypic interactions is not well established. Both ARF and IAA PB1 domains fold into two oppositely charged faces (“head” and “tail”), leading to potential oligomerization via head-to-tail electrostatic interactions [12-14]. Indeed, purified PB1

domains aggregate in large clusters *in vitro.* Whether these higher order complexes exist in plants, and what their biological relevance may be, remains unknown.

In addition to the interactions mediated by the PB1 domain, ARFs can dimerize through an N-terminal domain flanking the B3 DNA binding motif [17]. Dimerization through this domain is critical for the DNA binding and *in vivo* function of ARF5. The structure of an ARF5 DNA binding domain homodimer was solved bound to ER7, a short stretch of DNA containing inverted repeats of Auxin Response Elements (AuxREs). This structure revealed that each isolated domain contacted one of the AuxREs, suggesting that spacing and orientation of ARF binding sites contribute to the binding specificity of different ARFs. *In vitro* DNA binding studies supported this model, as DNA binding by ARF1 and ARF5 were differentially sensitive to the number of nucleotides between AuxREs [17]. These results add yet another dimension to possible models of auxin signaling, as the functional significance of multiple dimerization domains within full-length ARF proteins has not yet been determined.

Answering the many questions, old and new, about the functional molecular unit of auxin signaling requires a modular, quantitative assay that can fill in the wide gap between work *in vitro* and in plants. In the work described here, we assayed a number of synthetic Auxin Response Circuits in *Saccharomyces cerevisiae* (ARC^{Sc}) [18] to rigorously test current models of auxin-regulated transcription. ARC^{Sc} are user-defined circuits comprised of select IAA, ARF, and promoter sequences, combined with defined auxin input levels. ARC^{Sc} allowed direct, quantitative assessment of the functional importance of homo- and heterotypic interactions between auxin signaling components, while eliminating confounding factors like feedback or interference by other pathways.

Using this system, we demonstrated that ARFs exhibit promoter-specific activation activity and require dimerization at two distinct domains for effective transcriptional activation. Moreover, we discovered that IAA-IAA dimerization is unlikely to be of major biological significance, as it has little impact on the rate of auxin-induced degradation or the effectiveness of IAAs as repressors.

Results

ARF activity is promoter-specific

Several lines of inquiry, including recent structural studies, suggest that specificity in auxin responses reflect differences in ARF-DNA interaction. Using flow cytometry, we quantified the activity of a panel of ARFs, which included five activator ARFs (ARF5, ARF6, ARF7, ARF8, ARF19) and a repressor ARF (ARF2), on the native Arabidopsis *IAA19* promoter (*pIAA19*::*Venus*; Fig. 1A). As observed previously [18], ARF7 and ARF19 were effective activators of the *pIAA19*::*Venus* reporter. Though pIAA19 has five AuxREs within 300 nucleotides of the transcriptional start site, ARF8 was the only other ARF that activated *Venus* expression. These results suggest that the presence of AuxREs alone is not sufficient for ARF activity.

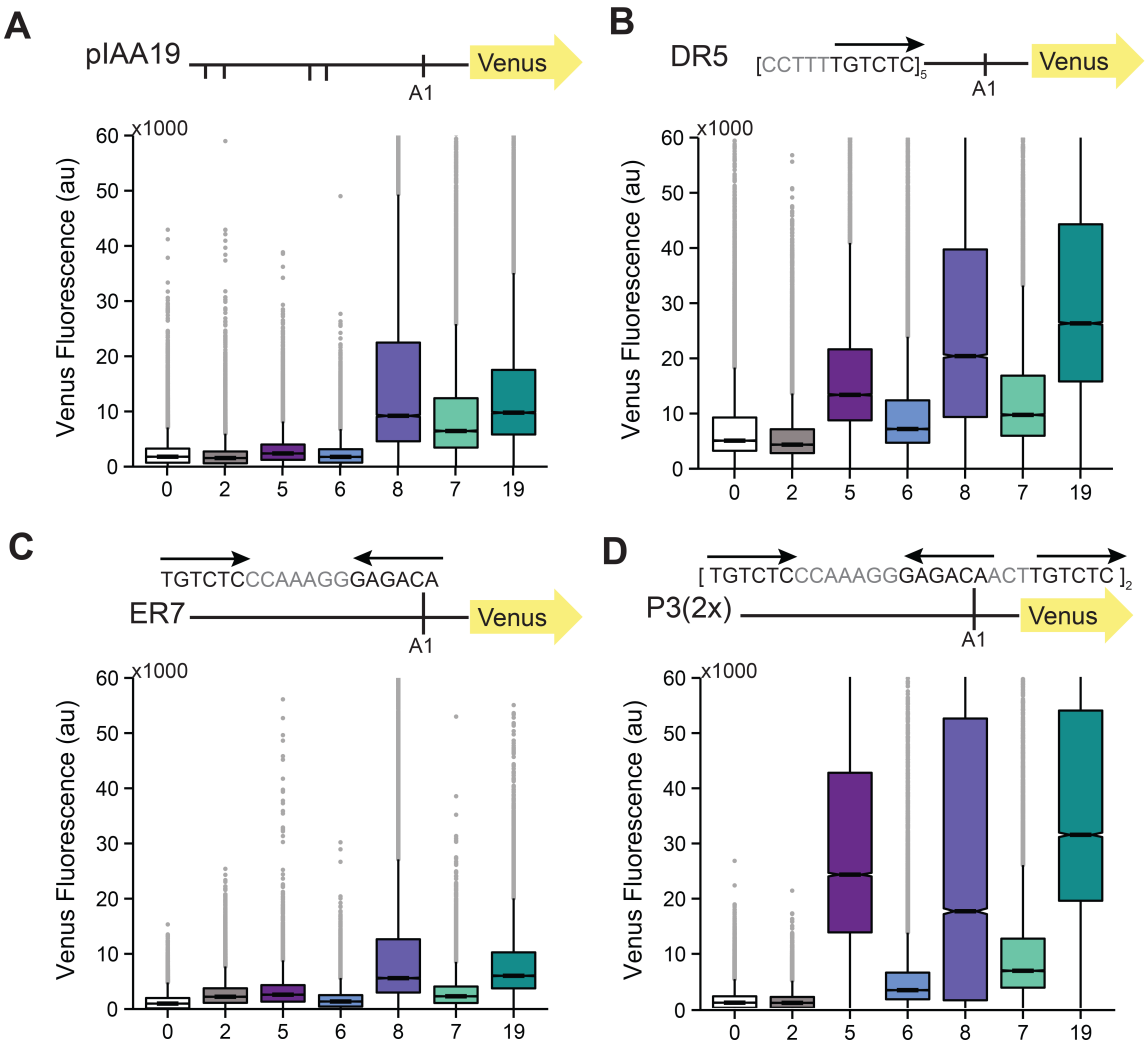

Fig 1. ARF transcription factors exhibit promoter-specific activity
(A) Comparison of ARF activity on the *pIAA19*::*Venus* reporter in yeast using flow cytometry. Each yeast strain contains the same reporter construct and differs only by the ARF expressed (2, 5, 6, 8, 7 or 19). "0" indicates absence of an ARF transcription factor. ARF expression levels are not correlated with activity (SI Fig. 1). Vertical lines in the reporter schematic indicate the location of an ARF binding site (AuxRE) in the native *IAA19* promoter (SI Fig. 1). The proximal site (A1) marks the insertion site of the AuxRE array variants in the following panels. **(B)** Comparison of ARF activity on the *DR5::Venus* fluorescent reporter in yeast. Five tandem repeats of the DR5 sequence replaced the pIAA19 sequence upstream of the A1 site. **(C)** Comparison of ARF activity on the *ER7::Venus* fluorescent reporter in yeast. The ER7 sequence containing an inverted pair of AuxREs was inserted in the middle of the A1 site in a pIAA19 reporter construct where all of the native AuxREs were mutated. **(D)** Comparison of ARF activity on the *P3(2x)::Venus* fluorescent reporter in yeast. A tandem repeat of the P3 sequence was inserted in the middle of the A1 site in a pIAA19 reporter construct where all the native AuxREs were mutated. Data is shown as Tukey box plots. The box in each column demarcates the first and third quartiles of all data. The inner band indicates the median with notches providing 95% confidence intervals around this value. Whisker lines span 1.5-times the inter-quartile range. Limits were set on the Cartesian coordinates to facilitate comparison across samples.

To distinguish between differences in activation strength and differences in affinity for different AuxRE configurations, we tested the same panel of ARFs against additional synthetic promoters. To limit any potential influence from flanking sequences, we generated promoter variants in the context of a mutated *IAA19* promoter where all of the AuxREs were rendered non-functional (SI Fig. 1). Into this ARF-insensitive promoter, we inserted previously characterized AuxRE arrays with variable number, spacing and orientation of sites [19]. The DR5 construct of direct AuxRE repeats has been used for decades to monitor auxin transcriptional effects in plants. Consistent with transient protoplast activation assays [20-22], all of the activator ARFs could activate a promoter containing a DR5-derived element in yeast (Fig. 1B). The strength of activation did vary, with ARF19 being the most active and ARF6 the least active.

Next, we introduced ER7, which is the pair of inverted AuxRE repeats utilized for the ARF DNA binding domain structural studies [17], as well as early biochemical assays [16]. Only ARF19 and ARF8 exhibited measurable activity on the ER7-containing promoter, and this effect was minimal in both cases (Fig. 1C). Notably ARF5, which has been shown to bind to this exact sequence *in vitro*, showed no activity. We then introduced tandem repeats of the P3 element [P3(2x)], which combines direct and inverted repeats and was used as a target for early biochemical binding assays and transient expression studies in protoplasts [16, 23]. Each P3 element is composed of an ER7 sequence separated from an additional AuxRE site by three nucleotides. Introduction of the P3(2x) element resulted in a dramatic increase in activation potential of ARF19, more than double the activity observed with the native pIAA19 (Fig. 1D). Strikingly, ARF5, which was nearly completely inactive on the native pIAA19 and ER7 variant,

activated the P3(2x)-containing promoter to similar levels as ARF19. Our data illustrate that the spacing and number of AuxREs can determine the strength and specificity of ARF activity.

ARFs activate as dimers

Working upstream from ARF-DNA interactions, we assessed the impact of homotypic interactions between ARFs on transcriptional activity. To maximize the sensitivity of these assays, we focused on the most active ARF-promoter combination: ARF19 and the *P3(2x)::Venus* reporter. To begin this analysis, we confirmed that ARF19 activity required the homologous residues identified as critical for ARF5 DNA binding (DB) and N-terminal dimerization (DD) [17]. As expected from the ARF5 data, the H138A (*db1*) and R188A (*db2*) DNA binding mutations resulted in the total loss of ARF19 activity (Fig. 2A, SI Table 1). G247I (*dd1*), which caused the most severe disruption of dimerization in ARF5, resulted in a complete loss of ARF19 activation activity. The A250N (*dd2*) and A255N (*dd3*) mutations retained modest levels of ARF19 activity, consistent with the observation that these mutations do not completely disrupt ARF5 dimerization [17].

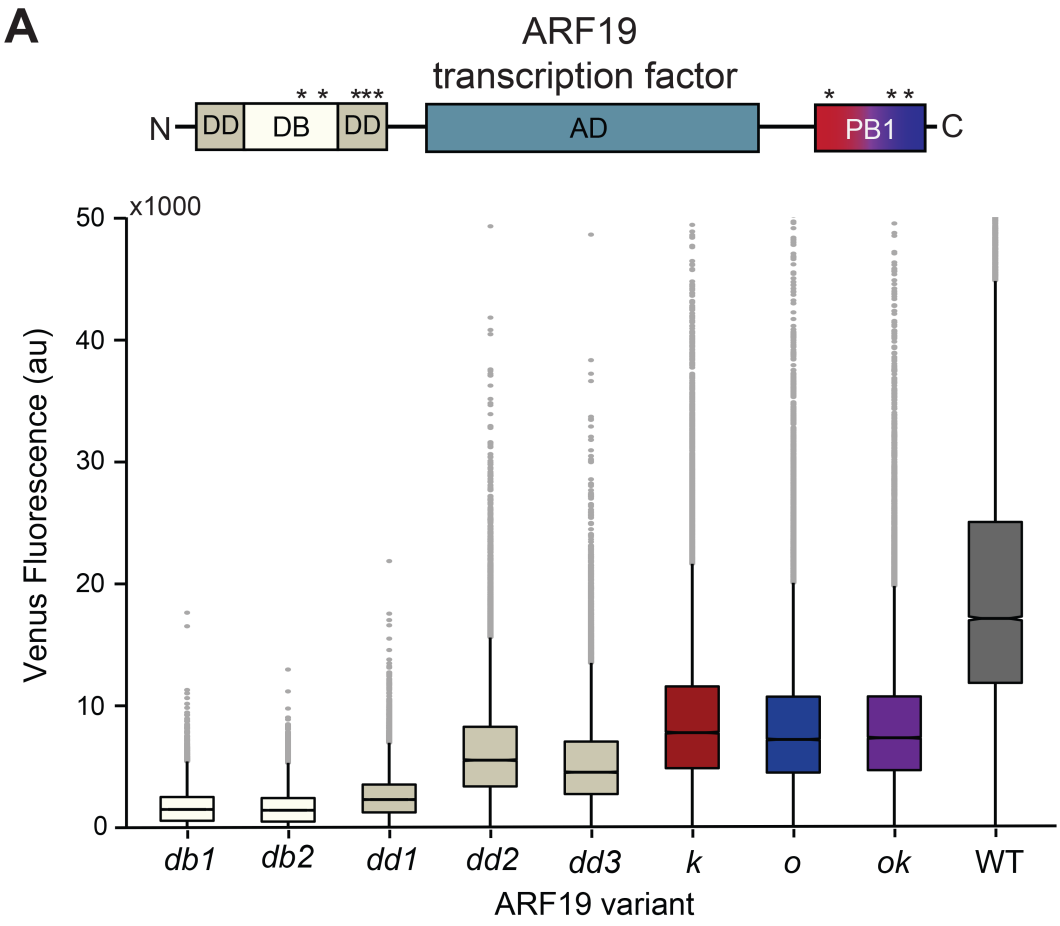
A
ARF19
transcription factor
N
DD
DB
DD
AD
PB1
C
* * ***
* **
x1000
50
40
30
20
10
0
Venus Fluorescence (au)
db1
db2
dd1
dd2
dd3
k
o
ok
WT
ARF19 variant

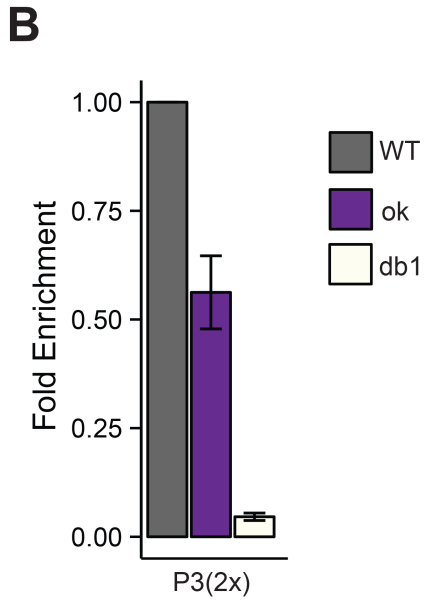
B
1.00
0.75
0.50
0.25
0.00
Fold Enrichment
P3(2x)
WT
ok
db1

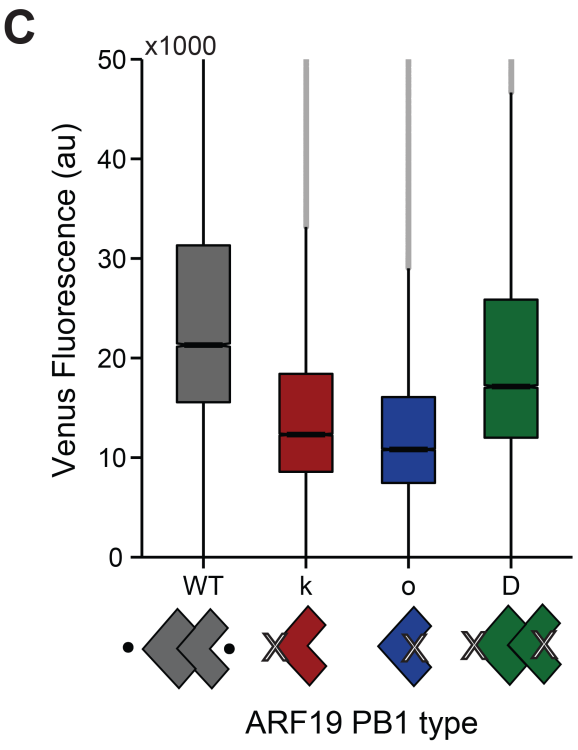
C
x1000
50
40
30
20
10
0
Venus Fluorescence (au)
WT
k
o
D
ARF19 PB1 type

Fig 2. ARFs activate as dimers
(A) ARF19 requires an intact PB1 domain for full activity. Activation of the *P3(2x)::Venus* fluorescent reporter by ARF19 variants in yeast. Asterisks above the ARF19 schematic indicate relative positions of point mutants. DB = DNA binding. DD=dimerization domain. AD= activation domain. PB1= C-terminal interaction domain. See SI Table 1 for specific residues that were mutated in each domain. Relative protein levels across the mutants were similar (SI Fig. S2). **(B)** PB1 mutations decrease DNA-binding by ARF19. Enrichment of 4xFLAG-ARF19 WT, double PB1 (*ok*), and DNA binding mutant (*db1*) at the P3(2x) locus. Results from three independent replicates are shown normalized to the enrichment of the wild-type ARF19. Error bars represent standard error. Relative activity of FLAG tagged ARFs was similar to untagged strains (SI Fig. 2). **(C)** Activity of ARF19 single PB1 mutants is rescued by co-expressing mutants with complementary interfaces to allow dimerization in the PB1 domain (D = *k* +*o*).

Next, we probed the impact of PB1 interactions on ARF19 activity. To do this, we engineered homologous mutations into ARF19 that were previously shown to compromise one or both PB1 interaction surfaces in ARF7 [13]. Specifically, we generated the following ARF19 variants: K962A (*k*) to disrupt the positively charged face (head), a double mutation D1012A and D1016A in the OPCA motif (*o*) to disrupt the negatively charged face (tail), and all three mutations in combination to disrupt interactions at both faces (*ok*) (Fig. 2A). Each mutant expressed on its own lack a complementary interface required for PB1 domain interactions, so each variant should provide a similar level of transcriptional activation representing the efficacy of an ARF19 PB1 monomer. Indeed, all variants exhibited similar and strongly diminished activity on the *P3(2x)::Venus* reporter when compared to wild-type ARF19 (Fig. 2A). Early *in vitro* studies using truncated ARFs indicated that PB1 interactions might be required to stabilize ARF binding to DNA [16]. We hypothesized that the observed reduction in transcriptional activation activity of ARF19 PB1 mutants might reflect reduced binding to the *P3(2x)* promoter. Chromatin immunoprecipitation assays supported this interpretation (Fig. 2B). ARF19 DNA binding was significantly reduced when the PB1

domain was mutated, although this reduced binding was still substantially stronger than what was observed when the DNA-binding domain was mutated. Thus, self-interaction at both the N-terminal DNA binding domain and the C-terminal PB1 domain are required for full ARF19 function.

The multimerization potential of the PB1 domain has led to speculation about the composition of the minimal functional unit needed for ARF action. While monomers showed a strong reduction or complete loss of activity, we wanted to test the activation potential of ARFs limited to dimers. To do this, we compared expression of the *P3(2x)::Venus* reporter in yeast transformed with either two copies of wild-type *ARF19*, two copies of either the *o* or *k* mutants, or a circuit containing one *k* and one *o* variant (Fig. 2C). We expected that wild-type ARF19 had the capacity to form dimers or higher order complexes, while *o* or *k* mutants were likely dimerized within the DNA binding domain but monomeric at the PB1 domains. A mixed *k* and *o* population allowed for dimerization at the DNA binding domain and only a single (dimer) interaction at the PB1 domain. As observed in yeast expressing only a single copy of the ARF19 variants, the monomeric PB1 mutants exhibited diminished activity on the *P3(2x)::Venus* reporter (Fig. 2C). Notably, the reconstituted PB1 dimer showed nearly the same activity as wild-type ARF19. This finding provides evidence that ARF dimers are functional, and that ARFs do not require higher-order complexes for efficient transcriptional activation.

IAAs can function as monomers

Continuing upstream in auxin response, we turned to the question of how many IAAs are required to effectively repress ARF activity. A number of models have been

proposed for ARF-IAA stoichiometry that depend upon the relative importance of different aspects of IAA function. In previous work, we demonstrated the importance of auxin-induced IAA degradation rate in tuning cellular sensitivity to auxin [18, 24, 25]. In the circuits examined here, IAA PB1 interactions had modest or no influence on IAA degradation rates (SI Fig. 3), supporting biochemical evidence that IAAs have only weak affinity for homotypic PB1 interactions compared to the strength of heterotypic interactions with ARF PB1 domains [12].

Multiple modes of IAA repression have been suggested by previous work. Structural studies suggest a potential mode of repression where IAAs directly interfere with ARF dimerization via occupation of ARF PB1 interaction surfaces [14]. Expression of an IAA alone has little impact on ARF activation in yeast [18]. This observation suggests that any insulating activity provided by ARF-IAA binding plays a minor role in repression, at least in conditions where both proteins are expressed at similar levels. In addition to potentially disrupting ARF-ARF interactions, IAAs repress transcription through the recruitment of TOPLESS (TPL) co-repressors [26]. As a member of the Groucho/Tup1 family of co-repressors, TPL likely recruits other components of the repression machinery and/or blocks co-activator binding once recruited to a DNA target site [26-28]. Co-expression of TPL with an IAA has no effect on reporter expression in ARC^{Sc}, but TPL:IAA fusions are effective repressors of ARF activity [18].

While a single PB1 interface is sufficient for ARF-IAA interaction in yeast two-hybrid and *in vitro* assays [12-14], there is conflicting evidence for whether this limited interaction is sufficient for repression [13, 14]. Through TPL:IAA fusions, we can directly measure the impact of each PB1 face on IAA repression strength. An N-terminal

fusion of the first 300 amino acids of TPL to IAA3 (TPLN300:IAA3) strongly represses ARF19 activity in a PB1-dependent manner (Fig. 3A). Mutations on both PB1 interaction surfaces of IAA3 (*ok*) showed a similar loss of repression ability as a complete PB1 deletion (ΔPB1). The single interface PB1 IAA mutants (*k* and *o*) maintain repression of ARF19, albeit with reduced strength. Similar results were observed for IAA14 and IAA7 (SI Fig. 4).

To further validate this observation, we transformed *Arabidopsis* seedlings with an auxin-insensitive form of *IAA14* (*solitary root, slr*) expressed from its own promoter. The *pIAA14::slr* transgenic plants largely recapitulate the phenotype of the *slr* mutant, where the initiation of nearly all lateral roots is inhibited (Fig. 3B). Single PB1 *slr* mutants maintain the ability to repress lateral root formation, in contrast to the large number of lateral roots made by plants expressing *slr* variants with both faces of the PB1 domain mutated. Together with the yeast assays, these results verify that an IAA monomer only able to interact with a single ARF PB1 surface can effectively repress ARF activity. This IAA-mediated repression is effective despite the fact that the target ARF can still form a homotypic dimer with a second ARF.

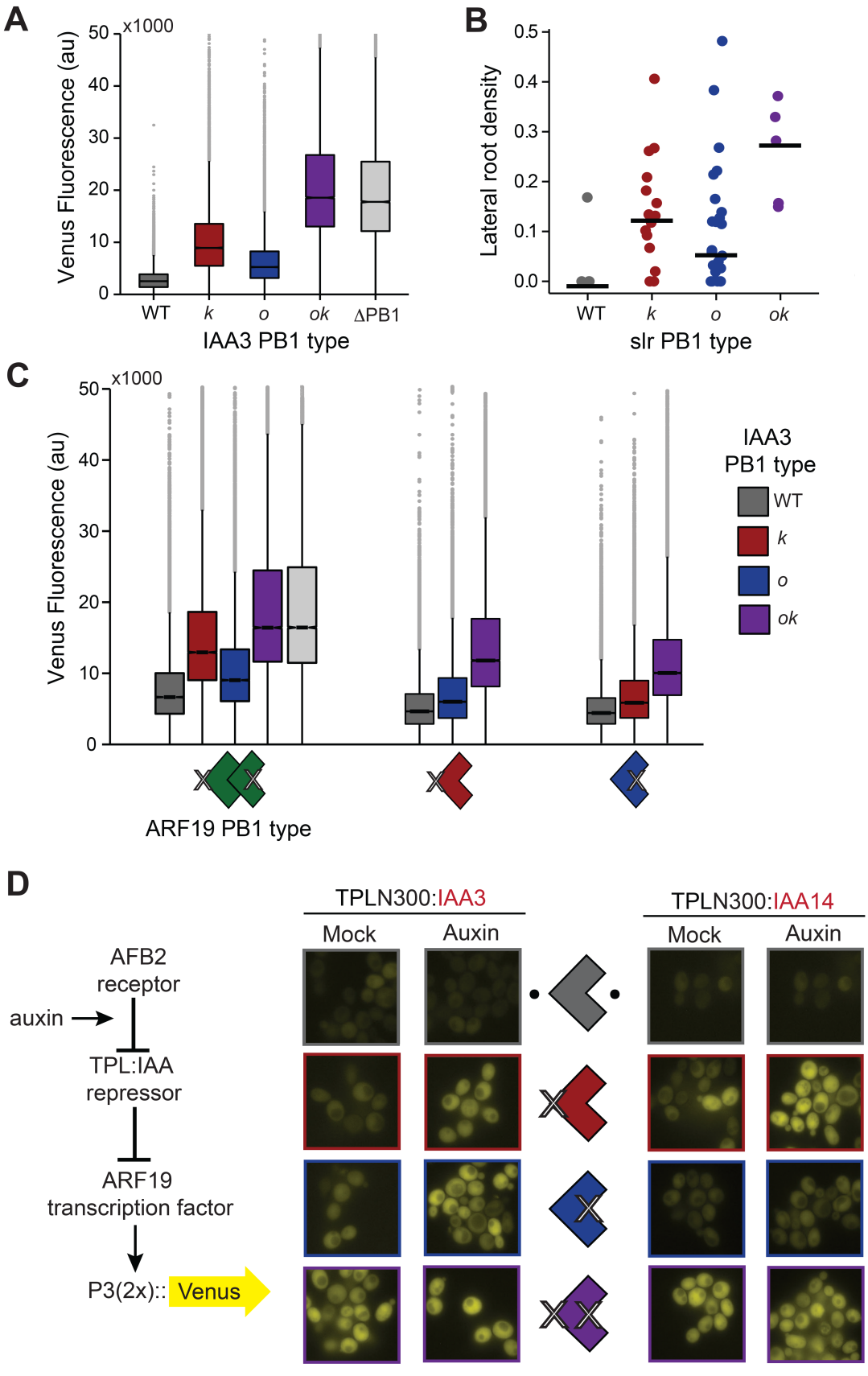
A
x1000
Venus Fluorescence (au)
50
40
30
20
10
0
WT
k
o
ok
ΔPB1
IAA3 PB1 type
B
Lateral root density
0.5
0.4
0.3
0.2
0.1
0.0
WT
k
o
ok
slr PB1 type
C
x1000
Venus Fluorescence (au)
50
40
30
20
10
0
ARF19 PB1 type
IAA3
PB1 type
WT
k
o
ok
D
AFB2
receptor
auxin
TPL:IAA
repressor
ARF19
transcription factor
P3(2x)::
Venus
TPLN300:IAA3
Mock
Auxin
TPLN300:IAA14
Mock
Auxin

Fig 3. IAAs can function as monomers
(A) Repression of ARF19 activity on the *P3(2x)::Venus* reporter by IAA3 fused to the TPLN300 fragment. Single PB1 mutants (*k* and *o*) maintain the ability to repress while the double mutant (*ok*) exhibits a complete loss of repression. Similar results were observed for IAA7 and IAA14 (SI Fig. 4).
(B) Single PB1 mutants (*k* and *o*) maintain the ability to repress ARF activity in plants. Lateral root density was measured in *pIAA14::slr* PB1 mutant lines. Each point represents the data from an independent T1 transgenic plant. The black horizontal line indicates the median root density for each genotype.
(C) IAA3 single PB1 mutants (*k* and *o*) can repress ARF19 PB1 monomers and dimers. Mutation of the *k* PB1 interface significantly reduces the repressive capability of IAA3 on the activity of an ARF19 PB1 dimer.
(D) Relief of TPLN300:IAA3 and IAA14 mediated repression in response to auxin treatment. Auxin responsiveness of single PB1 mutants (*k* and *o*) differs between IAAs.
Yeast strains were imaged using fluorescence microscopy 4 hrs after exposing to either an auxin (10 μM) or mock (95% EtOH) treatment. Flow cytometry was used to quantify fluorescence (SI Fig. 4).

To further refine the functional stoichiometry of ARF-IAA complexes, we assayed IAA repression strength when the PB1-mediated interaction potential of both the IAA and ARF partner were limited. IAA3 single PB1 mutants repressed almost as well as wild-type IAA3 when the ARF PB1 monomer had a complementary interaction surface (Fig. 3C; IAA3 *k* |ARF19 *o*; IAA3 *o*|ARF19 *k*). The IAA3 *k* mutant was a less effective repressor than the IAA3 *o* mutant in circuits where ARF19 PB1 variants were capable of self-dimerization, similar to what was seen in wild-type ARF19 circuits. This difference suggests that while either face is sufficient for repression, the positive (*K*) IAA PB1 interface may be the preferred surface for heterodimerization with an ARF. The functional relevance of this bias is further supported by a similar difference in repression strength seen in PB1 mutants expressed in plants (Fig. 3B).

ARF-IAA affinity tunes auxin sensitivity

Effective auxin signaling requires a sensitive balance between the strength of IAA interactions with ARFs and with auxin receptors. One measure of this balance is the

ease with which repression can be reversed following auxin exposure. By adding auxin to the TPL:IAA yeast strains, we could test whether loss of ARF affinity resulting from mutations in a single surface of the PB1 domain increased auxin sensitivity. This effect was exactly what we observed. Auxin could relieve repression of TPLN300-IAA *k* or *o* mutants (Fig. 3D), whereas repression is maintained when TPLN300 is fused to a wild-type IAA [18]. The relative affinity of the IAA PB1 mutant constructs for ARF19 could also be visualized by tracking their cellular localization (SI Fig 5). While fluorescence of YFP-IAA3 was diffuse throughout the cell when expressed alone, the addition of ARF19 strongly enhanced nuclear localization of the florescent signal. This is in contrast to the YFP-IAA3 PB1 mutants where localization remained diffuse even in the presence of ARF19.

Auxin sensitivity assays further supported a bias for the IAA K face for repression of ARF activity. While the *o* and *k* mutations in IAA3 were both moderately auxin-sensitive, there was a marked contrast in the auxin response of the IAA14 single PB1 mutants (Fig. 3D). The IAA14 *k* variant was quite sensitive to auxin, resulting in an almost total reversal of repression, whereas the strain expressing the IAA14 *o* variant exhibited only a modest response to auxin. IAA7 PB1variants followed a similar pattern as those observed for IAA14 (SI Fig. 4).

Why fusion of the TPLN300 domain to wild-type IAAs renders them auxin-insensitive is difficult to answer; however, a further truncation of TPL to the first 100 amino acids (TPLN100) leads to weaker but auxin-reversible repression [18]. Consistent with previous results, TPLN100:IAA3 repressed reporter activation (SI Fig. 6) albeit less stringently than the equivalent strains expressing TPLN300:IAA3 fusions. In contrast to

the results with TPLN300, all of the PB1 variants behaved like the PB1 deletion and could not repress ARF19 activity. As the TPLN300 and TPLN100 fusions are expressed at similar levels (SI Fig. 6), the difference in the sensitivity of repression activity to PB1 mutations may reflect different modes of repression enacted by the different TPL truncations. A recent structure of the N-terminal portion of TPL suggests that this result likely reflects the loss of a second TPL dimerization domain in the N100 fragment [28].

Discussion

To understand plants, one must understand auxin. The simple structure of the nuclear auxin signaling pathway, and its reliance on highly conserved and modular aspects of eukaryotic biology, has enabled remarkable progress towards this ambitious goal [29]. Synthetic recapitulation of auxin response in yeast provides a uniquely liminal testbed for sorting through the many competing models suggested by computational, *in vitro* and *in planta* experiments. Even an answer for the most straightforward question of what is the minimal functional unit of auxin signaling has been elusive. Synthetic auxin response circuits spanning promoter to receptor in yeast (ARC^{Sc}) have made it possible to quantitatively and systematically scrutinize the requirements for auxin response. In this process, we have validated some of the predicted structure-function connections, called others into question, and generated a new minimal model of auxin signaling (Fig. 4).

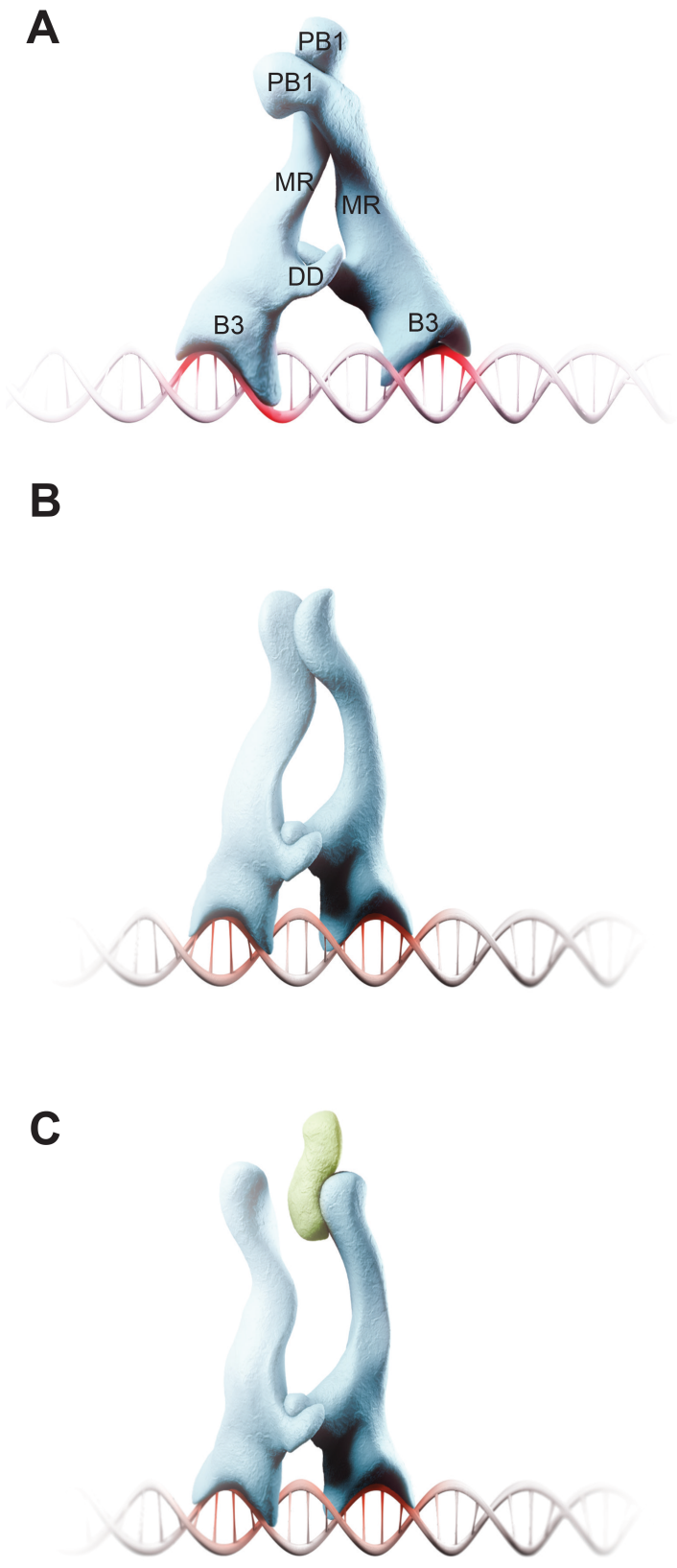

Fig 4. A minimal model of auxin nuclear signaling

(A) ARFs dimerize in both the N-terminal dimerization domain (DD) and the PB1 domain for robust transcriptional activation.
(B) Spacing and orientation of ARF binding sites likely drive conformation of the flexible middle region (MR). Secondary interactions in the PB1 domain may also contribute to conformation of the MR and stabilize an ARF dimer on the DNA.
(C) A single PB1 interaction allows for IAA-mediated repression of ARF activity. While either PB1 interface is capable of binding to an ARF, the positive (K) IAA surface may be preferred for heterodimerization with an ARF.

The strength and specificity of ARF activation is defined by promoter architecture. We quantified the activation strength of all activator ARFs on a panel of promoters, including one native promoter and several synthetic promoters used as field standards. The flexibility of ARF binding to direct or inverted repeats suggests that binding site orientation may drive differential conformation of the flexible middle-region, potentially leading to the recruitment of specific co-activators [30, 31]. Extensive bioinformatic analysis of transcriptome experiments reveals a surprising lack of AuxRE arrays in many early auxin response genes [32]. Rather, promoters of auxin-regulated genes are often enriched with binding sites for other transcription factors, often in proximity to an AuxRE [33-35]. Both bHLH and MYB transcription factors have been shown to interact with ARFs through the PB1 domain [36, 37]. Coupled with proximal binding sites to the ARFs, PB1-mediated interactions between an ARF and another transcription factor may provide the same enhanced binding we observed in ARF-ARF PB1-driven dimers. This would account for ARF dimer binding of single AuxRE sites as well as the integration of regulatory control from other signaling pathways.

The potential for oligomerization via PB1 domains has led to a large number of competing and complex models to explain auxin responses. The current study provides strong evidence that IAAs can repress as monomers, greatly simplifying the models that need to be considered. We have demonstrated that an IAA with a single PB1 interface can repress ARF activity, despite the associated decrease in affinity for the ARF. The differential auxin sensitivity of single PB1 mutants in different IAAs may therefore be indicative of basal differences in affinity for ARF19. Similar reasoning could account for the seemingly contradictory data from *in planta* repression assays [13, 14]. Some IAAs

may have such low basal affinity for one or more ARFs that further compromise of this interaction potential through a PB1 mutation renders them poor competitors for wild-type IAAs expressed in the same cells.

The mechanistic details of IAA-mediated repression remain elusive. Our data indicate that interaction between an IAA and an ARF is required but not sufficient for repression of ARF activity. TPL is essential for repression by an IAA in yeast, just as in plants. The requirement for a TPL:IAA fusion in yeast, along with the differences in strength and auxin reversibility of TPLN300 and TPLN100 repression, highlight the potential for multiple modes of TPL action. Much like the yeast Tup1 co-repressor, the N-terminal domain of TPL assembles into a tetramer and the C-terminal WD40 repeats likely fold into bladed propeller structures [28]. Thus, TPL recruitment would result in a large protein scaffold that could generate a multimeric complex of diverse transcriptional co-factors. These larger protein complexes could stabilize ARF-IAA interactions at the expense of ARF-ARF dimers, which would explain why IAAs expressed without TPL fusions are poor repressors in yeast. It is also possible that binding of the IAA repressor to the ARF could lead to conformational changes in the flexible middle region of the ARF that blocks recruitment of co-activators [31, 38]. Phosphorylation of the middle region in ARF7 and ARF19 has been shown to inhibit IAA interaction [39], indicating that signal integration from other pathways may take advantage of a link between an IAA interaction and the activity of the ARF middle region.

The nuclear auxin response pathway is a simple, robust and tunable circuit that underlies almost every aspect of plant growth and development. If considered in isolation, the simplicity of the circuit seems incongruous with the diverse repertoire of responses

elicited by auxin. It is becoming ever more apparent, however, that auxin does not work alone. Our work *in synthetica* has demonstrated the baseline for auxin response, which can now be used as a breadboard for testing additional layers of regulation. For example, a wealth of transcriptome data [32, 40] can now be re-evaluated and used to generate hypotheses about the likelihood of binding by a specific ARF through integration of cell-type specific expression maps of auxin signaling components [3] and binding site preferences from protein binding arrays [17]. ARC^{SC} provides a resource to rapidly test these hypotheses and inform experimental designs *in planta*. Our minimal experimental model would also facilitate further mathematical modeling by limiting the number of species that need to be included. By integrating studies in plants, *in vitro*, *in silico* and *in synthetica* we can uncover how evolution has tinkered with the auxin nuclear pathway to accommodate innovations in plant life.

Materials and Methods

Strain Construction

ARFs were driven by the yeast *ADH1* promoter and integrated at the *HIS3* locus into a W303-1A MATa strain containing a *pIAA19::Venus* reporter variant integrated at *URA3*. Haploid strains were assayed to measure activity of different promoter-ARF combinations. To maintain consistency across circuits of increasing complexity, ARF19 variant strains containing the *P3(2x)::Venus* reporter were mated to a MATα W814-29B strain containing the AFB2 auxin receptor integrated at *LEU2* (YNL 175) for measuring activity of ARF19 point mutants. For strains containing two genomically integrated copies of ARF19, the second copy of ARF19 was introduced at the *HIS3* locus of YNL175 prior to mating. IAAs were expressed from the yeast *GPD* promoter and N-terminally tagged with either a TPLN300 or TPLN100 fragment for repression assays or YFP for degradation assays as described previously [18]. IAAs were integrated at the *TRP1* locus into a MATα W814-29B strain containing the AFB2 auxin receptor integrated at *LEU2*. For repression assays, IAA strains were then mated to W303-1A MATa strains containing an ARF19 variant and the *P3(2x)::Venus* reporter. See Table S2 for a complete list of strains used in this study.

Plasmid Construction

ARF and Aux/IAA point mutants were generated in pDONR vectors through Gibson assembly [41]. Integrating yeast expression vectors were then generated through Gateway® cloning as previously described [18, 42]. For biochemical assays, epitope tags (4x-FLAG or 4x-MYC) were introduced as N-terminal fusions upstream of recombination sites in the *HIS3* targeting single integrating Gateway® vector [42] prior

to an LR reaction to introduce the ARF19 variant. The 300 bp native *IAA19* promoter sequence was ordered as a gBlock® gene fragment from Integrated DNA Technologies, Inc. (IDT) with a G->A mutation introduced at the second position of each AuxRE site (Figure S1). Gibson assembly was used to swap the mutated pIAA19 gene fragment for the native *IAA19* promoter sequence upstream of the Venus coding sequence in a *URA3* single integrating Gateway® vector. AuxRE arrays were ordered as oligos or gBlock® gene fragments with Gibson overhangs to introduce the sequences into the mutated *pIAA19::Venus* reporter construct. See Table S3 for oligo and gene fragment sequences.

Yeast Methods

Yeast transformations were performed using a standard lithium acetate protocol [43] into MATa W303-1A or MATα W814-29B (gifts from the Gottschling laboratory). Yeast Peptone Dextrose (YPD) and Synthetic Complete (SC) medium were made according to standard protocols and supplemented with 80 mg mL^{-1} adenine. MATa and MATα strains were mated by co-inoculating strains at low density into YPD medium, growing overnight at 30°C with shaking at 220rpm, streaking out to single colonies on SC plates lacking the appropriate amino acids to select for diploids, and isostreaking on YPD plates before glycerol stocking.

Flow Cytometry

Fluorescence measurements were taken with a custom BD Accuri™ SORP flow cytometer with a CSampler 96-well plate adapter using an excitation wavelength of 514 nm and an emission detection filter at 545/35 nm. A total of 20,000 events above a 40,000 FSC-H threshold (to exclude debris) were measured for each sample. Data was exported as FCS 3.0 files and processed in R using the flowCore, plyr, and ggplot2

software packages and custom scripts. Scripts and full datasets are available upon request.

ARF activity and IAA repression assays

A freshly grown colony was inoculated in 500 μl of SC media and grown at 30°C with shaking at 375 rpm in 2000 μl Eppendorf™ Deepwell™ Plates 96. After 16 hours of growth, cultures were either diluted 1:100 (haploid strains) or 1:200 (diploid strains) into fresh SC media. Fluorescence measurements were taken after 6 hours of additional growth. For auxin response assays, diluted cultures were grown for two hours before addition of 10μM auxin (indole-3-acetic acid) or mock treatment (95% [v/v] ethanol). Fluorescence measurements were taken after 4 hours of additional growth. The data for at least three independent replicates were pooled and plotted for each strain.

YFP-IAA expression and dose response assays

YFP-IAA strains were grown as described above. Basal YFP-IAA expression was measured in haploid strains lacking the presence of an auxin receptor. For dose response assays, diploid strains co-expressing the AFB2 auxin receptor and a YFP-IAA variant +/- ARF19 or ARF3 were diluted 1:200 into 4 separate wells containing 500 μl of fresh SC media. After 2 hours of additional growth, an auxin dose (0.05,.05, or 5 μM indole-3-acetic acid) or mock treatment (95% [v/v] ethanol) was added to one of the 4 identical wells for each strain. To compensate for differences between basal YFP-IAA expression levels, dose response fluorescence measurements were normalized by subtracting background autofluorescence and dividing by fluorescence levels of mock treated strains.

Western blotting

Yeast were grown overnight in 25-50 mL liquid YPD at 30°C with shaking at 225 rpm overnight. The next morning cultures were diluted to OD = 0.2 into fresh YPD media and

grown until OD=1.0-1.5. Cells were then pelleted at 4°C, rinsed once with TBS, and flash frozen in liquid nitrogen. Cell pellets were lysed by glass bead disruption in lysis buffer containing protease inhibitors [44]. Whole cell lysate protein concentrations were determined by Bradford assay, and equivalent amounts of protein were loaded onto 4-20% TGX gel (Bio-Rad). Anti-GFP (Sigma) was used to probe for YFP-tagged Aux/IAAs, anti-Myc was used to probe for Myc-ARF variants, and anti-PGK1 (Abcam) was used as a loading control.

Chromatin Immunoprecipitation

Yeast were inoculated in liquid YPD and grown at 30°C with shaking at 225 rpm. After 18 hrs of growth, cultures were diluted 1:50 in fresh YPD to a final volume of 200 mL. Four hours post-dilution, cells were treated with 20 mL of fix solution (11% formaldehyde, 0.1 M NaCl, 1 mM EDTA, 50 mM Hepes-KOH) for 20 min at room temperature with shaking. Cultures were further treated with 36 mL 2.5 M glycine for 5 minutes to quench the cross-linking. Cells were then pelleted at 4°C, washed twice with ice cold TBS and flash frozen in liquid nitrogen. Cells were lysed in breaking buffer containing 100mM Tris pH 8.0, 20% glycerol and 1 mM PMSF prior to sonication. Samples were processed in a Bioruptor® Plus sonication device at 50% for 25 cycles. The supernatent following centrifugation (to pellet cellular debris) was used for the IP reaction. Anti-FLAG M2 (Sigma) coupled to Protein G Dynabeads (Life Technologies) were used to probe for FLAG-tagged ARF19 variants. Following elution from the beads, samples were incubated overnight at 65°C to reverse cross-links. DNA was purified using a Qiaquick PCR purification kit (Qiagen). qPCR for three independent replicates was performed using iQ SYBR Green Supermix (Biorad) in a C100 thermocycler fitted with a

CFX96 Real-Time Detection System (Biorad).

Generation and Analysis of Transgenic Plants

A 2 kb fragment of the *IAA14* promoter [45] was cloned into pGREEN Gateway® compatible vectors. PB1 mutations were introduced through Gibson assembly in pDONR vectors containing the coding sequence for *slr*. Constructs were transformed into Col-0 wild-type plants using the floral dip method [46]. T1 seeds of transgenic plants were sown on 0.5x LS, 0.8% phytoagar plates supplemented with Kanamycin. Plates were stratified at 4°C for 2 days, and grown in continuous light conditions for 7 dpg. Following selection, transformants were transplanted to plain 0.5x LS, 0.8% phytoagar plates and grown vertically in continuous light. Plants were imaged at 14 dpg using an EPSON V500 scanner and root density was measured in ImageJ. Primary roots were traced using a Wacom Intuos Pro Medium tablet.

Microscopy

Yeast strains were grown overnight at 30°C with shaking at 220 rpm in SC medium. Overnight cultures were diluted 1:200 and grown for an additional 4.5 hours. Yeast samples were assembled on glass coverslips with 1% agarose pads placed over the cultures. Strains were immediately visualized using a Leica DMI 3000B microscope fitted with a Leica 100× N-PLAN 1.25 oil objective and illuminated with a Lumencor SOLA light source. Images were captured using Leica LAS AF version 2.6.0 software and a Leica DFC 345FX camera.

Acknowledgements

We thank Takato Imaizumi and Eric Klavins for careful reading of our manuscript; Richard Gardner and Toshio Tsukiyama for guidance on ChIP assays; members of the Nemhauser and Imaizumi Labs for helpful discussions and Jake Wegesin for the graphics shown in Figure 4.

References

1. Wang R, Estelle M. Diversity and specificity: auxin perception and signaling through the TIR1/AFB pathway. Curr Opin Plant Biol. 2014;21:51-8. Epub 2014/07/18. PubMed PMID: 25032902; PubMed Central PMCID: PMC4294414.

2. Chapman EJ, Estelle M. Mechanism of auxin-regulated gene expression in plants. Annu Rev Genet. 2009;43:265-85. PubMed PMID: ISI:000273580300012.

3. Rademacher EH, Moller B, Lokerse AS, Llavata-Peris CI, van den Berg W, Weijers D. A cellular expression map of the Arabidopsis AUXIN RESPONSE FACTOR gene family. Plant J. 2011;68(4):597-606. PubMed PMID: ISI:000297514900003.

4. Vernoux T, Brunoud G, Farcot E, Morin V, Van den Daele H, Legrand J, et al. The auxin signalling network translates dynamic input into robust patterning at the shoot apex. Mol Syst Biol. 2011;7. PubMed PMID: ISI:000293351900004.

5. Weijers D, Benkova E, Jager KE, Schlereth A, Hamann T, Kientz M, et al. Developmental specificity of auxin response by pairs of ARF and Aux/IAA transcriptional regulators. Embo J. 2005;24(10):1874-85. PubMed PMID:ISI:000229587500011.

6. Dreher KA, Brown J, Saw RE, Callis J. The Arabidopsis Aux/IAA protein family has diversified in degradation and auxin responsiveness. Plant Cell. 2006;18(3):699-714. PubMed PMID: ISI:000236004900017.

7. Muto H, Watahiki MK, Nakamoto D, Kinjo M, Yamamoto KT. Specificity and similarity of functions of the Aux/IAA genes in auxin signaling of arabidopsis revealed by promoter-exchange experiments among MSG2 IAA19, AXR2/IAA7, and SLR/IAA141. Plant Physiol. 2007;144(1):187-96. PubMed PMID: ISI:000246356300016.

8. De Smet I, Lau S, Voss U, Vanneste S, Benjamins R, Rademacher EH, et al. Bimodular auxin response controls organogenesis in Arabidopsis. P Natl Acad Sci USA. 2010;107(6):2705-10. PubMed PMID: ISI:000274408100062.

9. Lokerse AS, Weijers D. Auxin enters the matrix - assembly of response machineries for specific outputs. Curr Opin Plant Biol. 2009;12(5):520-6. PubMed PMID: ISI:000271137200002.

10. Rademacher Eike H, Lokerse Annemarie S, Schlereth A, Llavata-Peris Cristina I, Bayer M, Kientz M, et al. Different auxin response machineries control distinct cell fates in the early plant embryo. Dev Cell. 2012;22(1):211-22.

11. Guilfoyle TJ, Hagen G. Getting a grasp on domain III/IV responsible for Auxin Response Factor-IAA protein interactions. Plant Sci. 2012;190:82-8. Epub 2012/05/23. PubMed PMID: 22608522.

12. Han M, Park Y, Kim I, Kim EH, Yu TK, Rhee S, et al. Structural basis for the auxin-induced transcriptional regulation by Aux/IAA17. Proc Natl Acad Sci U S A. 2014;111(52):18613-8. Epub 2014/12/17. PubMed PMID: 25512488; PubMed Central PMCID: PMC4284525.

13. Korasick DA, Westfall CS, Lee SG, Nanao MH, Dumas R, Hagen G, et al. Molecular basis for AUXIN RESPONSE FACTOR protein interaction and the control of auxin response repression. Proc Natl Acad Sci U S A. 2014;111(14):5427-32. Epub 2014/04/08. PubMed PMID: 24706860.

14. Nanao MH, Vinos-Poyo T, Brunoud G, Thevenon E, Mazzoleni M, Mast D, et al. Structural basis for oligomerization of auxin transcriptional regulators. Nat Commun. 2014;5:3617. Epub 2014/04/09. PubMed PMID: 24710426.

15. Kim J, Harter K, Theologis A. Protein-protein interactions among the Aux/IAA proteins. P Natl Acad Sci USA. 1997;94(22):11786-91. PubMed PMID: ISI:A1997YD50600010.

16. Ulmasov T, Hagen G, Guilfoyle TJ. Dimerization and DNA binding of auxin response factors. Plant J. 1999;19(3):309-19. PubMed PMID: ISI:000082537000008.

17. Boer DR, Freire-Rios A, van den Berg WA, Saaki T, Manfield IW, Kepinski S, et al. Structural basis for DNA binding specificity by the auxin-dependent ARF transcription factors. Cell. 2014;156(3):577-89. Epub 2014/02/04. PubMed PMID: 24485461.

18. Pierre-Jerome E, Jang SS, Havens KA, Nemhauser JL, Klavins E. Recapitulation of the forward nuclear auxin response pathway in yeast. Proc Natl Acad Sci U S A. 2014;111(26):9407-12. Epub 2014/07/01. PubMed PMID: 24979769; PubMed Central PMCID: PMC4084466.

19. Hagen G, Guilfoyle T. Auxin-responsive gene expression: genes, promoters and regulatory factors. Plant Mol Biol. 2002;49(3-4):373-85. PubMed PMID: ISI:000175105500009.

20. Tiwari SB, Hagen G, Guilfoyle T. The roles of auxin response factor domains in auxin-responsive transcription. Plant Cell. 2003;15(2):533-43. PubMed PMID: ISI:000181008700018.

21. Ulmasov T, Hagen G, Guilfoyle TJ. Activation and repression of transcription by auxin-response factors. P Natl Acad Sci USA. 1999;96(10):5844-9. PubMed PMID: ISI:000080246500094.

22. Ulmasov T, Murfett J, Hagen G, Guilfoyle TJ. Aux/IAA proteins repress expression of reporter genes containing natural and highly active synthetic auxin response elements. Plant Cell. 1997;9(11):1963-71. Epub 1997/12/24. PubMed PMID: 9401121; PubMed Central PMCID: PMC157050.

23. Ulmasov T, Hagen G, Guilfoyle TJ. ARF1, a transcription factor that binds to auxin response elements. Science. 1997;276(5320):1865-8. Epub 1997/06/20. PubMed PMID: 9188533.

24. Moss BL, Mao H, Guseman JM, Hinds TR, Hellmuth A, Kovenock M, et al. Rate motifs tune Auxin/Indole-3-Acetic Acid degradation dynamics. Plant Physiol. 2015;169(1):803-13. Epub 2015/07/08. PubMed PMID: 26149575; PubMed Central PMCID: PMC4577399.

25. Guseman JM, Hellmuth A, Lanctot A, Feldman TP, Moss BL, Klavins E, et al. Auxin-induced degradation dynamics set the pace for lateral root development. Development. 2015;142(5):905-9. Epub 2015/01/31. PubMed PMID: 25633353; PubMed Central PMCID: PMC4352979.

26. Szemenyei H, Hannon M, Long JA. TOPLESS mediates auxin-dependent transcriptional repression during Arabidopsis embryogenesis. Science. 2008;319(5868):1384-6. PubMed PMID: ISI:000253712900042.

27. Wong KH, Struhl K. The Cyc8-Tup1 complex inhibits transcription primarily by masking the activation domain of the recruiting protein. Gene Dev. 2011;25(23):2525-39.

28. Ke J, Ma H, Gu X, Thelen A, Brunzelle JS, Li J, et al. Structural basis for recognition of diverse transcriptional repressors by the TOPLESS family of corepressors. Science Advances. 2015;1(6).

29. Pierre-Jerome E, Moss BL, Nemhauser JL. Tuning the auxin transcriptional response. J Exp Bot. 2013;64(9):2557-63. Epub 2013/05/01. PubMed PMID: 23630231.

30. Melcher K. The strength of acidic activation domains correlates with their affinity for both transcriptional and non-transcriptional proteins. J Mol Biol. 2000;301(5):1097-112. PubMed PMID: 10966808.

31. Wu MF, Yamaguchi N, Xiao J, Bargmann B, Estelle M, Sang Y, et al. Auxin-regulated chromatin switch directs acquisition of flower primordium founder fate. Elife. 2015;4. Epub 2015/10/16. PubMed PMID: 26460543; PubMed Central PMCID: PMC4600763.

32. Bargmann BO, Vanneste S, Krouk G, Nawy T, Efroni I, Shani E, et al. A map of cell type-specific auxin responses. Mol Syst Biol. 2013;9:688. Epub 2013/09/12. PubMed PMID: 24022006; PubMed Central PMCID: PMC3792342.

33. Berendzen KW, Weiste C, Wanke D, Kilian J, Harter K, Droge-Laser W. Bioinformatic cis-element analyses performed in Arabidopsis and rice disclose bZIP- and MYB-related binding sites as potential AuxRE-coupling elements in auxin-mediated

transcription. Bmc Plant Biol. 2012;12:125. Epub 2012/08/03. PubMed PMID: 22852874; PubMed Central PMCID: PMC3438128.

34. Ulmasov T, Liu ZB, Hagen G, Guilfoyle TJ. Composite structure of auxin response elements. Plant Cell. 1995;7(10):1611-23. Epub 1995/10/01. PubMed PMID: 7580254; PubMed Central PMCID: PMC161020.

35. Walcher CL, Nemhauser JL. Bipartite promoter element required for auxin response. Plant Physiol. 2012;158(1):273-82. Epub 2011/11/22. PubMed PMID: 22100645; PubMed Central PMCID: PMC3252081.

36. Shin R, Burch AY, Huppert KA, Tiwari SB, Murphy AS, Guilfoyle TJ, et al. The Arabidopsis transcription factor MYB77 modulates auxin signal transduction. The Plant Cell Online. 2007;19(8):2440-53.

37. Varaud E, Brioudes F, Szecsi J, Leroux J, Brown S, Perrot-Rechenmann C, et al. AUXIN RESPONSE FACTOR8 regulates Arabidopsis petal growth by interacting with the bHLH transcription factor BIGPETALp. Plant Cell. 2011;23(3):973-83. PubMed PMID: ISI:000289884200015.

38. Zhang F, Yao J, Ke J, Zhang L, Lam VQ, Xin XF, et al. Structural basis of JAZ repression of MYC transcription factors in jasmonate signalling. Nature. 2015;525(7568):269-73. Epub 2015/08/11. PubMed PMID: 26258305; PubMed Central PMCID: PMC4567411.

39. Cho H, Ryu H, Rho S, Hill K, Smith S, Audenaert D, et al. A secreted peptide acts on BIN2-mediated phosphorylation of ARFs to potentiate auxin response during lateral root development. Nat Cell Biol. 2014;16(1):66-76. Epub 2013/12/24. PubMed PMID: 24362628.

40. Lewis DR, Olex AL, Lundy SR, Turkett WH, Fetrow JS, Muday GK. A kinetic analysis of the auxin transcriptome reveals cell wall remodeling proteins that modulate lateral root development in Arabidopsis. Plant Cell. 2013;25(9):3329-46. Epub 2013/09/21. PubMed PMID: 24045021; PubMed Central PMCID: PMC3809535.

41. Gibson DG, Young L, Chuang RY, Venter JC, Hutchison CA, 3rd, Smith HO. Enzymatic assembly of DNA molecules up to several hundred kilobases. Nat Methods. 2009;6(5):343-5. Epub 2009/04/14. PubMed PMID: 19363495.

42. Havens KA, Guseman JM, Jang SS, Pierre-Jerome E, Bolten N, Klavins E, et al. A synthetic approach reveals extensive tunability of auxin signaling. Plant Physiol. 2012;160(1):135-42. Epub 2012/07/31. PubMed PMID: 22843664; PubMed Central PMCID: PMC3440190.

43. Gietz RD, Woods RA. Transformation of yeast by lithium acetate/single-stranded carrier DNA/polyethylene glycol method. Methods Enzymol. 2002;350:87-96. Epub 2002/06/21. PubMed PMID: 12073338.

44. Gerace E, Moazed D. Coimmunoprecipitation of proteins from yeast. Methods Enzymol. 2014;541:13-26. Epub 2014/03/29. PubMed PMID: 24674059; PubMed Central PMCID: PMC4370295.

45. Fukaki H, Tameda S, Masuda H, Tasaka M. Lateral root formation is blocked by a gain-of-function mutation in the SOLITARY-ROOT/IAA14 gene of Arabidopsis. Plant J. 2002;29(2):153-68. PubMed PMID: ISI:000173685000004.

46. Clough SJ, Bent AF. Floral dip: a simplified method forAgrobacterium-mediated transformation ofArabidopsis thaliana. The Plant Journal. 1998;16(6):735-43.

SI Figures

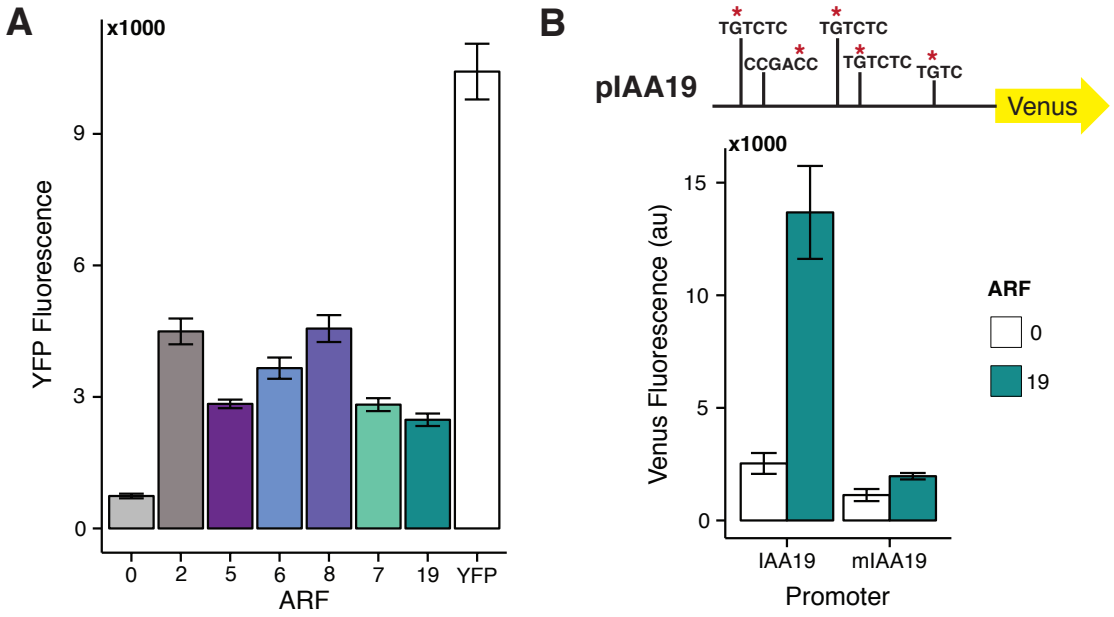

SI Fig. 1

A) ARF activity is not correlated to expression level. Expression of YFP:ARF fusion constructs are shown compared to yeast strains expressing no YFP (0) or YFP alone. The mean from three replicates is shown with error bars representing standard deviation.
B) Mutation of AuxRE sites in the *IAA19* promoter abolishes ARF19 activity. Red asterisks indicate location of G -> A mutations introduced into the 300 bp native IAA19 promoter sequence used for reporter constructs.

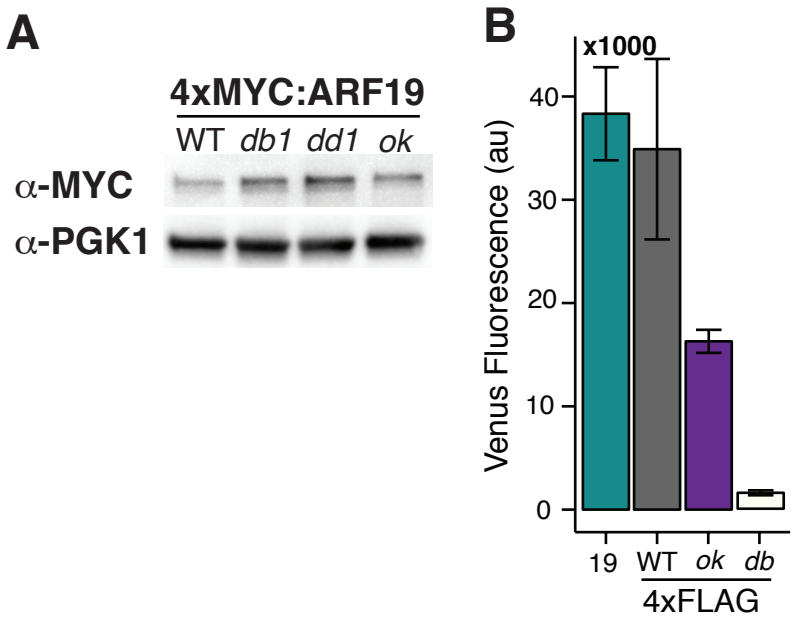

SI Fig. 2

A) Western blot of 4xMYC tagged ARF19 and mutant variants. Differences in ARF19 mutant variant activity are not due to differences in protein levels.
B) FLAG tagged ARF19 variants used in ChIP assays exhibit similar relative activation of the *P3(2x)::Venus* reporter as untagged constructs in Fig 2A. The mean from three replicates is shown with error bars representing standard deviation.

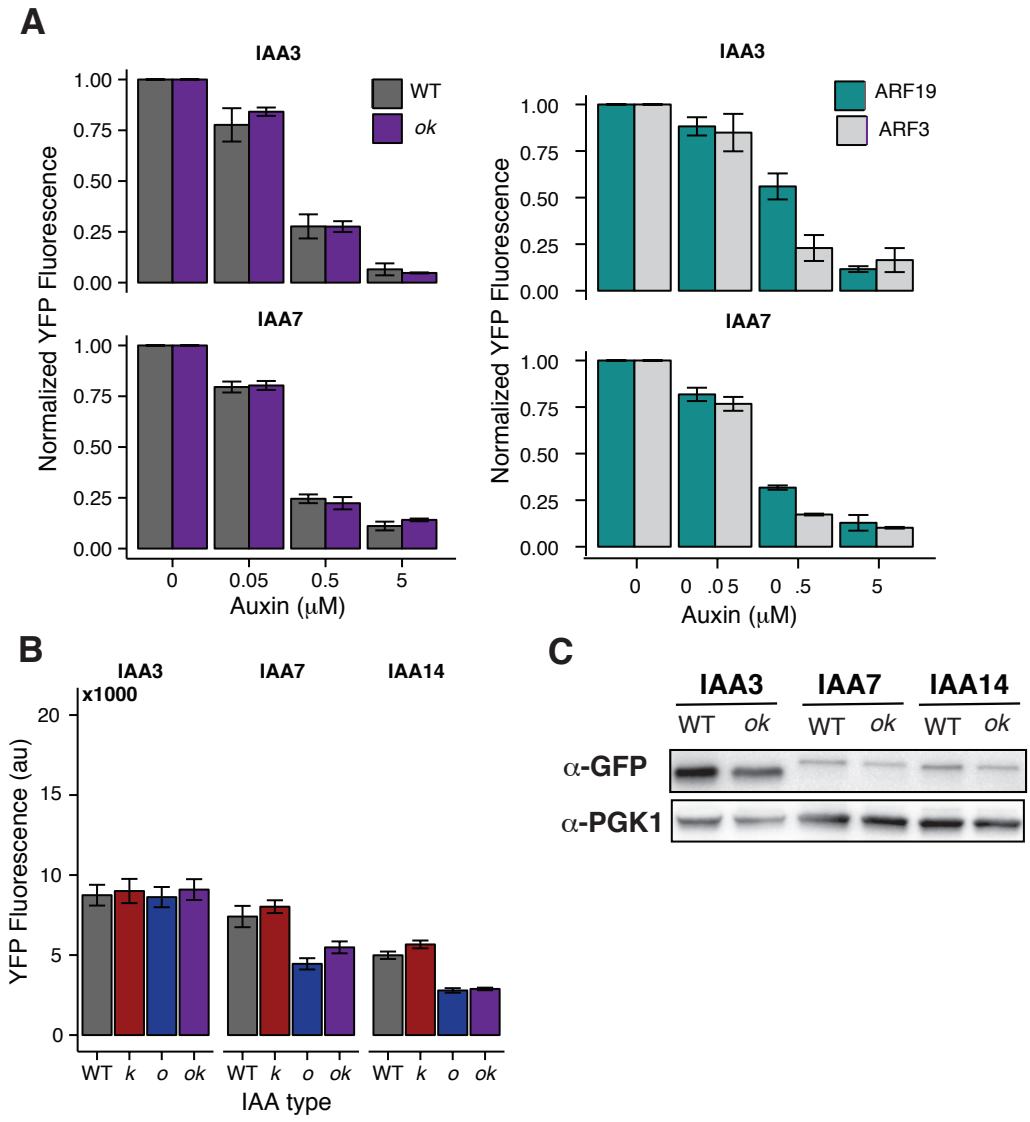

SI Fig. 3

A) Auxin dose response of YFP tagged IAA3 and IAA7 +/- ARF19. There is no difference in auxin-induced degradation between WT and *ok* YFP strains for both IAA3 and IAA7. ARF19 has only a modest effect on the auxin-induced degradation of IAA3 and no effect on IAA7. Fluorescence of YFP-WT and YFP-*ok* IAA strains in the presence of the AFB2 auxin receptor was measured 30 min post-auxin treatment. Fluorescence levels were normalized to mock treatment levels to compensate for differences in basal expression levels of IAAs.
B) Basal expression levels of YFP- IAA PB1 variants. PB1 mutations have little to no effect on the expression of IAA3 but the *o* and *ok* mutations decrease levels of both IAA7 and IAA14.
C) Western blot of YFP-IAA WT and *ok* variants. The *ok* mutations result in only a modest decrease of protein level compared to WT.

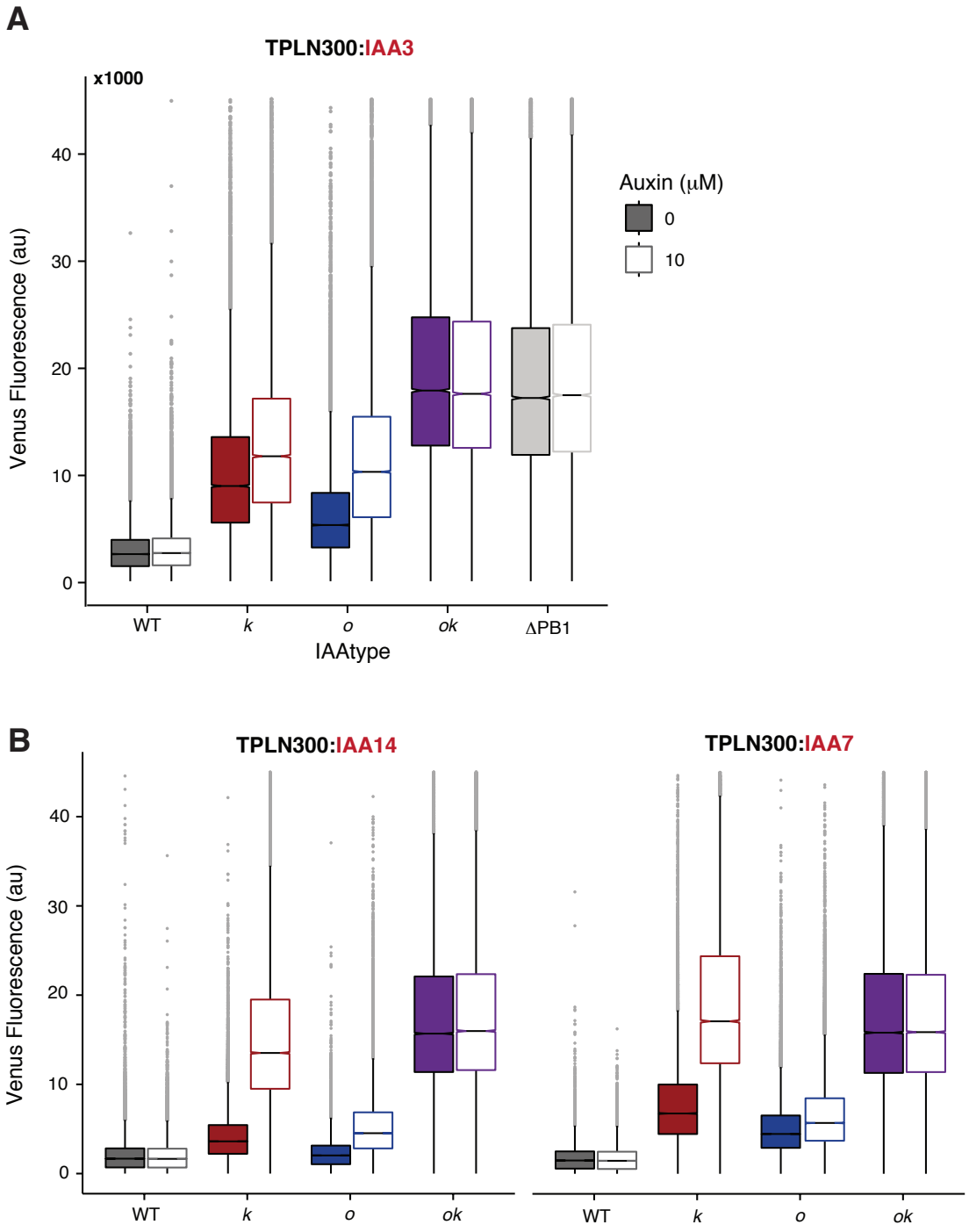

SI Fig. 4

A) Repression strength and auxin sensitivity of TPLN300:IAA3 PB1 mutant variants. Each strain was exposed to a 10 μM auxin or mock (95% EtOH v/v) treatment for 4 hours prior to fluorescence measurements using flow cytometry.
B) Repression strength and auxin sensitivity of TPLN300:IAA14 and TPLN300:IAA7 PB1 mutant variants are similar.

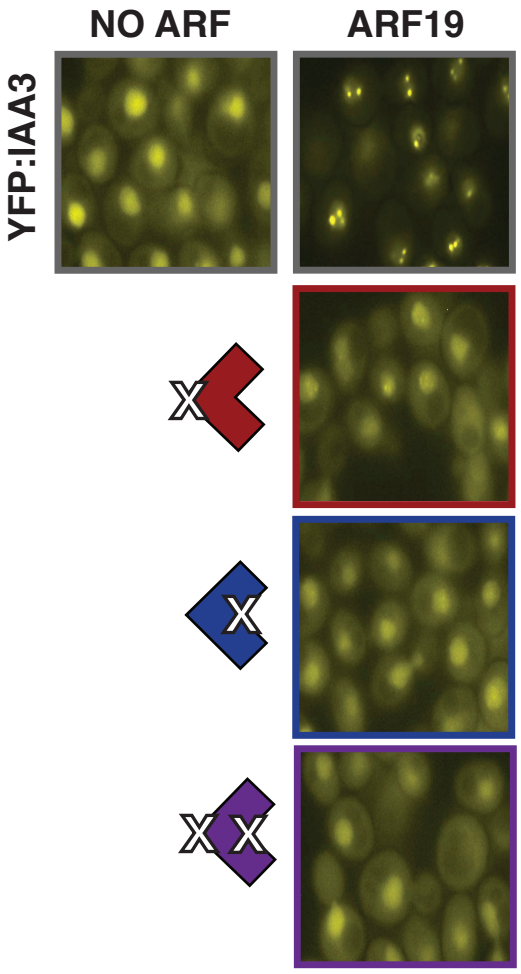

SI Fig. 5

Localization of YFP tagged IAA3 WT and PB1 mutants in the presence of ARF19. Wild-type IAA3 localization becomes strongly nuclear while localization remains diffuse when a PB1 face is compromised.

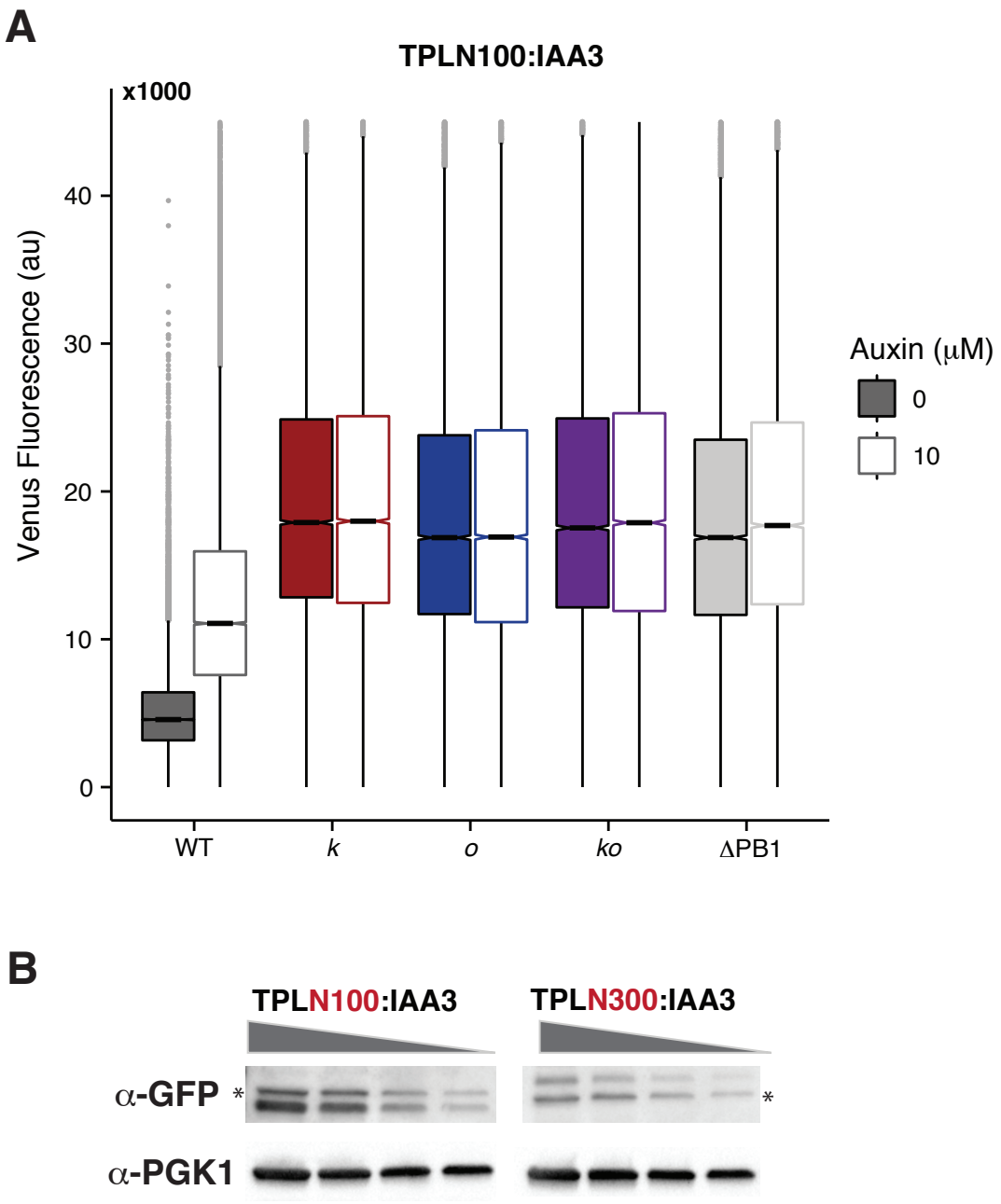

SI Fig. 6

A) Repression strength and auxin sensitivity of TPLN100:IAA3 PB1 mutant variants. Each strain was exposed to a 10 μM auxin or mock (95% EtOH v/v) treatment for 4 hours prior to fluorescence measurements using flow cytometry.
B) Western blot of YFP-TPL:IAA3 strains. Protein levels between TPLN100:IAA3 and TPLN300:IAA3 are similar. Grey wedge represents amount of total protein loaded (L-to-R: 30, 15, 7.5, 3.75 μg total protein). Asterisks mark a non-specific band.

SI Table 1. Positions of ARF19 and IAA3 mutations

ARF19 mutation	Corresponding ARF5 mutation*	ARF 5 complementation phenotype*	IAA3 mutation
DNA-Binding			
H138A (*db1*)	H170A	Small, bushy flower defects	-
R188A (*db2*)	R220A	Flower defects, sterile	-
Dimerization			
G247I (*dd1*)	G279I	Small plants, small fruits, sterile	-
A250N (*dd2*)	A282N	Flower defect, sterile	-
A255N (*dd3*)	A287N	Curled leaves, flower defect	-
PB1 domain			
K962A (*k*)	-	-	K96A (*k*)
D1012A,D1016A(*o*)	-	-	D151A, D155A(*o*)

* Boer DR, Freire-Rios A, van den Berg WA, Saaki T, Manfield IW, Kepinski S, et al. Structural basis for DNA binding specificity by the auxin-dependent ARF transcription factors. Cell. 2014;156(3):577-89.

SI Table 2. Yeast strains used in this study

Strain	Description	Figure
215	pGP6_pIAA19_UbiVenus-stop	1
2197	pGP6_DR5_UbiVenus-stop	1
2198	pGP6P3_2x_UbiVenus-stop	1
2531	W303-1A ADE2+, pGP6ER7_UbiVenus-stop	1
1986	pGP6_mpIAA19_UbiVenus_stop	S1
211	8A-ARF19, pGP6-pIAA19-Ubi-Venus-Stop	1
2200	pGP6DR5_UbiVenus-stop, pGP8A-ARF19	1
2201	pGP6P3_2x_UbiVenus-stop, pGP8A-ARF19	1,2
2532	pGP8A-ARF19, pGP6ER7_UbiVenus-stop	1
2068	pGP8A-ARF19, pGP6_mpIAA19_UbiVenus_stop	S1
1909	pGP6-pIAA19-Ubi-Venus-Stop, 8A-ARF7	1
2578	pGP6DR5_UbiVenus-stop, 8A-ARF7	1
2406	pGP6P3_2x_UbiVenus-stop, pGP8A_ARF7	1
2605	W303-1A ADE2+, pGP6ER7_UbiVenus-stop, 8A-ARF7	1
2597	pGP6-pIAA19-Ubi-Venus-Stop, 8A-ARF5	1
2576	pGP6DR5_UbiVenus-stop, 8A-ARF5	1
2407	pGP6P3_2x_UbiVenus-stop, pGP8A_ARF5	1
2604	W303-1A ADE2+, pGP6ER7_UbiVenus-stop, 8A-ARF5	1
2598	pGP6-pIAA19-Ubi-Venus-Stop, 8A-ARF6	1

2627	pGP6DR5_UbiVenus-stop, 8A-ARF6	1
2601	pGP6P3_2x_UbiVenus-stop, 8A-ARF6	1
2606	W303-1A ADE2+, pGP6ER7_UbiVenus-stop, 8A-ARF6	1
2599	pGP6-pIAA19-Ubi-Venus-Stop, 8A-ARF8	1
2602	pGP6P3_2x_UbiVenus-stop, 8A-ARF8	1
2607	W303-1A ADE2+, pGP6ER7_UbiVenus-stop, 8A-ARF8	1
2596	pGP6-pIAA19-Ubi-Venus-Stop, 8A-ARF2	1
2574	pGP6DR5_UbiVenus-stop, 8A-ARF2	1
2408	pGP6P3_2x_UbiVenus-stop, pGP8A_ARF2	1
2603	W303-1A ADE2+, pGP6ER7_UbiVenus-stop, 8A-ARF2	1
2678	8A-ARF8_pGP6DR5_UbiVenus-stop	1
2320	5G-AFB2 | pGP6P3_2x_UbiVenus-stop, pGP8A-ARF19	2
2456	5G-AFB2 | pGP6P3_2x_UbiVenus-stop, pGP8A_ARF19_k	2
2457	5G-AFB2 | pGP6P3_2x_UbiVenus-stop, pGP8A_ARF19_o	2
2458	5G-AFB2 | pGP6P3_2x_UbiVenus-stop, pGP8A_ARF19_ko	2
2459	5G-AFB2 | pGP6P3_2x_UbiVenus-stop, pGP8A_ARF7	2
2460	5G-AFB2 | pGP6P3_2x_UbiVenus-stop, pGP8A_ARF5	2
2461	5G-AFB2 | pGP6P3_2x_UbiVenus-stop, pGP8A_ARF2	2
2462	5G-AFB2 | pGP6P3_2x_UbiVenus-stop, pGP8A_ARF19_A287N	2
2463	5G-AFB2 | pGP6P3_2x_UbiVenus-stop, pGP8A_ARF19_A282N	2
2464	5G-AFB2 | pGP6P3_2x_UbiVenus-stop, pGP8A_ARF19_G279I	2

2465	5G-AFB2 | pGP6P3_2x_UbiVenus-stop, pGP8A_ARF19_R220A	2
2466	5G-AFB2 | pGP6P3_2x_UbiVenus-stop, pGP8A_ARF19_H170A	2
2507	pGP6P3_2x_UbiVenus-stop, pGP8A-3xFlag-GS-ARF19	2,S2
2508	pGP6P3_2x_UbiVenus-stop, pGP8A-3xFlag-GS-ARF19_ko	2,S2
2509	pGP6P3_2x_UbiVenus-stop, pGP8A-3xFlag-GS-ARF19_H170A	2,S2
2441	pGP5G-AFB2, 8A-ARF19 | pGP6P3_2x_UbiVenus-stop, pGP8A-ARF19	2
2444	pGP5G-AFB2, 8A-ARF19_k | pGP6P3_2x_UbiVenus-stop, pGP8A_ARF19_k	2
2445	pGP5G-AFB2, 8A-ARF19_o | pGP6P3_2x_UbiVenus-stop, pGP8A_ARF19_o	2
2446	pGP5G-AFB2, 8A-ARF19_k | pGP6P3_2x_UbiVenus-stop, pGP8A_ARF19_o	2
2310	5G-AFB2, 4GTPLN300-IAA3_k | pGP6P3_2x_UbiVenus-stop, pGP8A-ARF19	3,S4
2311	5G-AFB2, 4GTPLN300-IAA3_o | pGP6P3_2x_UbiVenus-stop, pGP8A-ARF19	3,S4
2312	5G-AFB2, 4GTPLN300-IAA3_ko | pGP6P3_2x_UbiVenus-stop, pGP8A-ARF19	3,S4
2316	5G-AFB2, 4GTPLN300-IAA3 | pGP6P3_2x_UbiVenus-stop, pGP8A-ARF19	3,S4
2317	5G-AFB2, 4GTPLN300-IAA3_t1 | pGP6P3_2x_UbiVenus-stop, pGP8A-ARF19	3,S4
2447	pGP6P3_2x_UbiVenus-stop, pGP8A_ARF19_o | pGP5G-AFB2, 8A-ARF19_k, 4GTPLRD2-IAA3_K96	3
2448	pGP6P3_2x_UbiVenus-stop, pGP8A_ARF19_o | pGP5G-AFB2, 8A-ARF19_o, 4GTPLRD2-IAA3_K96	3
2449	pGP6P3_2x_UbiVenus-stop, pGP8A_ARF19_o | pGP5G-AFB2, 8A-ARF19_k, 4GTPLRD2-IAA3_opca	3
2450	pGP6P3_2x_UbiVenus-stop, pGP8A_ARF19_o | pGP5G-AFB2, 8A-ARF19_k, 4GTPLRD2-IAA3_ko	3
2451	pGP6P3_2x_UbiVenus-stop, pGP8A_ARF19_o | pGP5G-AFB2, 8A-ARF19_k, pGP4G-TPLN300-IAA3.T1	3
2547	pGP6P3_2x_UbiVenus-stop, pGP8A_ARF19_o | pGP5G-AFB2, 8A-ARF19_o, 4GTPLRD2-IAA3_ko	3
2548	pGP6P3_2x_UbiVenus-stop, pGP8A_ARF19_o | pGP5G-AFB2, 8A-ARF19_o, pGP4G-TPLN300-IAA3	3

2549	pGP6P3_2x_UbiVenus-stop, pGP8A_ARF19_o | pGP5G-AFB2, 8A-ARF19_k, pGP4G-TPLN300-IAA3	3
2550	pGP6P3_2x_UbiVenus-stop, pGP8A_ARF19_k | pGP5G-AFB2, 8A-ARF19_k, 4GTPLRD2-IAA3_ko	3
2551	pGP6P3_2x_UbiVenus-stop, pGP8A_ARF19_k | pGP5G-AFB2, 8A-ARF19_k, 4GTPLRD2-IAA3_opca	3
2552	pGP6P3_2x_UbiVenus-stop, pGP8A_ARF19_k | pGP5G-AFB2, 8A-ARF19_k, pGP4G-TPLN300-IAA3	3
2436	pGP6P3_2x_UbiVenus-stop, pGP8A-ARF19 | 5G-AFB2, 4GTPLRD2-IAA14_KO	3,S4
2435	pGP6P3_2x_UbiVenus-stop, pGP8A-ARF19 | 5G-AFB2, 4GTPLRD2-IAA14_OPCA	3,S4
2434	pGP6P3_2x_UbiVenus-stop, pGP8A-ARF19 | 5G-AFB2, 4GTPLRD2-IAA14_K115	3,S4
2608	pGP6P3_2x_UbiVenus-stop, pGP8A-ARF19 | 5G-AFB2, 4GTPLRD2-IAA14	3,S4
449	4GY-ARF2	S1
451	4GY-ARF5	S1
452	4GY-ARF6	S1
453	4GY-ARF7	S1
454	4GY-ARF8	S1
455	4GY-ARF19	S1
2060	pGP6-pIAA19-Ubi-Venus-Stop, pGP8A_4xMyc_ARF19	S2
2063	pGP6-pIAA19-Ubi-Venus-Stop, pGP8A_4xMyc_ARF19_H170A	S2
2065	pGP6-pIAA19-Ubi-Venus-Stop, pGP8A_4xMyc_ARF19_G279I	S2
2252	pGP6-pIAA19-Ubi-Venus-Stop,pGP8A_4xMyc_ARF19_ko	S2
4	4GY-IAA3	S3
1694	pGP4GY-IAA3-OPCA	S3
1695	pGP4GY-IAA3-KO	S3

1732	4GY-IAA3_K96	S3
19	4GY-IAA14	S3
1691	pGP4GY-IAA14-K115	S3
1692	pGP4GY-IAA14-OPCA	S3
1693	pGP4GY-IAA14-KO	S3
6	4GY-IAA7	S3
1862	pGP4GY-IAA7-K	S3
1863	pGP4GY-IAA7-OPCA	S3
1864	pGP4GY-IAA7-KO	S3
47	5G-AFB2|4GY-IAA3	S3
49	5G-AFB2|4GY-IAA7	S3
1776	5G-AFB2 | pGP4GY-IAA3-KO	S3
1876	5G-AFB2 | pGP4GY-IAA7-KO	S3
2323	5G-AFB2, 8A-ARF19 | 4GY-IAA3	S3
2327	5G-AFB2, 8A-ARF19 | 4GY-IAA7	S3
2562	5G-AFB2, 8A-ARF3 | 4GY-IAA3_WT	S3
2564	5G-AFB2, 8A-ARF3 | 4GY-IAA7_WT	S3
2114	8A-ARF19|4GY-IAA3_KO	S5
2113	8A-ARF19|4GY-IAA3_OPCA	S5
2112	8A-ARF19|4GY-IAA3_K96	S5
2155	8A-ARF19|4GY-IAA3	S5

47	5G-AFB2|4GY-IAA3	S5
2438	pGP6P3_2x_UbiVenus-stop, pGP8A-ARF19 | 5G-AFB2, pGP4G-TPLN100-IAA3_k	S6
2439	pGP6P3_2x_UbiVenus-stop, pGP8A-ARF19 | 5G-AFB2, pGP4G-TPLN100-IAA3_o	S6
2440	pGP6P3_2x_UbiVenus-stop, pGP8A-ARF19 | 5G-AFB2, pGP4G-TPLN100-IAA3_ko	S6
2318	pGP6P3_2x_UbiVenus-stop, pGP8A-ARF19|5G-AFB2, 4GTPLN100-IAA3	S6
2319	pGP6P3_2x_UbiVenus-stop, pGP8A-ARF19|5G-AFB2, 4GTPLN100-IAA3_t1	S6
2239	pGP5G-AFB2, pGP4GYTPLN300-IAA3	S6
496	5G-AFB2, 4GY-TPLRD1-IAA3	S6
2315	pGP6P3_2x_UbiVenus-stop, pGP8A-ARF19|5G-AFB2, 4GTPLN300-IAA7	S4
2314	pGP6P3_2x_UbiVenus-stop, pGP8A-ARF19|5G-AFB2, 4GTPLN300-IAA7_ko	S4
2313	pGP6P3_2x_UbiVenus-stop, pGP8A-ARF19|5G-AFB2, 4GTPLN300-IAA7_o	S4
2437	pGP6P3_2x_UbiVenus-stop, pGP8A-ARF19 | 5G-AFB2, 4G-TPLN300-IAA7_k	S4

SI Table 3. Oligos used in this study

Synthesized oligos for promoter variants

mIAA19	cgccagggttttcccagtcacgacAAACAGCACCAAACTTATATCTCTCATGTGACCGATCACCGCATCC TCAGTTGACCTATCTCTGCCCCCACTTTATCTCCCCACACAAACTGAATAACAAGAAGAAGAAGA CTTTAGATATCAAATGACTCCACGTATCGATATTGGATTGGTTTTCATTGGTTGTATCGTGTGGAC CAACGAAGCAACATATAAAAAGCACGACGCGGTGCCATTACTACAATAAGAGAAGTGTAGGAG AAGAAAGTTCTCATTTCATAATTGTATCAAATTGTGAGAGGAAAAAAAGAAGTTCAAGAAaaaatg tctaaaggtgaagaattattc
DR5	agggttttcccagtcacgacCCCGGGccttttgtctccctttgtctccctttgtctccctttgtctccctttgtctccctttgtctccctttgtctcc cttttgtctcCCCGGGAGCAAGATCAAGATGTTTTC
ER7	cgccagggttttcccagtcacgacAAACAGCACCAAACTTATATCTCTCATGTGACCGATCACCGCATCCTC AGTTGACCTATCTCTGCCCCCACTTTATCTCCCCACACAAACTGAATAACAAGAAGAAGAAGAC TTTAGATATCAAATGACTCCACGTAtgtctcccaaagggagacaTCGATATTGGATTGGTTTTCATTGGTT GTATCGTGTGGACCAACGAAGCAACATATAAAAAGCACGACGCGGTGCCATTACTACAATAAGA GAAGTGTAGGAGAAGAAAGTTCTCATTTCATAATTGTATCAAATTGTGAGAGGAAAAAAAGAAGT TCAAGAA
P3(2x)	cgccagggttttcccagtcacgacAAACAGCACCAAACTTATATCTCTCATGTGACCGATCACCGCATCCTC AGTTGACCTATCTCTGCCCCCACTTTATCTCCCCACACAAACTGAATAACAAGAAGAAGAAGAC TTTAGATATCAAATGACTCCACGTAtgtctcccaaagggagacaacttgtctctgtctcccaaagggagacaacttgtctcT CGATATTGGATTGGTTTTCATTGGTTGTATCGTGTGGACCAACGAAGCAACATATAAAAAGCACG ACGCGGTGCCATTACTACAATAAGAGAAGTGTAGGAGAAGAAAGTTCTCATTTCATAATTGTATC AAATTGTGAGAGGAAAAAAAGAAGTTCAAGAA

Primers for targeted mutagensis using Gibson Assembly

2122	ARF19_A287N_R	AAGGGCTACTATTGGCATTATTATGAGCTGCAGCTGCAAGTATCC
2121	ARF19_A287N_F	AATAATGCCAATAGTAGCCCTTTTACCATCTTCT
2120	ARF19_A282N_R	CATGAGCTGCAGCGTTAAGTATCCCAATGTGCATACTGTCGCT
2119	ARF19_A282N_F	AACGCTGCAGCTCATGCTAATGCC
2118	ARF19_G279I_R	CTGCAGCTGCAAGTATGATAATGTGCATACTGTCGCTGGATATGAC
2117	ARF19_G279I_F	ATCATACTTGCAGCTGCAGCTCATGCTAAT
2116	ARF19_R220A_R	CTGTGGTAAGCAAGTGTGCTTTTGGTTGGCCTCGATAGATATGTCT
2115	ARF19_R220A_F	GCACACTTGCTTACCACAGGTTGGAGC
2114	ARF19_H170A_R	GTACAGAGAATCCACCAGCAGTGCTTGTGTCACTTGCAGTAAGAGTCTT
2113	ARF19_H170A_F	GCTGGTGGATTCTCTGTACCGCGT
2112	ARF19_OPCA_R	AGCGTTTTCGTGAGCGGTGTAGACGAGTTTCCAATCAGAG
2111	ARF19_OPCA_F	GCTCACGAAAACGCTATTTTACTAGTTGGTGATGATCCTTGGGAAGAG
2110	ARF19_K_R	CTCGTTTTTGAACCGCTGTATATGTTCGCATTCGTTGAGTCTGATT
2109	ARF19_K_F	GCGGTTCAAAAACGAGGGTCAGTAGGTAGAT
2100	IAA14_OPCA_R	GGCACCATCTTTGGCCTCGTAGCTTGGAACATACTCAGAACTGTTC
2099	IAA14_OPCA_F	GCCAAAGATGGTGCCTGGATGCTCGTTGGTGATGTC
2098	IAA14_K115_R	ATCCATGGAAACCGCCACAAAGGCGACGGTTCCTC
2097	IAA14_K115_F	GCGGTTTCCATGGATGGAGCTCCTTAT
2096	IAA7_OPCA_R	GGCACCATCTTTGGCCTCGTAGCTTGGCACATACTCAGAGC
2095	IAA7_OPCA_F	GCCAAAGATGGTGCCTGGATGCTCGTTGGCGAT
2094	IAA7_K128_R	GTCCATGGAGACCGCCACCAAGCCGGCTCCG
2093	IAA7_K128_F	GCGGTCTCCATGGACGGTGCTC
2092	IAA3_OPCA_R	AGCACCATCTTTGGCTTCATAAGTAGGCACAAAGTCTGAACCTTTATATCC
2091	IAA3_OPCA_F	GAAGCCAAAGATGGTGCTTGGATGCTCATTGGTGATGTTCC
2090	IAA3_K96A_R	GCACCATCCATACTTACTGCCACATAGATTCCTTGACCCTCATGCT
2089	IAA3_K96A_F	GCAGTAAGTATGGATGGTGCACCATACTTGAG

PERSPECTIVE

Evolution as Tinkering

"Evolution does not produce novelties from scratch. It works with what already exists, either transforming a system to give it new functions or combining several systems to produce a more elaborate one."

– Francois Jacob

When I started graduate school, the Auxin Synthetic Biology (AuxSynBio) project was just getting off the ground. I knew right away that I had to be a part of this project. It was ambitious, new and exciting. I don't think I even really appreciated how risky an undertaking it was until much later, when I was writing the manuscript describing the recapitulation of the entire pathway. I was always sure it was going it work, because getting the whole auxin pathway in yeast was only the first step. Five years and countless hours of cytometry later, I feel incredibly fortunate to have been here at the beginning and participate in the evolution of ARC^{Sc}. In building the pathway from perception to transcription, we were able to identify the minimal requirements for a transcriptional auxin response and generate a system that can be used to interrogate the underlying molecular mechanisms.

Why repress a repressor?

Auxin signaling, like many other regulatory pathways, pivots on the repression of a repressor. Robustness and tunability in auxin signaling is likely due in large part to the multifaceted IAA repressors. Auxin sensitivity, response dynamics and feedback are all directly mediated by the IAAs. In order to relay an auxin signal, an IAA must be able to interact with an AFB receptor, an ARF transcription factor and a TPL co-repressor. Each interaction is mediated through a different domain, each of which has the potential to vary across the large IAA gene family. Our work and that of many others has demonstrated that IAAs vary in their affinity for an AFB receptor, resulting in a range of degradation rates in response to auxin. In recapitulating the entire pathway, and only

allowing the identity of the IAA to vary between circuits, we were further able to demonstrate that IAA degradation rate tunes the rate of gene activation.

While preferential interactions between IAAs and ARFs have been posited as a source of specificity in auxin response, the only distinction appears to be that IAAs predominantly interact with the activator ARFs. Why this is the case when almost all ARFs contain the PB1 interaction domain is still unclear, as is the role of the repressor ARFs in general. The crystal structures of the IAA and ARF PB1 domains and the incorporation of additional ARFs into our yeast system may help shed new light. For example, the different auxin responses observed for PB1 mutants of IAA3 and IAA14 may actually be a reflection of a difference in affinity for ARF19. We have also seen some evidence that degradation of an IAA can be slowed by the presence of an ARF. Identifying which ARFs and IAAs are co-expressed within a cell would also help limit the number of interactions to characterize to those most likely to be of biological significance.

My work characterizing the behavior of the simplest forward response architecture and defining the molecular interactions involved also lays the groundwork to pursue the incorporation of additional layers of complexity. I have already shown that introducing a second IAA into an auxin response circuit typically results in an induction curve characteristic of one of the IAAs when expressed alone. It would be interesting to revisit this work when exploring potential differences in ARF affinity between IAAs. In addition, the new promoter variants and ARFs that are now functional in yeast may be only the tip of the iceberg. With stronger promoters and ARF specific activity, it may now be feasible to generate layered circuits that incorporate feedback.

What is repression?

While I have been able to demonstrate that we understand the broad strokes of the auxin response circuit by recapitulating the pathway in yeast, it is also clear that many details of the underlying molecular mechanisms have yet to be resolved. In particular, the mechanisms underlying IAA mediated repression (and relief of repression in response to

auxin) are still poorly understood. As a result, engineering IAA mediated repression of ARF activity was one of the biggest hurdles in recapitulating the auxin pathway in yeast. Our circuits therefore rely on a TPL:IAA fusion to connect auxin perception to transcription. I soon recognized, however, that our system could be used as a simple functional assay of TPL repression to try and identify the domain critical for repression as well as conserved interactions with transcriptional co-factors that may mediate that repression. While there is a lot left to do there, insight into TPL recruitment and repression is likely key to understanding transcriptional regulation by auxin and numerous other signaling pathways.

In their paper describing the lac operon, Jacob and Monod state, "The remarkable similarity of induction and repression suggests that the two effects represent different manifestations of fundamentally similar mechanisms." Therefore in order to understand repression, we need to understand activation. In terms of auxin signaling, asking how ARFs activate may shed light into how they are repressed when TPL is recruited by the IAAs. ARC^{Sc} would facilitate further interrogation of how promoter architecture influences ARF activity. Coupled with biochemical assays, it might be possible to distinguish ARF affinity for a certain DNA sequence from the ability of an ARF to recruit additional transcriptional factors. While we tend to think of proteins primarily in terms of their modular domains, it is likely that the flexible middle region, which ascribes an ARF its transcriptional ability, is influenced by the interactions occurring in the well-characterized domains that flank it.

I have many more questions to ask, but the ones I am most excited about are relevant for much more than auxin signaling. That's the beauty of molecular biology.

"Almost all aspects of life are engineered at the molecular level, and without understanding molecules we can only have a sketchy understanding of life itself. All approaches at a higher level are suspect until confirmed at the molecular level."
-Francis Crick, What Mad Pursuit

VITA

Edith Pierre-Jerome grew up in San Diego, CA. In 2008, she earned a Bachelor of Sciences in Genetics and Plant Biology and a Bachelor of Arts in Art History from the University of California, Berkeley.